The role of soluble guanylate cyclase in metabolism

Dissertation zur
Erlangung des Doktorgrades (Dr. rer. nat.)
der
Mathematisch-Naturwissenschaftlichen Fakultät
der
Rheinischen Friedrich-Wilhelms-Universität Bonn

vorgelegt von

Jennifer Naumann

aus

Nordhausen, Deutschland

Bonn, Juli 2017

Angefertigt mit Genehmigung der Mathematisch-Naturwissenschaftlichen Fakultät der Rheinischen Friedrich-Wilhelms-Universität Bonn

1. Gutachter: Prof. Dr. Alexander Pfeifer
2. Gutachter: Prof. Dr. Klaus Mohr

Tag der Promotion: 26.01.2018

Erscheinungsjahr: 2018

Table of contents

Table of contents ..... **I**

List of figures ..... **V**

List of tables ..... **VII**

List of abbreviations ..... **VIII**

1 Introduction **1**

1.1 Obesity and adipose tissue 1

1.1.1 White adipose tissue (WAT) *2*

1.1.2 Brown adipose tissue (BAT) *4*

1.1.3 Beige adipose tissue *6*

1.2 NO/sGC/cGMP pathway 7

1.2.1 Production of NO *8*

1.2.2 Guanylate cyclases *9*

1.2.2.1 Particular guanylate cyclase (pGC) 9

1.2.2.2 Soluble guanylate cyclase (sGC) 10

1.2.3 sGC as a drug target *11*

1.2.4 Effector molecules of the second messenger cGMP *12*

1.3 Aim of the thesis 14

2 Materials and Methods **15**

2.1 Materials 15

2.1.1 Reagents *15*

2.1.2 Chemicals *17*

2.1.3 Cell culture *17*

2.1.4 Lab wares *18*

2.1.5 Equipment *18*

2.2 Animal studies 20

2.2.1 Animal housing *20*

2.2.2 Thermography *21*

2.2.3 Body composition *21*

2.2.4 Glucose tolerance test (GTT) *22*

2.2.5 Plasma parameters *22*

2.2.6 Indirect calorimetry *22*

2.2.7 NE-stimulated thermogenesis *22*

2.2.8 TG measurement ex vivo 23
2.2.9 Radioactive-labeled lipid uptake 24
2.3 Immunohistochemistry 24
2.3.1 Preparation of paraffin sections 24
2.3.2 Hematoxylin/Eosin (H/E) staining 25
2.3.3 UCP1 staining of paraffin sections 25
2.4 Cell culture 26
2.4.1 Isolation of mesenchymal stem cells 26
2.4.2 Immortalization of primary BAT-MSCs 27
2.4.3 Cryo conservation and thawing of cells 27
2.4.4 Adipogenic differentiation of brown adipocytes 28
2.4.4.1 Substances 29
2.4.5 cGMP Elisa 29
2.4.6 Oil RedO staining of mature BA 30
2.4.7 Quantification of triglyceride accumulation in adipocytes 30
2.4.8 Lipolysis 31
2.5 Biochemical methods 32
2.5.1 Preparation of total protein lysates from adherent cells and tissue 32
2.5.2 Determination of protein content using Bradford 33
2.5.3 Gel electrophoresis of proteins (SDS-PAGE) 33
2.5.4 Western blotting 34
2.5.5 Immunodetection 35
2.6 Molecular biological methods 37
2.6.1 Phenol/chloroform extraction of genomic DNA 37
2.6.2 Isolation of ribonucleic acid (RNA) from differentiated adipocytes and tissues 38
2.6.3 Polymerase chain reaction (PCR) 38
2.6.4 Genotyping sGC$\beta_1^{-/-}$ and WT mice 41
2.6.5 Agarose gel electrophoresis 42
2.7 Statistics 42
3 Results 43
3.1 Expression pattern of sGC in pre- and mature adipocytes 43
3.2 sGCβ_1 deficiency leads to alteration in body composition of newborn and adult mice 44

3.2.1 sGC is crucial for body temperature of newborn mice 44
3.2.2 Loss of sGC leads to a reduction of adipose tissue in adult mice 45
3.3 sGC deficiency impairs BA function 46
3.3.1 Deletion of sGC influences cGMP production and lipid accumulation 46
3.3.2 Deletion of sGC affects the adipogenic and thermogenic program 48
3.3.3 sGC deletion impairs mitochondrial biogenesis and lipolysis ... 50
3.4 Pharmacological stimulation of sGC enhances BA function 53
3.4.1 Stimulation of sGC influences cGMP production and lipid accumulation 53
3.4.2 sGC stimulator BAY 41-8543 enhances thermogenic and adipogenic program in BAs 54
3.5 sGC stimulation protects against diet-induced obesity..... 58
3.5.1 Pharmacological stimulation of sGC protects against weight gain 58
3.5.2 Enhanced metabolic effects after sGC stimulation 60
3.5.3 sGC stimulator BAY 41-8543 enhances glucose clearance. 61
3.6 Metabolic changes in brown adipose tissue after sGC stimulation . 63
3.6.1 Acute NE stimulation increases BAT activity in mice treated with sGC stimulator..... 63
3.6.2 Treatment with the sGC stimulator BAY 41-8543 increases lipid uptake in BAT..... 64
3.6.3 Mice treated with the sGC stimulator BAY 41-8543 exhibit improved BAT function..... 66
3.7 Metabolic changes in white adipose tissue after sGC stimulation .. 68
3.7.1 Stimulation of sGC leads to an improved lipid uptake in WATi and reduces adipocytes diameter 68
3.7.2 Browning effect in WATi after sGC stimulation with BAY 41-8543 69
3.8 sGC stimulation influences muscle metabolism 70
3.8.1 Increased lipid uptake into muscles after treatment with BAY 41-8543 70
3.8.2 Muscle fiber type switch in mice fed a HFD+BAY 41-8543 73

3.9 BAY 41-8543 protects against liver steatosis 74
3.10 Effects of sGC stimulator BAY 41-8543 on already established obesity 76
3.10.1 sGC stimulator BAY 41-8543 influences body weight. 76
3.10.2 BAY 41-8543 increases energy expenditure and improves glucose clearance..... 77
3.10.3 The sGC stimulator BAY 41-8543 decreases adipose tissue weight and plasma level of insulin, leptin and adiponectin 79
3.11 Effects of sGC stimulator BAY 41-8543 on mice fed a CD..... 81
3.11.1 sGC stimulator BAY 41-8543 does not influence body weight nor body composition 81
3.11.2 The sGC stimulator BAY 41-8543 improves glucose clearance, but does not affect NE-induced thermogenesis..... 82
4 Discussion 84
4.1 sGC is crucial for BA differentiation and thermogenesis..... 84
4.2 Stimulation of sGC with BAY 41-5843 influences adipogenesis of brown adipocytes..... 87
4.3 The effect of pharmacological stimulation of sGC on metabolism .. 88
4.3.1 Stimulation of sGC increases BAT activity and browning of WAT in vivo 88
4.3.2 Pharmacological stimulation of sGC decreases fatty liver and enhances muscle function 91
4.3.3 sGC stimulation as a potential therapeutic approach against obesity 95
5 Summary 99
6 References..... 100

List of figures

Figure 1: Location of brown, white and beige adipocytes in mice and humans (modified from (Bartelt and Heeren, 2014)). 2
Figure 2: Different types of adipocytes (modified from (Pfeifer and Hoffmann, 2015)). 3
Figure 3: Effect of NO/sGC/cGMP pathway in brown adipocytes. 8
Figure 4: Effector molecules of cGMP (modified from (Pfeifer et al., 2013)). 12
Figure 5: Schematic illustration of the *in vivo* experiments perfomed in WT mice. 21
Figure 6: sGC is highly expressed in mature brown adipocytes. 43
Figure 7: sGC is crucial for thermogenesis in newborn mice. 44
Figure 8: Loss of sGC leads to a reduction of adipose tissue weight in adult mice. 46
Figure 9: sGC mediated cGMP production and lipid accumulation. 47
Figure 10: Loss of sGC influences adipogenic program. 48
Figure 11: Loss of sGC influences thermogenic program. 49
Figure 12: sGC deficiency leads to reduced mitochondrial biogenesis and BAs function. 52
Figure 13: Stimulation of sGC influences cGMP production and lipid accumulation. 54
Figure 14: Chronic stimulation of sGC increases adipogenic program. 55
Figure 15: Chronic stimulation of sGC increases thermogenic program. 56
Figure 16: Pharmacological stimulation of sGC leads to an enhanced BAT function. 57
Figure 17: Pharmacological stimulation of sGC protects against weight gain. 59
Figure 18: Metabolic measurements after 12 weeks feeding with CD, HFD and HFD+sGC stimulator. 61
Figure 19: sGC stimulator BAY 41-8543 enhances glucose clearance after 12 weeks on a HFD. 62
Figure 20: sGC stimulator BAY 41-8543 enhances BAT activity after acute cold stimulation. 63
Figure 21: sGC stimulator BAY 41-8543 increases lipid uptake in BAT. 65
Figure 22: sGC stimulator BAY 41-8543 enhances BAT function. 67

Figure 23: sGC stimulator BAY 41-8543 influences lipid uptake in WATi. .. 68
Figure 24: sGC stimulation leads to decreased adipocyte sizes. 69
Figure 25: sGC stimulator enhances browning effect of WATi. 70
Figure 26: sGC stimulator enhances lipid uptake in muscle 71
Figure 27: sGC stimulator leads to a muscle fiber type switch. 74
Figure 28: sGC stimulator enhances liver metabolism. 75
Figure 29: Effects of sGC stimulator BAY 41-8543 on already established obesity. 77
Figure 30: BAY 41-8543 increases energy expenditure after already established obesity. 77
Figure 31: BAY 41-8543 improves glucose clearance after already established obesity. 78
Figure 32: BAY 41-8543 decreases adipose tissue weight and improves insulin and leptin secretion after already established obesity. 80
Figure 33: Effects of sGC stimulator BAY 41-8543 on body weight and composition in mice fed a CD. 81
Figure 34: Enhanced glucose clearance after BAY 41-8543 treatment in CD mice. 83
Figure 35: Pharmagological sGC stimulation counteracts against obesity. . 98

List of tables

Table 1: Different concentrations of SDS-PAGE gel compounds 34
Table 2: Transferring conditions of proteins with different sizes 35
Table 3: List of primary antibodies for immunblotting 35
Table 4: List of secondary antibodies for immunblotting 36
Table 5: List of mitochondrial pirmer for qRT-PCR 39
Table 6: List of murin primer for qRT-PCR 40

List of abbreviations

AC	adenylyl cyclase
ANP	Atrial natriuretic peptide
aP2	fatty acid binding protein 4 (Fabp-4)
ATF2	activating transcription factor 2
ATP	adenosine triphosphate
AUC	area under the curve
β3-AR	beta-3 adrenergic receptor
BAs	brown adipocytes
BAT	brown adipose tissue
BAY 41-8543	sGC stimulator
BMI	body mass index
BMP7	bone morphogenetic protein 7
BNP	B-type natriuretic peptide
BSA	bovine serum albumin
cAMP	3’, 5’ cyclic adenosine monophosphate
cGMP	3’-5’cyclic guanosine monophosphate
CAT	catalase
CD	control diet
CD36	fatty acid translocase
DNA	deoxyribonucleic acid
cDNA	complementary DNA
CEBP	CCAAT/enhancer-binding protein
cGMP	cyclic guanosine-3’, 5’-monophosphate
CNP	C-type natriuretic peptide
Co1	cytochrome c oxidase subunit 1
Cpt1b	carnitine palmitoyltransferase 1B
CREB	cAMP response element-binding protein
CT	cycle threshold
Cytb	cytochrome b
Cytc	cytochrome c
DETA/NO	diethylenetriamine/nitric oxide
DIO	diet-induced obesity
DMEM	Dulbecco's modified eagle medium
DMSO	dimethyl sulfoxide
DNA	deoxyribonucleic acid
dNTPs	deoxynucleotide triphosphate

EDTA	ethylene diamine tetraaceitic acid
ELISA	enzyme linked immunoSorbent assay
EE	energy expenditure
eNOS	endothelia nitric oxide synthase
EtOH	ethanol
FBS	fetal bovine serum
FFA	free fatty acids
GC	guanylate cyclase
Gcp6	glucose-6-phosphatase
GLP-1	glucagon-like peptide-1
GTP	guanosine triphosphate
GTT	glucose tolerance test
HCN	hydrogen cyanide
H/E	Hematoxylin/Eosin
HFD	high fat diet
HSL	hormone-sensitive lipase
IBMX	3-isobutyl-methyl-xanthine
iNOS	inducible nitric oxide synthase
IRS1	insulin receptor substrate 1
LPL	lipoprotein lipase
MHC	myosin heavy chains
mRNA	messenger RNA
MSC	mesenchymal stem cell
mt DNA	mitochondrial DNA
mtTFA	mitochondrial transcription factor
Nd1	NADH dehydrogenase
NE	norepinephrine
NMR	nuclear magnetic resonance
NO	nitric oxide
NOS	nitric oxide synthase
nNOS	neuronal nitric oxide synthase
NP	natriuretic peptide
NPR	Natriuretic peptide receptors
NRF	nuclear respiratory factor
P/S	penicillin/streptomycin
PAGE	polyacrylamide gel electrophoresis
PBS	phosphate-buffered saline

PDE	phosphodiesterase
PFA	paraformaldehyde
PGC-1a	peroxisome proliferator-activated receptor gamma coactivator 1-alpha
PKA	activate protein kinase A
PKG	cGMP-dependent protein kinase
PPARg	peroxisome proliferator-activated receptor gamma
PRDM16	PRD1-BF-1-RIZ1 homologous domain containing-16
qRT-PCR	quantitative reverse transcription polymerase chain reaction
RIPA	radio immunoprecipitation assay
RMR	resting metabolic rate
RNA	ribonucleic acid
ROS	reactive oxygen species
SEM	standard error of the mean
sGC	soluble guanylate cyclase
SLC27A3	very long-chain acyl-CoA synthetase homolog 3
SLC2A1	gene of Glut-1 receptor
SLC2A4	gene of Glut-4 receptor
SVF	stromal vascular fraction
TG	triglyceride
TM	transmembrane domain
Ucp1	uncoupling protein 1
Ucp2	uncoupling protein 2
Ucp3	uncoupling protein 3
VASP	vasodilator-stimulated phosphoprotein
VEGF	vascular endothelial growth factor
VO_2	oxygen consumption
WAs	white adipocytes
WAT	white adipose tissue
WATg	gonadal white adipose tissue
WATi	inguinal white adipose tissue
WHO	world health organization
WT	wild type

unity

A	ampère
bp	base pair
°C	degree
µg	microgram
µl	microliter
g	gravity
h	hour
kb	kilo base pair
kDa	kilodalton
mg	milligram
min	minutes
ml	milliliter
mM	millimolar
ng	nanogram
nM	nanomolar
nm	nanometer
rpm	rotations per minute
V	volt

1 Introduction

1.1 Obesity and adipose tissue

Obesity is defined as an imbalance between energy uptake and energy consumption which leads to an abnormal increase in body fat (Klish, 1995). According to the world health organization (WHO) more than 1.9 billion adults were overweight and more than 600 millions of these were obese in 2014 (WHO, 2016). Overweight and obesity can be classified by the body mass index (BMI). Adults with a BMI between 26-29.99 are overweight whereas adults with a BMI larger than 30 are obese (WHO, 2016). Obesity can be accompanied by several comorbidities like hypertension, diabetes mellitus type II, gout, gallbladder disease, and cardiovascular diseases. These diseases are a growing worldwide problem as the number of obese people doubled since 1980 (WHO, 2016). Obesity places an enormous burden for the society and health care systems as well as on the afflicted individuals themselves (Khaodhiar et al., 1999; Lobstein et al., 2015) (WHO, 2017). Consequently, the funding for research aiming to identify potential targets, aiding to treat obesity-associated diseases has been substantially increased. Recent studies have revealed that targeting the adipose tissue could be a solution (Harms and Seale, 2013).

The adipose tissue is an important organ as it is responsible for the storage of lipids as major energy source and thereby it controls the energy homeostasis (Galic et al., 2010). Importantly, different types of adipose tissue exist in mammals with discrete functions. Mammalian adipose tissue is classically categorized into two different types, the white and the brown adipose tissue. Each of these is characterized by a specific population of adipocytes and is found at distinct regions. Furthermore, beige adipose tissue can occure within the classical white adipose tissue (Figure 1).

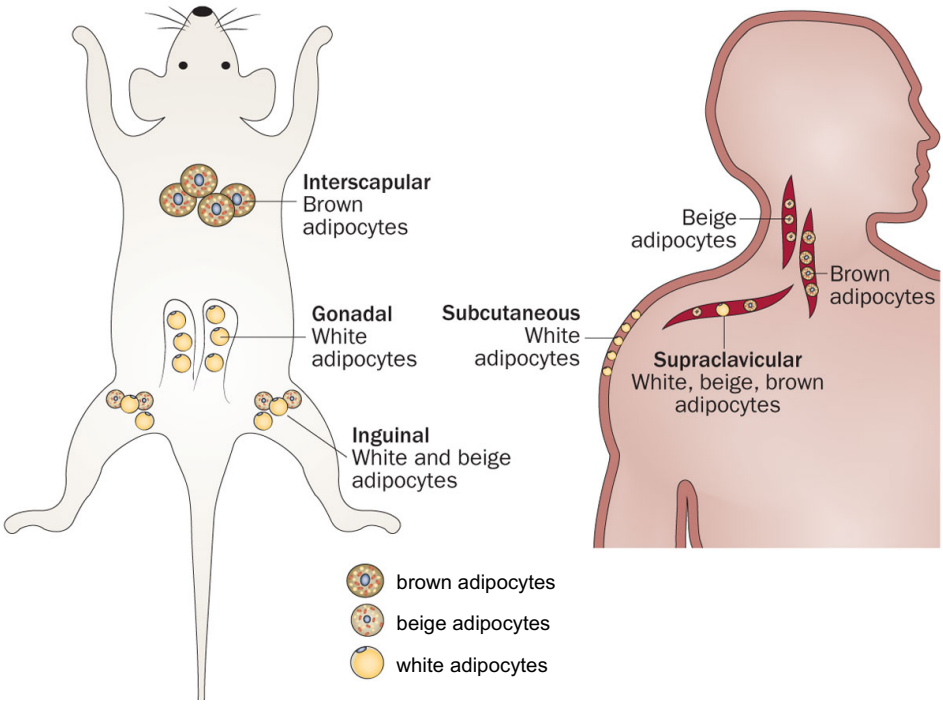

Figure 1: Location of brown, white and beige adipocytes in mice and humans (modified from (Bartelt and Heeren, 2014)).

In mice, brown adipocytes are located in the interscapular region. The inguinal adipose tissue contains a mixture of beige and brown adipocytes and the gonadal adipose tissue only contains white adipocytes. In humans, brown adipocytes can be found deep in the neck, close to muscle tissue. The subcutaneous adipose tissue only contains white adipocytes. Moreover, supraclavicular is characterized by the expression of white, beige and brown adipocytes.

1.1.1 White adipose tissue (WAT)

The white adipose tissue (WAT) is found predominantly around the gonads (WATg, gonadal white adipose tissue) and subcutaneously close to the hind limbs (WATi, inguinal white adipose tissue) in mice. In humans, the major sites of WAT are located under the skin (subcutaneous WAT) or associated with the digestive tract (visceral WAT) (Bartelt and Heeren, 2014; Cinti, 2005). Morphologically, white adipocytes (WAs) contain one large lipid droplet which is located in the cytoplasm of the cell (also called unilocular) (Cinti, 2005) (Figure 2).

The main function of WAT is energy storage. However, in case of chronic excessive energy intake, fatty acids are no longer safely cleared from systemic circulation and accumulate in other organs such as the liver and the muscle (Frayn et al., 2006). This is known as lipid spillover or ectopic lipid deposition (Unger and Scherer, 2010). Apart from an energy repository, WAT functions as an endocrine organ, secreting hormones (like leptin and adiponectin) chemokines and cytokines and thereby influencing the metabolic homeostasis, inflammatory processes and vascular homeostasis (Galic et al., 2010; Ouchi et al., 2011; Trayhurn and Beattie, 2001). Thus far, no specific markers for WAT have been identified. However, several genes including fatty acid binding protein (aP2), peroxisome proliferator-activated receptor γ (PPARγ) and CCAAT/enhancer-binding protein α (C/EBPα) are highly expressed in WAT and have an important role in WAT differentiation (Shao and Lazar, 1997). The transcription factor C/EBPα is crucial for the regulation of energy metabolism, whereas PPARγ influences glucose metabolism and insulin sensitivity (Choi et al., 2010).

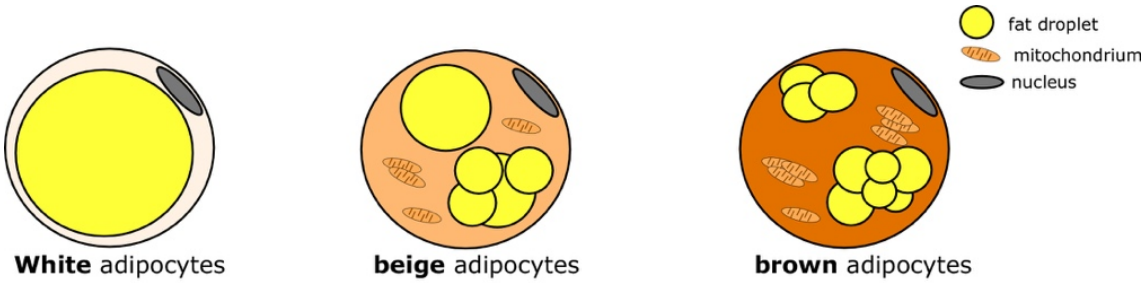

Figure 2: Different types of adipocytes (modified from (Pfeifer and Hoffmann, 2015)).
For decades, the different types of adipocytes were divided into two groups: the white adipocytes, which contain one single large lipid droplet and the brown adipocytes containing multilocular lipid droplets and high abundancy of mitochondria. Recently, an intermediate type was discovered: the beige adipocytes. Those are characterized by multilocular lipid droplets and a high number of mitochondria, however they are located in classical WAT.

1.1.2 Brown adipose tissue (BAT)

The second type of adipose tissue is the brown adipose tissue (BAT) which consumes energy for non-shivering thermogenesis instead of storing energy. Previously, it was widely accepted that BAT is only present in newborns and atrophies during growth. In 2009, innovative studies by using positron-emission-tomography/computed tomography (PET/CT) showed that human adults have active BAT (Virtanen et al., 2009). In humans, BAT is located in the neck region, supraclavicular and perirenal (van Marken Lichtenbelt et al., 2009; Virtanen et al., 2009). In rodents, BAT is located in the interscapular region, between the shoulder blades, and to a lesser extent as perirenal and axillary BAT (Figure 1) (Lidell et al., 2013). Brown adipocytes (BAs) and WAs both have the capacity to store lipids, although they are derived from different precursor cells (Seale et al., 2008). The precursor cells of BAs are derived from the same lineage as skeletal muscle cells. BA progenitors express bone morphogenic protein 7 (BMP7) and PRD1-BF-1-RIZ1 homologous domain containing protein-16 (PRDM16) during development and this drives them into mature BAs (Seale et al., 2008; Tseng et al., 2008). In contrast to WAs, BAs contain multiple smaller lipid droplets (multilocular), and they are rich in mitochondria (Cinti, 2005) (Figure 2).

Thermogenesis by BAT is controlled by the sympathetic nervous system. Upon stimulation by stimuli such as cold exposure, sympathetic nerves in BAT release Norepinephrine (NE). NE then binds to and activates β3-adrenergic receptors (β3-AR) on the surface of the BAs. This leads to increased intracellular 3', 5' cyclic adenosine monophosphate (cAMP) levels, which activates protein kinase A (PKA) (Matthias et al., 2000). PKA activates the hormone-sensitive lipase (HSL), which catalyzes the hydrolysis of free fatty acids (FFA) (Shih and Taberner, 1995). The FFA mediate the activation of uncoupling protein 1 (UCP1) (Cannon and Nedergaard, 2004; Sell et al., 2004). UCP1 is a polypeptide that serves as a proton transporter in the inner mitochondrial membrane and disrupts the electrochemical proton gradient (Cannon and Nedergaard, 2004; Cinti, 2005). By this, UCP1 allows the uncoupling of respiration from ATP synthesis. This uncoupling in turn drives high levels of substrate oxidation (especially glucose and fat)

and results in generation of heat (Cannon and Nedergaard, 2004; Kozak and Harper, 2000; Yamada et al., 1992). Additionally, stimulation of PKA activates the P38 mitogen-activated protein kinase that activates and phosphorylates PGC-1α through activating transcription factor 2 (ATF2) (Cao et al., 2004). PGC-1α directly interacts with nuclear respiratory factor (NRF), like NRF1 and NRF2, to stimulate *de novo* mitochondrial biogenesis and additionally with different protein complexes to induce the transcription of UCP1 (Robidoux et al., 2006; Rosen et al., 2000; Thonberg et al., 2002).

It has been suggested that in humans BAT activity can contribute 5 % of the basal metabolic rate, mediated by UCP1 expression. This indicates a regulatory role of BAT in energy balance and hence body weight (van Marken Lichtenbelt and Schrauwen, 2011). In adult humans, UCP1 expression in BAT is negatively correlated with obesity and its expression diminishes with age (Saito et al., 2009; van Marken Lichtenbelt et al., 2009). Studies on severely obese patients demonstrate that weight loss induced by bariatric surgery increases BAT activity (Vijgen et al., 2012; Vijgen et al., 2011). Furthermore, investigations on healthy Japanese men revealed that single nucleotide polymorphisms in human *UCP1* and *ADRB3* (Gene of β3-AR) result in increased age-related decline of BAT activity and visceral fat accumulation (Nakayama et al., 2013; Yoneshiro et al., 2011; Yoneshiro et al., 2013). Nevertheless, studies to increase BAT mass and activity in humans after repetitive cold exposure showed increased glucose clearance and insulin sensitivity (Blondin et al., 2014; Lee et al., 2014b). These results unravel the adipose tissue as a valuable therapeutic target to treat metabolic diseases and obesity in humans.

1.1.3 Beige adipose tissue

Recently, an intermediate type of adipocytes has been identified: the beige or brite (**br**own in wh**ite**) adipocytes (Wu et al., 2012). Beige adipocytes share several characteristics of BAs like multilocular lipid droplets, a high number of mitochondria and expression of UCP1, but they are located in classical WAT (Bordicchia et al., 2012; Gnad et al., 2014; Mitschke et al., 2013; Rosen and Spiegelman, 2014; Seale et al., 2011) (Figure 1). The origin of beige fat cells is not well understood and different hypotheses exist: one idea is that beige fat cells can arise directly from Myh11+ smooth muscle precursor cells (Long et al., 2014). Long et al. crossed transgenic mice expressing Myh11-driven Cre with GFP reporter mice. Cold exposure increased the number of beige adipocytes in WATi but not in BAs. They also demonstrated in fate mapping experiments and UCP1-TRAP data that mature Myh11-expressing cells suppress their smooth muscle gene signature during differentiation into mature beige adipocytes. Classical brown adipocytes have been described to derive from the same $Pax7^{+}/Myf5^{+}$ lineage as skeletal muscle cells, whereas white und beige adipocytes derive from $Pax7^{+}/Myf5^{-}$ cells (Seale et al., 2008). Other notions are that beige cells derive from preadipocytes or mesodermal stem cells or through transdifferentiation from white to beige adipocytes (so called browning) (Asano et al., 2014; Kajimura and Saito, 2013; Sanchez-Gurmaches et al., 2015; Sanchez-Gurmaches et al., 2012). Several situations might be true in different adipose depots, as the abundance of beige cells varies dramatically between them. Beige adipocytes content in WATg is not as high as of WATi. WATi is responsive to browning even with mild NE stimulation, whereas WATg of male mice is largely resistant to beige adipocyte recruitment (Kim et al., 2016; Okamatsu-Ogura et al., 2013; Shabalina et al., 2013). In addition, studies on human white adipose tissue reveal also browning capacity (Jespersen et al., 2013; Wu et al., 2012).

1.2 NO/sGC/cGMP pathway

The nitric oxide (NO)/ soluble guanylate cyclase (sGC)/ 3'-5'cyclic guanosine monophosphate (cGMP) pathway plays an important role in different physiological processes, for example relaxation of the smooth muscle cells, platelet aggregation and cell differentiation (Ignarro et al., 1999; Pfeifer et al., 1998). The NO/cGMP pathway is also important for the differentiation of BAs, shown in Figure 3. NO is a gaseous molecule produced by different nitric oxide synthases (NOS). It binds to sGC and thereby activates sGC to produce cGMP from guanosine triphosphate (GTP) (Forstermann and Sessa, 2012). Treatment of BAs during differentiation with NO and cGMP increases the expression of the transcription factor PGC-1α and UCP1 (Nisoli et al., 1998). Endothelial NOS (eNOS) knockout mice have a higher body weight in comparison to wild type (WT) mice (Nisoli et al., 2003). These results reveal that a deficiency in eNOS function leads to a reduced energy consumption, favoring weight gain. cGMP functions as a second messenger in the cell and affects different phosphodiesterases (PDEs), cyclic nucleotide gated cation channels (HCN) as wells as cGMP-dependent protein kinase (PKG) (Biel et al., 1999; Francis et al., 2010a; Francis et al., 2010b; Pfeifer et al., 1999). Employing gain and loss of function models Haas et al. demonstrated the importance of the cGMP/PKGI pathway for the differentiation of BAs (Haas et al., 2009). The loss of PKGI leads to an impairment of adipogenesis in BAs. PKGI knockout mice have decreased expression levels of aP2 and PPARγ as well as the thermogenic marker UCP1 compared to WT mice (Haas et al., 2009). In contrast, overexpression of PKGI leads to increased expression of adipogenic markers and UCP1 as well as improved mitochondrial biogenesis and protection from diet-induced obesity (DIO) (Miyashita et al., 2009). One important downstream target of PKGI is RhoA. PKGI phosphorylates RhoA and thereby releases the inhibitory effect of RhoA/ROCK on insulin signaling. The insulin receptor substrate 1 (IRS1) transmits insulin binding to its receptor into mitochondrial biogenesis and adipogenic differentiation(Haas et al., 2009).

A major downstream (phosphorylation) target of PKGI is the vasodilator-stimulated phosphoprotein (VASP). Deletion of VASP results in increased cGMP signaling in adipocytes and enhanced browning of WATi, indicative of a negative feedback loop regulating cGMP levels in BAs (Jennissen et al., 2012). The pathway has been explained in more detail in the following chapters.

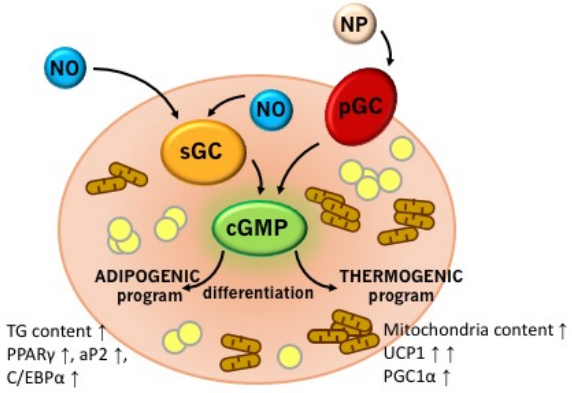

Figure 3: Effect of NO/sGC/cGMP pathway in brown adipocytes.
Two GC exist that generate cGMP from GTP, one is the sGC stimulated by NO and the other one is pGC which is activated by NPs. Increased cGMP leads to activation of the adipogenic (increased PPARγ, aP2 expression and TG content) and thermogenic program (increased expression of UCP1 and PGC-1α) in BAs.

1.2.1 Production of NO

The gaseous signaling molecule NO is produced endogenously by NOS from the amino acid L-arginine that is either also produced endogenously or generated from food intake (Mayer and Hemmens, 1997; Murad, 2006). Three different subtypes of NOS have been identified so far: neuronal NOS (nNOS) which is expressed in neurons, heart, and skeletal muscle cells and produces NO after binding to Calmodulin (Weissman et al., 2002). NO produced by nNOS is an important neurotransmitter mainly in non-adrenergic non-cholinergic nerves (Bowman et al., 1986; Gillespie et al., 1989). eNOS is located in endothelial cells and the activation of eNOS is regulated by fluid shear stress (Forstermann and Sessa, 2012). The third subtype is inducible NOS (iNOS) which is present in macrophages/ glia cells, and its expression can be induced by lipopolysaccharides, glucocorticoids and cytokines (Daff, 2010; Murad, 2006; Stuehr et al., 1991). The production of NO by the different subtypes of NOS leads to the activation of the major enzyme class guanylate cyclase (GC).

1.2.2 Guanylate cyclases

The GCs are members of the nucleotide cyclase class and catalyze the conversion of GTP to cGMP. GCs are classified in sGC and particular GCs (pGC) (Lucas et al., 2000; Tesmer and Sprang, 1998). While pGCs are active as a monomer, sGC is only catalytically active when present as a heterodimer (Lucas et al., 2000; Tesmer and Sprang, 1998).

1.2.2.1 Particular guanylate cyclase (pGC)

Natriuretic peptide receptors (NPRs) are activated by atrial natriuretic peptide (NP) (ANP), B-type NP (BNP) as well as C-type NP (CNP) (Kuhn, 2009, Potter et al 2009). NPRA (GC-A) is activated by ANP and BNP, whereas NPRB (GC-B) is only activated by CNP. The stimulation of GC-A by ANP and BNP for example regulates blood pressure and prevents fibrosis (Kuhn, 2003; Potter et al., 2006), whereas activation of GC-B by CNP inhibits the proliferation of fibroblasts in the heart, for instance (Bocciardi et al., 2007; Obata et al., 2007). The ligands guanylin and uroguanylin bind to GC-C and regulate intestinal fluid balance. Other subtypes of pGC are expressed in the olfactory neuroepithelium (GC-D), in the retina (GC-E and GC-F) (Potter, 2011) or in the intestine, lung and skeletal muscle cells (GC-G). The subtypes GC-D to GC-G are also known as orphan receptors (Lucas et al., 2000). All pGCs exhibit the same structure, an extracellular ligand binding domain, a transmembrane domain (TM), a kinase homology domain and a high conserved catalytic domain (Potter et al., 2006).

1.2.2.2 Soluble guanylate cyclase (sGC)

sGCs are heterodimeric heme-binding proteins consisting of α and β subunits, organized in heterodimer combinations of α_1/β_1 and α_2/β_1 (Friebe and Koesling, 2009b; Potter, 2011; Russwurm et al., 1998). The function of the β_2 subunit remains elusive (Derbyshire and Marletta, 2012). The heterodimer α_1/β_1 is ubiquitously expressed, whereas the α_2/β_1 combination of sGC is highly expressed in lung, brain, adipose tissue, spleen, uterus, placenta, heart and colon (Bellingham and Evans, 2007; Budworth et al., 1999; Jennissen et al., 2012; Potter, 2011).

The structure of sGC is characterized by an N-terminal regulatory domain, a C-terminal catalytic domain, a Per/Ant/Sim (PAS) domain and an α-helix. For the dimerization of the α and β subunits the PAS domain and the α-helix are necessary (Ma et al., 2008). The heme binding site is located in the N-terminal regulatory domain and is required for stimulation of sGC by NO. The catalytic domain of sGC is responsible for the conversion of GTP to cGMP and is located in the C-terminal part (Chang et al., 2005; Lucas et al., 2000).

Deletion of the β_1 subunit ablates sGC enzymatic activity (Friebe et al., 2007). Genetically modified mice lacking the sGCβ_1 subunits exhibit a severe phenotype with higher blood pressure, reduced heart rate and a dysfunctional contraction of the gastrointestinal tract (Friebe et al., 2007). Overall, sGCβ_1 knockout mice have a shorter lifespan in comparison to WT mice. These findings underpin the central and crucial role of sGC for the entire organism (Friebe and Koesling, 2009a; Friebe et al., 2007).

1.2.3 sGC as a drug target

sGC has been used as a drug target since 1860 (Murrell, 1879). First, organic nitrates such as glyceryl nitrate were used as treatments for angina pectoris (Sandler et al., 1963). Nitrates are metabolized to release NO, which is relieving the acute symptoms of arterial hypertension and coronary artery disease. However, nitrate tolerance rapidly emerges and reduces the efficiency of these compounds, potentially in part through a mechanism leading to sGC heme oxidation (Jabs et al., 2015; Munzel et al., 1995).

More recent discovered compounds directly target and increase sGC activity. The first NO-independent stimulator was the benzylindazole derivate YC-1. Due to its NO-independent sGC-stimulating properties YC-1 was used as a lead structure for the synthesis of BAY 41-2272 and BAY 41-8543. These compounds possess a stronger affinity to sGC and thereby further enhance the stability of the NO-heme complex compared to YC-1 (Schmidt et al., 2003; Stasch et al., 2002a; Stasch et al., 2002b).

Different studies showed that BAY 41-2272 and BAY 41-8543 inhibit platelet aggregation, decrease proliferation of vascular smooth muscle cells and lead to vasodilation (Nossaman et al., 2012; Stasch et al., 2002b). The clinical application of BAY 41-8543 is precluded by adverse drug metabolism and pharmacokinetic properties, including high clearance and dose non-linearity of plasma concentrations (Mittendorf et al., 2009).

Further optimization of these compounds resulted in the discovery of a new sGC stimulator. *In vitro* studies revealed that treatment with Riociguat (BAY 63-2521) activates sGC in a dose dependent manner. In addition, it exhibits a higher degree of specificity and no side effects towards inhibition of PDE compared to the earlier sGC stimulator (Schermuly et al., 2008). Riociguat has a superior profile of drug metabolism and pharmacokinetics compared to other drugs of this family. It also has a favored oral bioavailability and hemodynamic profile. Recently, Riociguat completed phase III clinical trials and is now approved by the FDA and EMA for treatment of pulmonary hypertension (Ghofrani et al., 2013a; Ghofrani et al., 2013c; Mittendorf et al., 2009).

1.2.4 Effector molecules of the second messenger cGMP

cGMP is affecting different cGMP-gated ion channels (HCN), phosphodiesterases (PDEs) and cGMP-dependent protein kinase G (PKG) and thereby mediating signaling transmission (Biel et al., 1999; Francis et al., 2010a; Francis et al., 2010b; Pfeifer et al., 1999) (Figure 4).

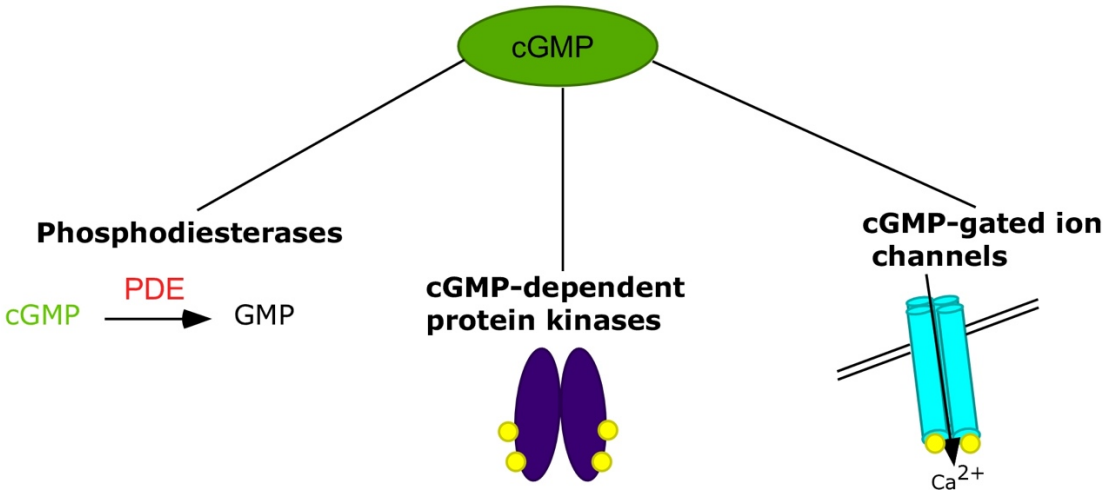

Figure 4: Effector molecules of cGMP (modified from (Pfeifer et al., 2013)).
The second messenger cGMP mediates its effects by binding to phosphodiesterases (PDE), cGMP dependent protein kinases or cGMP-gates ion channels.

The HCN possess an important function in the signaling pathway of retinal photoreceptors and olfactory receptor neurons as they regulate the influx of potassium and sodium (Biel et al., 1999).

PDEs break down cGMP and cAMP to GMP and AMP, respectively. Until now 11 members of the PDE family have been identified and they are classified based on their substrate specificity. The class of cAMP-specific PDEs include PDE 4,7 and 8 and the class of cGMP-specific PDEs include PDE 5, 6 and 9 while other PDEs can hydrolyze both, cAMP and cGMP (1, 2, 3, 10 and 11) (Levy et al., 2011). PDE5 is expressed in muscle cells and PDE3 in adipose tissue (Boswell-Smith et al., 2006). PDE3B plays an important role in insulin, IGF1 and leptin signaling (Degerman et al., 1997). Overexpression of PDE3B in beta-cells diminishes insulin secretion and glucose tolerance in mice (Degerman et al., 1997).

The crucial mediator of cGMP effects in adipocytes is PKG (Haas et al., 2009). PKG belongs to the family of serine/threonine kinases and two isoforms have been identified, PKGI and PKGII. Both kinases exhibit a similar structure: two cGMP binding sites and a catalytic domain (Hofmann et al., 2006). PKGI is predominantly localized in the cytoplasm, whereas PKGII is anchored to the plasma membrane (Gudi et al., 1997; Vaandrager et al., 1996). The 70 kDa PKGI protein is mostly expressed in vascular smooth muscle cells, platelets and different neurons (Hofmann, 2005). The main function of PKGI is relaxation of smooth muscle cells (Pfeifer et al., 1998). In contrast, PKGII is mostly expressed in secretory epithelial cells, and influences bone development and growth (Pfeifer et al., 1996). Controversial results are described regarding the function of PKGI on platelet aggregation. In earlier studies it was reported that PKGI inhibits platelet aggregation (Massberg et al., 1999), whereas more recently, Lie et al. showed a novel PKG-dependent platelet aggregation pathway wherein, PKGI promotes platelet activation (Li et al., 2003). Studies on PKGI knockout mice revealed that the deletion of PKGI leads to severe dysfunction of vascular and intestinal function due to dysregulated smooth muscle cells relaxation (Pfeifer et al., 1998).

1.3 Aim of the thesis

Several research groups have shown that the NO/cGMP signaling pathway has a positive effect on BA differentiation and browning of WAT (Haas et al., 2009; Mitschke et al., 2013; Nisoli et al., 2003). Results obtained from sGCβ_1 knockout mice indicate a central role of sGC in the differentiation of BAs (Jennissen et al., 2012). Although many effectors of the NO/cGMP pathway have already been analyzed for their precise roles in adipocytes, not much is known about the effects of sGC stimulation on adipose tissue and whole body metabolism. The main aim of this thesis was to identify the role of sGC in BA differentiation and function. This work also aims to identify sGC stimulators as novel pharmacological tools to develop therapies against obesity and its associated diseases.

Accordingly, the following questions were raised:

- What is the consequence of loss of sGC during BA differentiation *in vitro* and *in vivo*?
- Does the pharmacological sGC stimulator (using BAY 41-5843) affect adipocyte differentiation *in vitro*?
- What are the effects of sGC stimulation on metabolism *in vivo*?

To this end, pharmacological and genetic tools (sGC$\beta_1^{-/-}$ mice) were used for detailed *in vitro* and *in vivo* studies.

2 Materials and Methods

2.1 Materials

2.1.1 Reagents

4-Morpholineethanesulfonic acid	Sigma-Aldrich
Acetic acid	Sigma-Aldrich
ADP	Sigma-Aldrich
Agarose	PeqLab
ammonium persulfate (APS)	Merck
ATP	Sigma-Aldrich
Bromphenol blue	Roth
BSA	Roth
BSA (essential fatty acid free)	Sigma-Aldrich
CaCl2	Roth
Chloroform	Roth
Complete® EDTA-free	Roche
Coomassie brilliant blue G-250	Merck
Desoxy-cholic acid-Na	Sigma-Aldrich
Digitonin	Sigma-Aldrich
Dithiothreitol	Sigma-Aldrich
Enhanced chemiluminescence (ECL) reagent	Amersham Biosciences
EGTA	Sigma-Aldrich
Eosin G	Merck
Ethanol	Roth
Ethidium bromide	Carl Roth GmbH
Ethylendiamintetraacetate (EDTA)	Sigma-Aldrich
2,2'(Hydroxynitrosohydrazano)bis-ethanime (DETA/NO)	Sigma-Aldrich
8-(4-Chlorophenylthio)guanosin-3'5'-cyclic monophophosphate (8-pCPT-cGMP)	Biolog
Acrylamide,Rotiphorese®Gel 30	Carl Roth GmbH

Arteronol	Sanofi
control diet D12450B	Ssniff
Entwicklerkonzentrat T-Matic	ADEFO-CHEMIE GmbH
Fixierkonzentrat T-Matic	ADEFO-CHEMIE GmbH
Free Glycerol Reagent	Sigma-Aldrich
Glucose	SERAG
Glycerol Standard Solution	sigma-Aldrich
HCl	Roth
HEPES	Sigma-Aldrich
High fat diet D12492	Ssniff
Hydrogen peroxide	Roth
IMMU-MOUNT	Thermo Scientific, Waltham
Isopropyl alcohol (99%)	Roth
KCl	Roth
KH2PO4	Roth
L-(-)-Norepinephrine bitartate salt monohydrate (NE)	Sigma-Aldrich
LightCycler® SYBR Green I Master mix	Roche
Mayers hemalaun	Merck
Methanol	Roth
MgCl 2	Roth
Na-Citrate	Roth
Na2HPO4	Roth
Na3VO4	Sigma-Aldrich
NaCl	Roth
NaF	Roth
NP-40	Roth
Oil RedO	Sigma-Aldrich
Oligomycin	Sigma-Aldrich
Paraffin	Roth

Paraformaldehyde	Sigma-Aldrich
Phosphoric acid	Sigma-Aldrich
Precision plus All Blue Standard	BioRad
Protease inhibitor cocktail, Complete® EDTA-free	Roche
Proteinase K	Roche
Roti® Phenol/C/I	Carl Roth GmbH
Roti®-Histokitt	Carl Roth GmbH
SDS	Sigma-Aldrich
Skimmed milk	Sigma-Aldrich
Sodium ascorbate	Sigma-Aldrich
T4 DNA ligase	Invitrogen
TaqCOREkit	Qbiogen
TEMED	Sigma-Aldrich
Transcriptior First Strand Synthesis Kit	Roche
Triglyceride Reagent	Sigma-Aldrich
Triton X-100	VWR
Tween 20	Sigma-Aldrich
Xylencyanol FF	Sigma-Aldrich
Xylol	Sigma-Aldrich
β-mercaptoethanol	Sigma-Aldrich
cGMP Elisa	Cayman chemical
innuSOLV	Analytik Jena AG

2.1.2 Chemicals

All chemicals used in this thesis were purchased from following companies, if not further specified: Carl Roth (Karlsruhe), Calbiochem (Darmstadt), Gibco-Invitrogen (Karlsruhe), Merck (Darmstadt), Roche (Mannheim), Sigma-Aldrich (Steinheim) or VWR (Darmstadt). The water that was used for all the experiments was purified and distilled with an UV/UF system (PURELAB classic, ELGA LabWater, Celle)

2.1.3 Cell culture

Collagenase II	Worthington, Lakewood
Dexamethason	Sigma-Aldrich
DMSO	Roth
DMEM	Gibco
Dulbecco's modified Eagle's medium (DMEM) liquid (4.5 g/L D-glucose)	Gibco
Fetal bovine serum (FBS)	Biochrom AG
Insulin	Sigma-Aldrich
Isobutylmethylxanthine (IBMX)	Sigma-Aldrich
Penicillin, Streptomycin (P/S)	Biochrom AG
Triiodothyronine-Na	Sigma-Aldrich
Trypan blue 0.4% solution	Sigma-Aldrich
Trypsin-EDTA 0.05%	Invitrogen

2.1.4 Lab wares

100 mm dish	Labomedic
15 ml / 50 ml Falcon tube	Amersham Biosciences
5 ml / 10 ml / 25 ml pipette	Sarstedt
6-well / 12-well cell culture plate	Sarstedt
Cell scraper	Sarstedt
Chemiluminescence films, Hyperfilm®	Marienfeld GmbH
Cryogenic vials	Sarstedt
Microscope Cover Glasses	Sarstedt
needle (26G)	Millipore
Nylon mesh	VWR
PVDF membranes, Immobilon®P 0.45µm	Millipore
Sterile filter 0.22 µm	BD
Syringe 1 ml	B.Braun

2.1.5 Equipment

AccuCheck with test stripes for GTT	Roche
Autoclave, Varioklav 135 T	Faust
Casting platforms	EmbiTech
Centrifuge, 5415R	Eppendorf
Centrifuge, Biofuge Primo	Heraeus
Electrophoresis chamber	Peqlab
Electrophoresis/blotting system, Mini Trans Blot System	BioRad
Film processor, CP100	Agfa
Fluorescence microscope, LEICA DMIL4000 B	Leica
Incubator, HeraCell 150	Heraeus
Infrared camera IC060	Trotec
Laminar air flow, HeraSafe	Heraeus
Leica Application Suite V3	Leica Microsystems GmbH
Micro plate reader, SUNRISE-BASIC TECAN	Tecan
Microsystems GmbH, WetzlarAxioCam camera and AxioVision software	Zeiss
Microsystems GmbH, WetzlarCamera, LEICA DFC425C	Leica
Microwave	Severin
Neubauer counting chamber	Labomedic
NMR device minispec	Bruker Corporation
Phenomaster device	TSE System
Photometer, Biophotometer	Eppendorf
Power supply, Consort E835	Peqlab
QuantityOne® Software	BioRad
Real-time PCR machine, StepOnePlusTM Real-Time PCR System	Applied Biosystems
Thermocycler, T1	Biometra
Thermomixer, 5350	Eppendorf
UV light transilluminator, GelDoc®XR	BioRad
WetzlarMicrotome, HM335E	Microm

2.2 Animal studies

2.2.1 Animal housing

Transgenic mice used in this study were established by Prof. Friebe, Würzburg and were transferred to Bonn for direct use (Friebe et al., 2007). Newborns from $sGC\beta_1^{-/-}$ mice and their littermates were used directly after birth. 8-week old $sGC\beta_1^{-/-}$ mice and their WT littermates were bred and housed in Würzburg and afterwards sent to Bonn for direct experiments.

5-week old male C57Bl/6J mice were purchased from Charles River. High fat diet (HFD) (60% of calories from fat, D12492) and control diet (CD) (D12450B) were purchased from Ssniff GmbH, Germany. 300 mg kg^{-1} BAY 41-8543 were directly added to the diet as indicated.

In the first *in vivo* study mice were treated for 12 weeks with CD, HFD or HFD+BAY 41-8543 (Figure 5).

In the second *in vivo* study mice were first treated for 12 weeks with a HFD and then for 6 more weeks with HFD or HFD+B41-8543 or with a CD or CD+B41-8543 (Figure 5).

In the third *in vivo* study mice were treated for 12 weeks with a CD or CD+B41-8543 (Figure 5).

All mice were maintained on a daily cycle of 12 hours light (0600 to 1800) and 12 hours darkness (1800 to 0600), at 24 ± 1°C, and were allowed free access to diets and water. During the studies mice were weighed weekly.

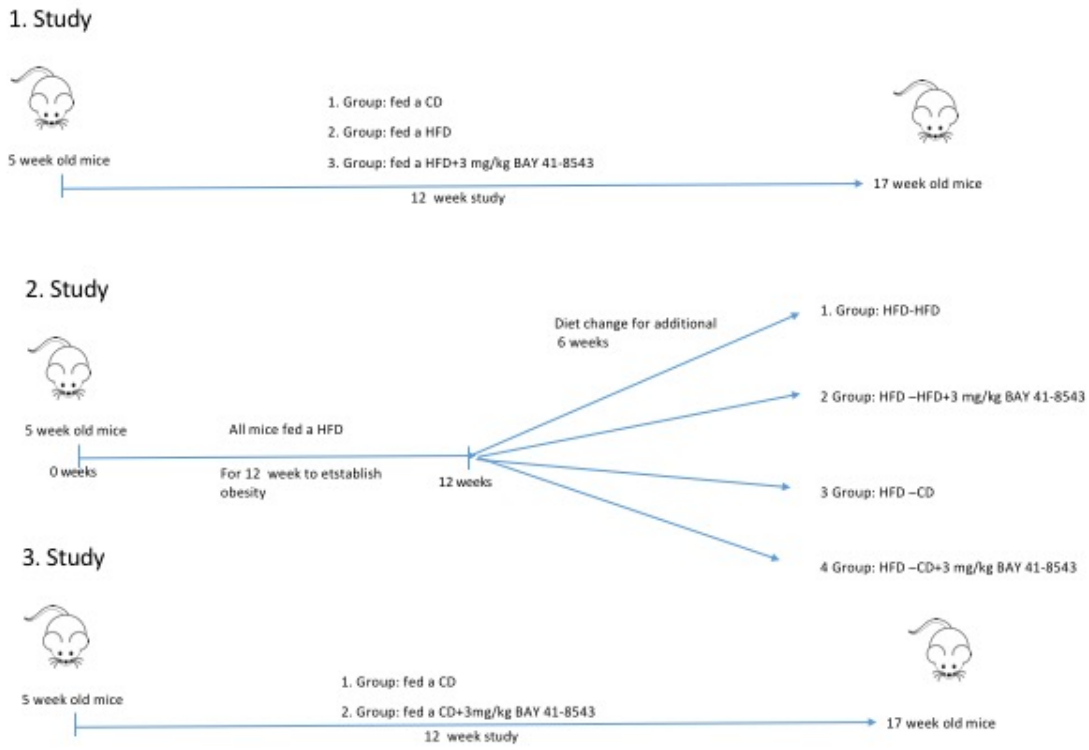

Figure 5: Schematic illustration of the *in vivo* experiments perfomed in WT mice.

2.2.2 Thermography

Infrared thermography was performed on WT and sGCß$_1^{-/-}$ newborns (directly after birth). Therefore, newborns were kept for 10 min in 37°C separated from the mother to allow the newborn to reach same body temperature. Afterwards pictures were taken at ambient temperature using a hand-held infrared camera (IC060, Trotec GmbH). The images were analyzed using IC-Report software 1.2 (Trotec GmbH) (Haas et al., 2009).

2.2.3 Body composition

In the last week of each study, body composition (lean mass, water and fat mass) of the mice was measured. Therefore, body weight of mice was measured and afterwards body composition in conscious mice was determined with the use of a benchtop NMR device Minispec (Bruker Corporation).

2.2.4 Glucose tolerance test (GTT)

Animals were fasted for 5 h before starting GTT. Prior to starting GTT all mice were weighed and then tail veins were punctured with a scalpel to measure starving glucose levels (time point 0) in duplicates using AccuCheck test stripes (Roche). The difference between both measurements was not more than 27 mg/dl. Then a glucose solution (0.25 g/ml) was *i.p.* injected (8 µl/g body weight) with a syringe (1 ml) and a needle (26G). Glucose levels were further monitored was measured 30, 60, 90 and 120 min post injection in blood drawn from the tail vein as described above.

2.2.5 Plasma parameters

Insulin was measured using a commercially available ELISA following manufacturer's instructions (Crystal Chem). LDL and triglycerides were measured using a Cobas device (Roche).

2.2.6 Indirect calorimetry

Individual oxygen consumption (VO_2) and CO_2 production (VCO_2) were measured using a Phenomaster device (TSE systems) at ambient temperature. During measurement mice had ad libitum access to food and water. Furthermore, food intake and motility was recorded by the Phenomaster device. Energy expenditure (EE) was calculated using the following equation: EE [kJ/hour] = [4.44 + 1.43 x (VO_2/VCO_2)] x VO_2 [ml O_2/hour] x 360.

2.2.7 NE-stimulated thermogenesis

The resting metabolic rate (RMR) was measured at 30°C for 4 h in a Phenomaster device individually for each mouse. After reaching an O_2 baseline, mice were weight and then NE (Arterenol, Sanofi) was injected subcutaneous (in the interscapular region) in a final concentration of 1 mg/kg bodyweight after reaching a O_2 baseline. Afterwards, mice oxygen consumption was measured for 2 h.

2.2.8 TG measurement *ex vivo*

Triglycerides (TG) are ester of fatty acids and glycerol. To detect TGs an enzyme coupled assay was used.

Glycerol + ATP t→ GK → G-1-P +ADP

G-1-P+O2 → GPO → DAP+H_2O_2

H_2O_2 + 4-AAP +ESPA → POD → Quinoneimine (colour) + H_2O

ATP	Adenosine-5-triphosphate	DAP	Dihydroxyacetone phosphate
G-1-P	Glycerol-1-phosphate	H_2O_2	Hydrogenperoxid
ADP	Adenosine-5-diphosphate	POD	peroxidase
GK	Glycerol kinase	4-AAP	4-Aminoantipyrine
GPO	Glycerol phosphate oxidase	ESPA	sodium-ethyl-N-(3sulfopropyl)m-anisidin

TG Assay reagent was prepared from free glycerol reagent and triglyceride reagent (Sigma) following the manufacturer's instructions. Livers, WATi and muscles of mice were weighed and transferred to TGTx lysis buffer. Tissues were cut into small pieces, sonicated and resuspended.
The 20 µl of the tissue suspension was added to 100 µl TG assay reagent. Following, the sample was measured at 540 nm in a TecanReader (Sunrise). The increase in absorption is directly proportional to the glycerol content. The Glycerol content was calculated from the resulting values and normalized to the wet weight of the sample.

Glycerol content:

$(A_{sample}-A_{Blank})-(A_{Standard}-A_{blank})$ x concentration of the standard (mg/dl)

TGTx lysis buffer

NaCl	150 nM	
Tris-HCl	10 nM	pH 8.0
Triton-X 100	0.05 %	

The buffer was sterile filtered before use and then stored at -20°C. Before use 40 µl/ml Complete® was added as a protease Inhibitor.

TG Assay reagent	
Free glycerol reagent	80 %
Triglyceride reagent	20 %

2.2.9 Radioactive-labeled lipid uptake

Radioactive-labeled lipid uptake was not performed in our lab, it was done in cooperation with the laboratory of Jörg Heeren, Hamburg.
For this, mice were fed CD, HFD or HFD + BAY 41-8543 for 8 weeks and 1 mg/kg BAY 41-8543 or vehicle was i.p. injected, to guarantee high plasma levels. Lipid uptake into tissues was measured with radioactive-labeled triolein (PerkinElmer) which was administered by oral gavage. Mice were killed 2 h post injection and organs were harvested. Radioactivity was counted in solubilized organs by scintillation counting. To calculate total lipid uptake estimated organ weights were used.

2.3 Immunohistochemistry

2.3.1 Preparation of paraffin sections

Paraffin embedding is a common method to cut thin sections of a variety of tissues. Paraformaldehyde (PFA) was used for fixation as it cross-links proteins while retaining their antigenicity. In order to prepare paraffin sections from BAT and WATi, mice were sacrificed and dissected. Interscapular BAT and WATi was removed, transferred to PFA fixative (4 % PFA in PBS) and incubated at 4°C for 2 days. Afterwards, tissue samples were dehydrated by successive incubations in ethanol of ascending concentrations (50 %, 70 %, 96 %, 100 %) at RT for 30 min each. Subsequently, samples were incubated in xylol 3 times for 10 min at RT and placed in paraffin 3 times for 1 h at 60°C. Tissue samples were embedded with fluid paraffin (60°C) and paraffin blocks were stored afterwards at RT. 5 µm thick sections of the embedded tissues were cut using a microtome (Microm). Slides were dried at RT and stored at RT.

2.3.2 Hematoxylin/Eosin (H/E) staining

H/E staining is a widely used technique to visualize numerous tissue structures. Cell nuclei are stained in blue by hematoxylin whereas the cytoplasm and connective tissue appear in a variety of pink nuances, caused by the eosin staining. H/E stains were performed at RT. Paraffin sections were incubated for 2 min in xylol (deparaffinization), then in ethanol of descending concentrations (100 %, 96 %, 70 %, 50 %) and finally in water (rehydration) 2 min each. Afterwards, slides were treated with hematoxylin (Mayers hemalaun, Merck) for 1 min, washed in water for 15 min. Then slides were stained with eosin (Eosin G, Merck) for 1 min and again washed in water. Sections were dehydrated in ethanol of ascending concentrations (70 %, 90 %, 96 %, 100 %) and xylol for 2 min each and mounted with Roti®-Histokitt (Carl Roth GmbH). Images were taken using a LEICA DMI4000 B microscope (Leica Microsystems GmbH) equipped with a LEICA DFC425 C camera (Leica Microsystems GmbH). Adipocyte diameter was measured using ImageJ.

2.3.3 UCP1 staining of paraffin sections

Four-micrometer paraffin-embedded sections from interscapular BAT region from newborn sGC$\beta_1^{-/-}$ mice and their WT littermates as well as BAT and WATi from adult mice were blocked with 2 % normal chicken serum–TBS (tris-buffered saline) for 30 min at RT and washed three times with 1 % BSA–TBS. Primary antibody against UCP (Sigma-Aldrich) 1, diluted 1:50, was applied overnight at 4°C temperature. After washing three times with PBS-T, secondary antibody against rabbit (SignalStain Boost IHC, Cell Signaling) was applied for 1 h at RT and developed with DAB Kit (Vector Laboratories) according to the manufacturer's instructions. After DAB development, sections were incubated with Hematoxylin for 10 sec and covered with Roti Histo-Kitt (Roth). Sections were dehydrated in ethanol of ascending concentrations (70 %, 90 %, 96 %, 100 %) and xylol for 2 min each and mounted with Roti®-Histokitt (Carl Roth GmbH). Images were taken using a LEICA DMI4000 B microscope (Leica Microsystems GmbH) equipped with a LEICA DFC425 C camera (Leica Microsystems GmbH).

2.4 Cell culture

2.4.1 Isolation of mesenchymal stem cells

The mesenchymal stem cells (BAT-MSC) were isolated from interscapular BAT pads of newborn sGCß$_1^{-/-}$ mice and their WT littermates as previously described (Haas et al., 2009). After isolation of the fat pads they were transferred to the isolation buffer. This suspension was shaken every 5 min for in total 30 min in a water bath with 37°C. The tissue carryover was removed by filtration through a 100 µM nylon mesh (Millipore). After filtration the BAT-MSC suspension was placed on ice for 30 min. After this time, 3 phases of the BAT-MSC suspension are obtained and the middle phase was again filtered through a 30 µM nylon mesh. After filtration the suspension was centrifuged for 10 min at 700 g. The pelleted cells were resuspended in culture media. The cells of one newborn were plated in one 6-well and incubated at 37°C and 5 % CO_2.

Isolation buffer

NaCl	123 mM
KCl	5 mM
$CaCl_2$	1.3 mM
Glucose	5 mM
HEPES	100 mM

All substances were solved in water, the pH was adjusted to 7.4. The buffer was and then sterile filtered and stored at 4°C.

Shortly before use, following substances were added

BSA	1.5 %
Collagenase	0.2 %

and again sterile filtered.

Culture media

DMEM Glutamax I +4500mg/dl Glucose

FBS	10 %
P/S	1 %
Insulin	4 nM
Triiodothyronine-Na	4 nM
HEPES	10 nM
Sodium ascorbate	25 μg/ml

2.4.2 Immortalization of primary BAT-MSCs

Primary BAT-MSCs were immortalized 24 h after isolation with a lentivirus which contains the large T-antigen expressing the Simian Virus 40 (SV40) under control of the phosphoglycerate kinase (PGK) promoter. After infection the cells were cultivated with growth media at 37°C and 5 % CO_2. When the cells reached confluence they were splitted 1:5. All experiments were done with cells of the passage 4.

Growth media

DMEM Glutamax I +4500 mg/dl Glucose

FBS	10 %
P/S	1 %

2.4.3 Cryo conservation and thawing of cells

The cells were cultured in growth media at 37°C and 5 % CO_2 as described above. The confluent cells were washed with PBS and to detach the cells they were incubated for 5 min with Trypsin-EDTA at 37°C and 5 % CO_2. The detached cells were resuspended in growth media and centrifuged for 5 min at 1000 rpm.

Afterwards the cell pellet was resuspended in freezing medium. The cells were transferred to a cryo vial and placed on ice for 15 min. Afterwards, the cryo vials were stored at -80°C for 24 h before transferring them to -150°C for long-term storage.

freezing medium

DMEM Glutamax I +4500 mg/dl Glucose	
FBS	10 %
P/S	1 %
Dimethyl sulfoxide(DMSO)	10 %

The cryo-preserved cells were quickly placed in the water bath at 37°C. Afterwards the 10-fold volume of pre-warmed growth media was added to the cells and centrifuged 5 min at 37°C. The cell pellet was resuspended in growth media and the cell number was determined using a Neubauer chamber. After adjustment of the cell number, cells were plated in 6–well plates.

2.4.4 Adipogenic differentiation of brown adipocytes

The SVF of brown adipocytes was seeded at a density of $1.8x10^5$ in each well of a 6-well plate (d-4). After 48 h the medium was changed to differentiation media (d-2). On day 0 cells were confluent and the media was changed to induction media for additional 48 h. Starting from d2 onwards, the media was changed every second day with differentiation media until BAT-MSCs were differentiated to mature BAs (d7).

Differentiation media

DMEM Glutamax I +4500 mg/dl Glucose	
FBS	10 %
P/S	1 %
Insulin	4 nM
Triiodothyronine-Na	4 nM

Induction media

DMEM Glutamax I +4500 mg/dl Glucose	
FBS	10 %
P/S	1 %
Insulin	4 nM
Triiodothyronine-Na	4 nM
Dexamethasone	1 μM
IBMX	0.5 mM

2.4.4.1 Substances

As indicated in respective experiments, cells were treated with following substances, which were added freshly after every medium change.

PKG activator

As a PKG activator 8-pCPT-cGMP was used. The stock solution was 10 mM solved in water and diluted in the media to an end concentration of 200 μM in the well.

NO donor

The NO donor 2,2'-(Hydroxynitrosohydrazono)bis-ethanimine (DETA/NO) was used in the experiments. The substance has a half life of 20 h when incubated at pH 7.4 and 37°C. Shortly before the media change DETA/NO was dissolved in a 10 mM NaOH solution and the stock was 10 mM as diluted to the requested concentration in the media.

sGC stimulator

BAY 41-8543 (gift from BAYER HealthCare GmbH) was used as sGC stimulator to activate the enzyme. The concentration which was used for cell culture experiments was 3 μM. The stock solution was 3 mM solved in DMSO and then diluted in the media.

2.4.5 cGMP Elisa

The cGMP levels in brown adipocytes were measured by EIA (Cayman Chemical) following the manufacturer's instructions. Therefore, sGC$\beta_1^{-/-}$ cells and WT cells were differentiated to mature adipocytes in 6-well plates. Mature adipocytes were acutely treated either with 3 μM BAY 41-8543 or 50 μM DETA/NO or a combination of both substances for 15 min at 37°C and 5 % CO_2. After washing with PBS, cells were lyzed with 200 μl 0.1 M HCl/well for 15 min at RT. Afterwards cells were scraped with a cell scraper from the plate and centrifuged at 600 g for 5 min. Supernatants were used to perform the enzyme immunoassays. Results were normalized to protein content of the cells using the Bradford protein assay.

2.4.6 Oil RedO staining of mature BA

Oil RedO staining was used to visualize the lipid droplets of the cells. During differentiation of adipocytes the lipids accumulate to lipid droplets and these lipid droplets can be stained with Oil RedO. Therefore, the differentiated adipocytes where washed three times with PBS and then cells were fixed with 4 % Paraformaldehyde (PFA) for 15 min at RT. Later, the PFA was washed out with PBS and cells were incubated with Oil RedO solution (3 mg/ml in isopropyl alcohol) for 4 h at RT and finally washed three times with water.

Oil RedO stock solution

Isopropyl alcohol (99%)	100 ml
Oil RedO	0.5 g

dissolved overnight on a magnetic stir bar and stored at RT.

Oil RedO working solution

Water	4 ml
Oil RedO stock solution	6 ml

Filtered two times through a paper filter the day of use.

2.4.7 Quantification of triglyceride accumulation in adipocytes

Detailed explanation of this experiment is shown in 2.2.8.

Free glycerol reagent and triglyceride reagent were used following the manufacturer's instructions. The BAT-MSC were differentiated to mature brown adipocytes (d7) and then washed with PBS. 400 µl TGTx lysis buffer was added to the cells on day 7. Subsequently, the cells were frozen at -80°C und stored there until the assay was performed.

After the cells were thawed on ice, the adipocytes were scraped from the plate and resuspended. Subsequently, the suspension was centrifuged for 10 min at 14 000 rpm and 4°C. After centrifugation 2 µl of the supernatant was used to measure the protein content with the aid of the Bradford assay (2.5.2).

The pellet was resuspended and 20 µl of the suspension was added to 100 µl TG assay reagent. Following, the sample was measured at 540 nm (TecanReader, Sunrise). The increase in absorption is direct proportional to the glycerol content. The measured glycerol content was normalized to the protein content.

2.4.8 Lipolysis

Lipolysis is a process where TGs are enzymatically hydrolyzed to free fatty acids and glycerol. The release of stored TGs in adipocytes is controlled through lipolytic hormones like for example catecholamines. To detect the lipolytic activity in BA, cells were differentiated in 6-well plates until d7 and then washed three times with lipolysis media (37°C). After the washing step the cells were incubated with 800 µl lipolysis media for 2 h at 37°C and 5 % CO_2. As a positive control cells were stimulated with 10 µM norepinephrine (NE). After the incubation time 40 µl of the supernatant was used for the assay. The supernatant was mixed with 60 µl of the free glycerol reagent and incubated for 5 min at 37°C. As control only the lipolysis media was used and a standard glycerol reagent was used to calculate the glycerol concentration in the cells. All samples were pipetted in a 96-well plate and measured in a TecanReader (Sunrise) at 540 nm. The glycerol release was normalized to the protein content of the cells, which was determined using Bradford assay (see 2.5.2).

Lipolysis media

DMEM (4.5 g/l D-glucose, -pyruvate, without phenol red)
BSA free fatty acid free 2 %

2.5 Biochemical methods

2.5.1 Preparation of total protein lysates from adherent cells and tissue

Mature BA were washed with ice cold PBS and following 200 µl lysis buffer (radio immunoprecipitation (RIPA)) was added to each wells. With the aid of the lysis buffer and a cell scraper the cells were detached from the plate. The lysate was centrifuged at 4°C and 14.000 rpm for 20 min. The supernatant was transferred to a fresh tube. The protein content was detected by Bradford assay. The protein content was adjusted and afterwards the calculated volume of 3x laemmli was added (Laemmli, 1970). The adjusted proteins were cooked for 5 min at 95 °C (Thermoblock) and either used directly or frozen at -20°C until they were used for the sodium dodecyl sulfate polyacrylamide gel electrophoresis (SDS-PAGE).

Tissue protein lysates were generated by using a small piece of BAT and sonicated in 250 µl lysis buffer (radio immunoprecipitation (RIPA)) until the suspension was homogeneous. Afterwards, the lysate was centrifuged at 4°C and 14.000 rpm for 20 min. And

Lysis buffer (RIPA)

TrisHCl	10 mM	
NaCl	150 mM	
NP-40	1 %	pH 7.4
sodium dodecyl sulfate (SDS)	0.1 %	
sodium deoxycholate	1 %	

The buffer was sterile filtered and stored at 4 °C.

Before use, following substances were added

Complete® EDTA free	40 µl/ml
NaF	10 mM
Na_3VO_4	1 mM

3 x laemmli buffer

TrisHCl	125 mM
Glycerol	20 %
SDS	17 %

Bromophenol blue	0.015 %

Dissolved in water and stored at -20°C.

Before use, 5 % β-mercaptoethanol was added.

2.5.2 Determination of protein content using Bradford

The protein content in BA and of the BAT tissue was calculated using the Bradford method (Bradford, 1976). The protein concentration of the investigated lysates was determined in a photometer using a defined BSA standard curve. Therefore, 2 µl cell/tissue lysate and 98 µl 0.15 M NaCl solution was mixed, 1 ml coomassie solution was added and incubated for 2 min. After the incubation time the absorption was measured at 595 nm in a TecanReader (Sunrise).

Coomassie solution

Coomassie brilliant blue G250	0.01 %
EtOH	5 %
Phosphoric acid	8.5 %

All substances were dissolved in water and stored at 4°C protected from light.

2.5.3 Gel electrophoresis of proteins (SDS-PAGE)

Using SDS-PAGE, denatured proteins were separated according to their molecular weight. Therefore, first the resolving and afterwards the stacking gel were poured between two glass plates (BioRad). The two glass plates were fixed in a casting stand and the resolving gel was poured. After 20 min the gel was polymerized. Afterwards the stacking gel was poured on top of the resolving gel and a comb was inserted and after polymerization removed. The gel was inserted in an electrophoresis chamber with running buffer and then the samples were loaded into the pockets of the stacking gel. In each pocket either 15 µg or 50 µg were loaded, depending on the protein analyzed. The proteins were separated at 100 V and 300 mA for 2.5 h.

Table 1: Different concentrations of SDS-PAGE gel compounds

Resolving gel		
	10 %	**15 %**
Water	4 ml	2.3 ml
Rotiphorese®Gel 30	3.3 ml	5 ml
1.5 M TrisHCl pH 8.8	2.5 ml	2.5 ml
APS 20%	0.05 ml	0.05 ml
TEMED	0.004 ml	0.004 ml

Stacking gel	
	4 %
Water	3.4 ml
Rotiphorese®Gel 30	0.83 ml
1.5 M TrisHCl pH 6.8	0.63 ml
APS 20 %	0.025 ml
TEMED	0.005 ml

10 x SDS-PAGE running buffer

Tris	250 mM
Glycine	2 M
SDS	0.1 %

Dissolve all substances in water and store at RT.

2.5.4 Western blotting

After the SDS-PAGE the separated proteins were transferred to a nitrocellulose membrane. This transfer is a wet electrophoresis according to Towbin (Towbin et al., 1979). To do so, the gel was taken out from the electrophoresis chamber and after separating the stacking gel was removed. The gel, nitrocellulose membrane and whatman paper were laminated without air bubbles in sandwich principle. The sandwich was transferred to a chamber with transfer buffer and the electron transfer according to protein size of the analyzed protein, as shown in the following table.

Table 2: Transferring conditions of proteins with different sizes

Protein size	Volt	Ampere	Time	temperature
15-30 kDa	100 V	300 mA	45 min	With ice package
30-75 kDa	100 V	300 mA	1h 15 min	With ice package

Transfer buffer

10 x SDS.PAGE running buffer 10 %
Methanol 20 %
Dissolve in water and store at 4°C.

2.5.5 Immunodetection

After the protein transfer the membrane was blocked in blocking solution for 1 h, to block unspecific binding sites. Afterwards, the membrane was washed 3 times with TBS-T and then incubated with the primary antibody over night at 4°C.

Table 3: List of primary antibodies for immunblotting

Primary antibody	Company	Dilution
aP2	Santa Cruz, Santa Cruz, USA	1/1000
PPARg	Santa Cruz, Santa Cruz, USA	1/1000
Cytochrome C	BD Bioscience, Franklin Lakes, USA	1/1000
UCP1	Sigma	1/500
sGCα1	Sigma	1/1000
sGCα2	Abcam	1/500
sGCβ2	Cayman	1/1000
β-Actin	Santa Cruz, Santa Cruz, USA	1/1000

Tubulin	Dianova, Hamburg, Germany	1/1000

Table 4: List of secondary antibodies for immunblotting

Secondary antibody	**Company**	**dilution**
Rabbit-HRP	Cell-signaling, Danvers, USA	1/5000
Mouse-HRP	Dianova, Hamburg, Germany	1/10000
Goat-HRP	Chemicon, Schwalbach, Germany	1/5000

The day after, the membrane was washed 3 times 5 min with TBS-T. Afterwards, the membrane was incubated with the secondary antibody for 1 h at RT. After this, the membrane was again washed 3 times 5 min with TBS–T. The immunoreactivity bands were detected with the aid of chemiluminescence. The principle of chemiluminescence is the reaction of the ECL solution with the HRP-conjugated secondary antibody and then the band can be detected. For this, the membranes were incubated with ECL solution for 2 min and then developed in the dark room using ECLHyperfilm™. The film was scanned with the aid of a scanner and then quantified with the software QuantityOne (BioRad). After detection of one desired protein, antibodies were stripped off the membrane with stripping solution for 30 min. After a 5 min wash with PBS, the whole immunodetection procedure could be repeated on the same membrane to detect different proteins.

10x TBS

Tris 100 mM
NaCl 1.4 M

Dissolved in water and the pH was adjusted to 8.0 and afterwards stored at RT.

TBS-T

10 x TBS 10 %
Tween-20 0.1 %

Dissolved in water and stored light protected at RT.

Blocking solution

Milk powder	5 %

Dissolved in TBS-T and then stored at 4°C.

Stripping solution

Glycine	2.5 M
SDS	1 %

Dissolved in water, pH adjusted to 2 and stored at RT.

2.6 Molecular biological methods

2.6.1 Phenol/chloroform extraction of genomic DNA

For the isolation of mitochondrial DNA from BAs and tissue following protocol was used. For cells, 1 ml Proteinase K buffer was added to one 6-well, cells were scraped from the plate and transferred to a fresh tube. These tubes were incubated at 55°C and 550 rpm overnight in a Thermomixer. The day after 500 µl phenol/chloroform (Rothi®-phenol, Carl Roth GmbH) was added and shaken carefully. Afterwards, the DNA solution was centrifuged 10 min at 13000 rpm. The upper part of the solution was transferred to a fresh tube and 500 µl chloroform was added and shaken carefully. The solution was again centrifuged 10 min at 13000 rpm. After centrifugation two phases were visible, the upper one was transferred to a new tube. In this new tube 800 µl isopropanol was added and the tube was inverted to precipitate the DNA. After an additional centrifugation of the solution for 10 min at 13000 rpm and a washing step with 75 % EtOH, the pellet was dried at RT. Finally, the DNA was dissolved in 50 µl or more water and the concentration was measured at NanoDrop.

Protein Kinase K buffer

TrisHCl	100 mM
NaCl	200 mM
EDTA	5 mM
SDS	0.2 %
Proteinkinase K	0.1 mg/ml

The amount of mtDNA (mt-Co1, mt-Nd1, and mt-Cytb) was normalized to the amount of chromosomal DNA (H19).

2.6.2 Isolation of ribonucleic acid (RNA) from differentiated adipocytes and tissues

The isolation of RNA from cells and tissues was performed with the aid of InnuSOLV reagent. Therefore, 1 ml InnuSOLV reagent was added to the cells or minced tissues and 200 µl chloroform was added. The mix was shaken powerful for 15 sec.

Afterwards, the solution was incubated for 5 min at RT and centrifuged for 10 min at 13000 rpm and 4°C. After the centrifugation three phases were visible and the middle one was transferred to a new tube. Afterwards, 500 µl isopropanol was added, shaken and centrifuged for 10 min at 13000 rpm and 4°C. The resulting RNA pellet was washed with 75 % ethanol, dried and dissolved in DEPC-water. To determine the RNA concentration, the samples were measured at the NanoDrop.

For the reverse transcription polymerase chain reaction (RT-PCR) 500 ng RNA were reverse transcribed to complementary DNA (cDNA) with the aid of transcription first strand synthesis kit (Roche). The master mix was used as described in the manufacturer's instructions.

2.6.3 Polymerase chain reaction (PCR)

For the quantitative determination of mRNA levels, quantitative real-time (qRT) PCR using SYBR green was performed on the cDNA samples. SYBR Green is a fluorescent dye, which intercalates in the double strained DNA. This interaction leads to a fluorescent signal, which is proportional to the amount of DNA. The SYBR Green qRT-PCRs were performed with the aid of LightCycler® SYBR Green I master Mix (Roche) or Power SYBR Green PCR Master Mix (AppliedBiosystems) and the following program and primer sequences.

SYBR Green qRT-PCR

cDNA	5 µl
forward primer (5 pmol/µl)	0.5 µl
reverse primer (5 pmol/µl)	0.5 µl
SYBR Green I Master Mix	5 µl

SYBR Green qRT-PCR program for mt DNA

Steps	Time (seconds)	Temperature (°C)
1	900	95
2	10	95
3	20	33
4	30	72
5	5	82
6	60	25

Steps 2 to 5 were repeated 40 time

Table 5: List of mitochondrial pirmer for qRT-PCR

Primer	Forward	reverse
Nd1	AATCGCCATAGCCTTCCTAACAT	GCCGTCTGCAAATGGTTGTAA
Cytb	TTCTGAGGTGCCACAGTTATT	GAAGGAAAGGTATTAGGGCTAAA
Co1	CCCAATCTCTACCAGCATC	GGCTCATAGTATAGCTAGGAG
H19	GTACCCACCTGTCGTCC	GTCCACGAGACCAATGACTG

SYBR Green qRT-PCR program for thermogenic markers

Steps	Time (seconds)	Temperature (°C)
1	600	95
2	10	95
3	15	72
4	90	72
5	1	82

Steps 2 to 5 were repeated 40 times

Table 6: List of murin primer for qRT-PCR

Primer	Forward	reverse
ATPsyn	AGTTGGTGTGGCTGGATCA	GCTGCTTGAGAGATGGGTTC
CD36	TGGCCAAGCTATTGCGACAT	AGGCATTGGCTGGAAGAACA
Cpt1b	GGCACCTCTTCTGCCTTTAC	TTTGGGTCAAACATGCAGAT
Cox8b	GAACCATGAAGCCAACGACT	GCGAAGTTCACAGTGGTTCC
Glut-4	GACGACGGACACTCCATCTG	AGCTCTGCCACAATGAACCA
Dio2	GCGATGGCAAAGATAGGTGA	GAATGGAGCTGGGTGTAGCA
HPRT	ACATTGTGGCCCTCTGTGTGCTCA	CTGGCAACATCAACAGGACTCCTCGT
HPRT(ABI)	GTCCCAGCGTCGTGATTAGC	TCATGACATCTCGAGCAAGTCTTT
Lpl	AGCAGCAAGACCTTCGTGG	TCTCTCTTGTACAGGGCGGC
Nrf1	TGTGGCAACAGGGAAGAAACGGAA	TCCGTAATGCCTGGGTCCATGAAA
PGC-1α	GCACACACCGCAATTCTCCCTTGTA	ACGCTGTCCCATGAGGTATTGACCA
PPARδ	ACTGCAGCCCCCTATAGT	GGATCAGTTGGGTCAGTGGG
Slc27a3	TGGATTTGGTTCGGACTGGC	CTGGCTCATCCACTTGGTCT
ß3AR	ATCTTCTCTCTGTGCTGGCTGCCCT	CATCGGTTCTGGAGCGTTGGAGAGT
UCP1 (ABI)	TAAGCCGGCTGAGATCTTGT	GGCCTCTACGACTCAGTCCA
VEGF	GGAGATCCTTCGAGGAGCACTT	GGCGATTTAGCAGCAGATATAAGAA

Power SYBR Green qRT-PCR

cDNA	4 µl
forward primer (5 pmol/µl)	0.5 µl
reverse primer (5 pmol/µl)	0.5 µl
SYBR Green I Master Mix	5 µl

SYBR Green qRT-PCR program for ABI primer

Steps	Time (seconds)	Temperature (°C)
1	600	95
2	15	95
3	60	60
4	1	25

Steps 2 to 3 were repeated 40 times

The relative quantification of the mRNA level was performed with the aid of the $\Delta\Delta C_t$ method. The PCR products increase exponential until they reached a plateau. C_t value is defined as the time when the fluorescence is exceeding the background. HPRT or GAPDH were used as housekeeper genes.

2.6.4 Genotyping sGC$\beta_1^{-/-}$ and WT mice

For genotyping, a small biopsy of the ear punch was digested in 88 µl water plus 10 µl PCR buffer with $MgCl_2$ and 2 µl proteinase K at 55°C and 600 rpm in a thermomixer (Eppendorf) overnight. Afterwards DNA was isolated as described in 2.6.1. For PCR, 1 µl DNA was used.

Primer

IoxP-β1-U1 5'- AAGATGCTGAAGGGAAGGATCG-3'
IoxP-β1-L1 5'- CAGCCCAAAGAAACAAGAAGAAAG-3'
del -β1-L1 5'- GATGTGGGATTGTTTCTGAGGA-3'

Genotyping PCR program

Steps	Time (seconds)	Temperature (°C)
1	180	94
2	60	95
3	45	60
4	420	72
Steps 2 to 4 were repeated		30 times

Bands detected for WT mice were 680 bp and sGCβ_1 knockout mice 830 bp.

2.6.5 Agarose gel electrophoresis

Agarose gel electrophoresis is used for separating, identifying and purifying DNA fragments. For gel preparation, 0.8 % agarose was added to 1x Tris-acetic acid-EDTA (TAE) buffer and boiled in a microwave (Severin). Afterwards 800 ng/ml ethidium bromide was added and the solution was poured into casting platforms (EmbiTech). After polymerization at RT, the gel was placed in an electrophoresis chamber (Peqlab) containing 1x TAE buffer. For electrophoretic separation, 6x loading dye was added to the PCR products and loaded on the agarose gel. Electrophoresis was performed at 100 V. DNA bands were visualized using a UV light transilluminator (GelDoc®XR, BioRad) at 366 nm using QuantityOne® Software (BioRad).

1x TAE buffer

Tris	100 mM
acetic acid	0.11 %
Na2-EDTA	1 mM

6x loading dye

Ficoll Typ 400	18 %
EDTA	0.12 mM
Bromphenol blue	0.15 %
Xylencyanol FF	0.15 %
in 1x TAE buffer	

2.7 Statistics

Statistical analysis was performed with GraphPad prism 5 software. Two-tailed Student's t-tests or analysis of variance (ANOVA) with Bonferroni post-hoc tests for multiple comparisons were used as indicated under the figures. *P* values below 0.05 were considered significant. All data are represented as mean ± SEM.

3 Results

3.1 Expression pattern of sGC in pre- and mature adipocytes

To study the expression of sGC in BAs, SVF from WT and sGC$\beta_1^{-/-}$ mice were isolated and the containing MSC and preadipocytes were differentiated into mature BAs using the established protocol described above (2.4.4). The protein expression level of all three sGC subunits was determined by Western blot analysis. sGC$\beta_1^{-/-}$ cells were used to study potential differences in the expression pattern compared to WT cells. Surprisingly, expression of β_1 subunit was absent in WT preadipocytes. Mature brown WT adipocytes express all three sGC subunits, as monitored by detection of sGCα_1, sGCα_2 and sGCβ1. Moreover, expression levels of all subunits were highly increased following maturation. As expected, sGC$\beta_1^{-/-}$ cells do not possess the β_1 subunit (Figure 6). In comparison to WT cells, there is a lower expression of sGCα_1 and sGCα_2 in mature brown sGC$\beta_1^{-/-}$ adipocytes (Figure 6).

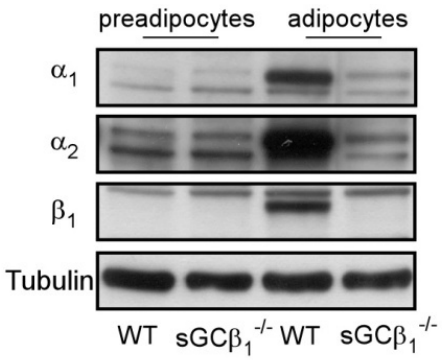

Figure 6: sGC is highly expressed in mature brown adipocytes.
Western blot analysis of the expression levels of the distinct sGC subunits (sGCα_1, sGCα_2 and sGCβ_1) in preadipocytes and adipocytes from WT and sGC$\beta_1^{-/-}$ mice. Tubulin was used as loading control.

3.2 sGCβ$_1$ deficiency leads to alteration in body composition of newborn and adult mice

3.2.1 sGC is crucial for body temperature of newborn mice

The main function of BAT is non-shivering thermogenesis in newborns (Barnard, 1977), however only little is known about this effect in sGCβ$_1^{-/-}$ mice. The impact of sGC deficiency on BAT thermogenesis was investigated in newborn sGCβ$_1^{-/-}$ mice and their WT littermates. Therefore, the surface temperature of the interscapular region (where BAT is located) was measured by using infrared thermography. Furthermore, the BAT weight and UCP1 expression in BAT were determined.

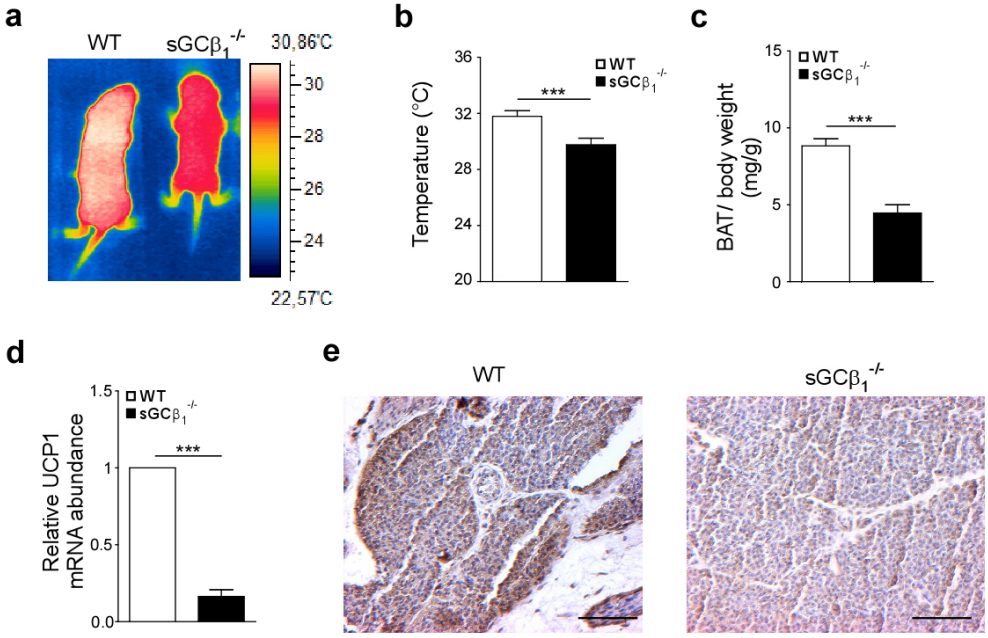

Figure 7: sGC is crucial for thermogenesis in newborn mice.

(a) Representative thermographic image of newborn WT and sGCβ$_1^{-/-}$ mice. (b) Interscapular temperature of WT and sGCβ$_1^{-/-}$ newborn mice measured with infrared thermography. (c) Weight of brown adipose tissue related to the whole body weight. (d) UCP1 mRNA expression in brown adipose tissue of newborn mice. (e) Representative images of brown adipose tissue sections stained with UCP1 (brown color), scale bar 100 µM. (b, c, d): n=8-9 mice per genotype. All data are represented as mean ± SEM and statistical testing was performed using Student`s t-test, ***p<0.005.

The surface temperature of the sGC$\beta_1^{-/-}$ mice was significantly reduced by 2.0 °C compared to WT mice (Figure 7a,b). Furthermore, BAT weight was significantly reduced by 50.1 % in comparison to WT littermates (Figure 7c). Interestingly, UCP1 mRNA expression was diminished by 83.5 % in sGC$\beta_1^{-/-}$ mice compared to WT mice (Figure 7d). Histological examination of BAT revealed a reduction of UCP1 in sGC$\beta_1^{-/-}$ mice compared to the WT littermates (Figure 7e). Together, these results indicate that sGC is crucial for BAT function in newborn mice.

3.2.2 Loss of sGC leads to a reduction of adipose tissue in adult mice

The influence of sGC on the amount of white and brown adipose tissue was analyzed in 8-week old sGC$\beta_1^{-/-}$ mice and their WT littermates. Body weight of sGC$\beta_1^{-/-}$ mice was significantly reduced by 21.1 % in comparison to WT littermates (Figure 8a).

Deletion of sGC$\beta_1^{-/-}$ significantly reduced BAT weight by 6.0 ± 0.7 mg/g bodyweight compared to WT littermates (Figure 8b). As cGMP is also crucially involved in the differentiation of WAs (Mitschke et al., 2013), WATi of sGC$\beta_1^{-/-}$ mice and WT littermates was analyzed graphimetrically and histologically. In sGC$\beta_1^{-/-}$ mice weight of WATi was significantly reduced in comparison to WT littermates (Figure 8c). Histology did not reveal any obvious differences in WATi morphology between WT and sGC$\beta_1^{-/-}$ mice (Figure 8d). In adult mice, sGC deficiency resulted in weight decrease of BAT and WATi whereas the morphology of the latter remained unchanged. Importantly, sGC$\beta_1^{-/-}$ mice exhibit severe phenotypes including impaired smooth muscle function, intestinal abnormalities and increased blood pressure (Friebe et al., 2007). Therefore, only few adult mice were available for analysis and the metabolic phenotype of adult mice might be affected by the wide spread alterations observed in the knockout mice.

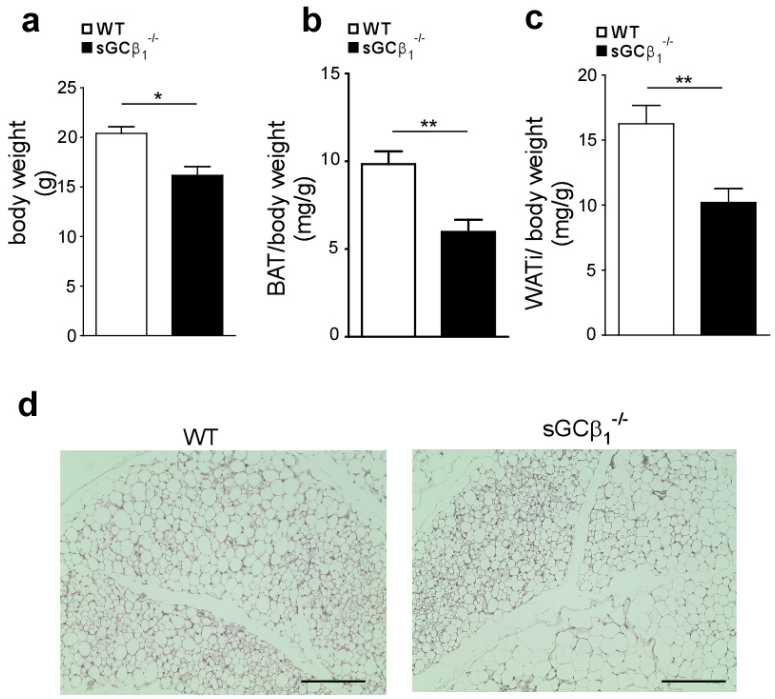

Figure 8: Loss of sGC leads to a reduction of adipose tissue weight in adult mice.
Analyses of 8-week old WT and sGC$\beta_1^{-/-}$ mice on (a) Body weight. (b) Weight of BAT WT and sGC$\beta 1^{-/-}$ mice related to the whole body weight. (c) Weight of WATi related to the whole body weight. (d) Representative image of WATi stained with hematoxylin and eosin. n=6 mice per genotype, scale bar 100 µM. All data are represented as mean ± SEM and statistical testing was performed using Student t-test *p<0.05; **p<0.01.

3.3 sGC deficiency impairs BA function

3.3.1 Deletion of sGC influences cGMP production and lipid accumulation

Furthermore, the role of sGC on differentiation and function of BAs was investigated in more detail. Therefore, SVF from sGC$\beta_1^{-/-}$ mice and their WT littermates were isolated and differentiated into mature BAs. The addition of 200 µM cGMP has been shown to increase differentiation of BAs (Haas et al., 2009).

In order to investigate the impact of sGCβ_1 on cGMP production, cGMP concentration was measured in mature sGC$\beta_1^{-/-}$ and WT BAs. The NO Donor DETA/NO was used to stimulate sGC. After 15 min incubation with DETA/NO the cGMP level was significantly (10.2 fold) increased in comparison to untreated WT cells (Figure 9a).

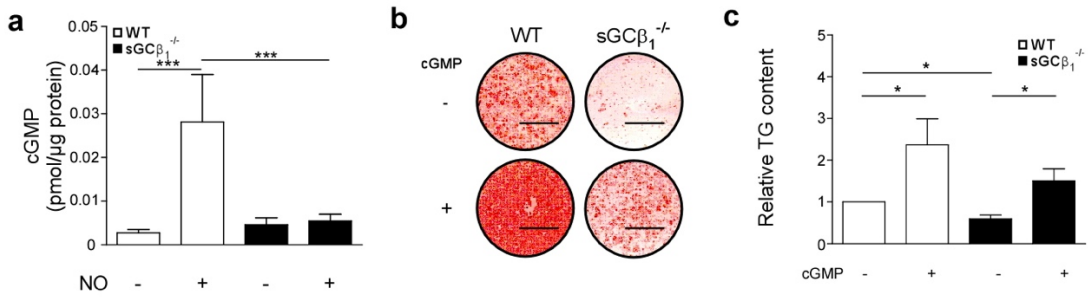

Figure 9: sGC mediated cGMP production and lipid accumulation.

(a) Basal and NO-stimulated cGMP content in WT and sGC$\beta_1^{-/-}$ brown adipocytes, n=5 independent cell cultures. (b) Brown WT and sGC$\beta_1^{-/-}$ adipocytes differentiated in absence or presence of 200 µM 8-pCPT-cGMP and then stained with Oil RedO. (c) Intracellular triglyceride (TG) content in WT and sGC$\beta_1^{-/-}$ cells differentiated in absence or presence of 200 µM 8-pCPT-cGMP; n=5 independent cell cultures. All data are represented as mean ± SEM and statistical testing was performed using Student t-test *p<0,05; ***p<0.005.

To test whether cGMP is produced in the absence of sGCβ_1, cGMP production was measured in sGC$\beta_1^{-/-}$ BAs. In contrast to WT cells treated with DETA/NO, sGC$\beta_1^{-/-}$ cells produced significantly lower amounts of cGMP (a). Additionally, the acute treatment of sGC$\beta_1^{-/-}$ cells with 50 µM DETA/NO did not significantly increase the cGMP content (Figure 9a).

Chronic treatment with 200 µM cGMP throughout differentiation increased the lipid content in WT cells as shown by Oil RedO staining (Figure 9b). In comparison to untreated WT cells, untreated sGC$\beta_1^{-/-}$ cells exhibited a decreased lipid content. sGC$\beta_1^{-/-}$ cells treated chronically with 200 µM cGMP differentiated more efficiently than sGC$\beta_1^{-/-}$ cells without treatment (Figure 9b). For quantification, TG content of BAs was measured. 200 µM cGMP increased the TG content in WT cells by 2.4 ± 0.6 fold in comparison to untreated WT cells (Figure 9c). In contrast, sGC$\beta_1^{-/-}$cells stored 41.0 % less TG than untreated WT cells (Figure 9c). Chronic treatment of sGC$\beta_1^{-/-}$ cells with 200 µM cGMP throughout differentiation increased the TG content 1.5 ± 0.3 fold compared to untreated WT cells (Figure 9c). In comparison to untreated sGC$\beta_1^{-/-}$cells, sGC$\beta_1^{-/-}$cells treated with cGMP stored 2.6 fold more lipids. These data demonstrate, that deletion of sGC$\beta_1^{-/-}$ leads to an impaired TG storage, which could be rescued by addition of cGMP.

3.3.1.1 Deletion of sGC affects the adipogenic and thermogenic program

The influence of sGC deficiency on the adipogenic and thermogenic program of BAs was analyzed in differentiated WT and sGC$\beta_1^{-/-}$ BAs *in vitro*. PPARγ and aP2 were used as adipogenic markers whereas UCP1 and cytochrome c (Cytc) were used as marker for the thermogenic program.

Western blot analysis showed that cGMP increased the PPARγ abundance to 694.0 ± 168.1 % in comparison to untreated WT cells (Figure 10a). In contrast to un treated WT cells, protein level of PPARγ was downregulated by 60.8 % in untreated sGC$\beta_1^{-/-}$ cells (Figure 10a). Treatment of sGC$\beta_1^{-/-}$ cells with cGMP significantly increased PPARγ expression by 453.6 ± 58.0 % compared to untreated WT cells (Figure 10a). In comparison to untreated sGC$\beta_1^{-/-}$ cells, sGC$\beta_1^{-/-}$ cells treated with cGMP significantly increased the expression of PPARγ (11.6 fold) (Figure 10a). However, PPARγ protein levels in sGCβ1$^{-/-}$ cells treated with cGMP were still 196 % lower than PPARγ expression measured in WT cells treated equally (Figure 10a).

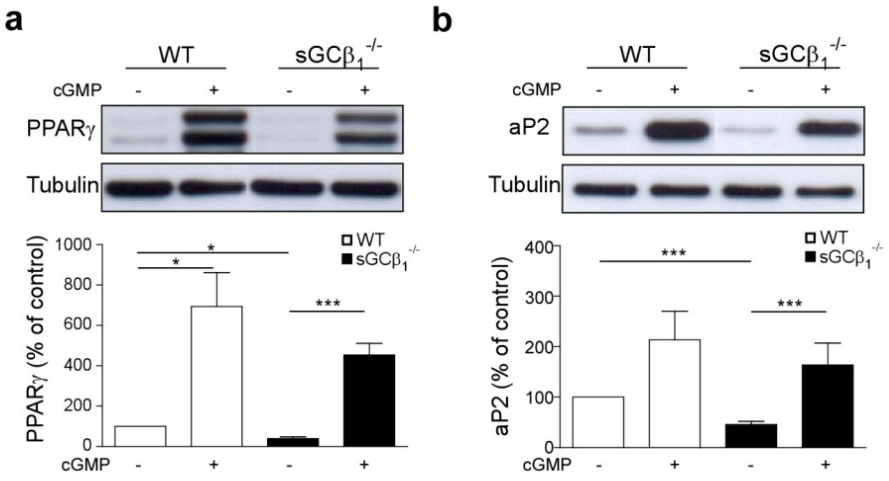

Figure 10: Loss of sGC influences adipogenic program.

Western blot analysis of brown WT and sGC$\beta_1^{-/-}$ adipocytes differentiated in the absence or presence of 200 µM 8-pCPT-cGMP. (a) Upper part representative Western blot of PPARγ, lower part densitometric quantification normalized to Tubulin. (b) Upper part representative Western blot of aP2, lower part densitometric quantification normalized to Tubulin; n>4 independent cell cultures. All data are represented as mean ± SEM and statistical testing was performed using Student t-test *p<0.05; ***p<0.005.

Similar results were observed for the adipogenic marker aP2. Treatment of WT cells with cGMP led to a 213.3 ± 57.3 % increase of the aP2 expression compared to untreated WT cells (Figure 10b). The loss of $sGC\beta_1$ in these cells led to a 54.1 % decrease in aP2 protein compared to untreated WT cells (Figure 10b). $sGC\beta_1^{-/-}$ cells treated with cGMP increased aP2 expression to 163.7 ± 43.45 % in comparison to untreated WT cells (Figure 10b). In $sGC\beta_1^{-/-}$ cells treated with cGMP aP2 expression was 3.6 fold increased in comparison to untreated $sGC\beta_1^{-/-}$ cells (Figure 10b). However, also aP2 expression levels in $sGC\beta_1^{-/-}$ cells remained reduced compared to WT cells when equally treated with cGMP.

The protein level of UCP1 in WT cells treated with cGMP was significantly increased to 216.8 ± 31.3 % compared to untreated WT cells (Figure 11a). In contrast, $sGC\beta_1^{-/-}$ cells expressed 45.4 % less UCP1 than untreated WT cells (Figure 11a). Chronic treatment of $sGC\beta_1^{-/-}$ cells with cGMP increased the UCP1 protein level to 182.8 ± 25.8% compared to untreated WT cells (Figure 11a). In comparison to untreated $sGC\beta_1^{-/-}$ cells, UCP1 expression in $sGC\beta_1^{-/-}$ cells treated with cGMP was 3.4 fold increased (Figure 11a).

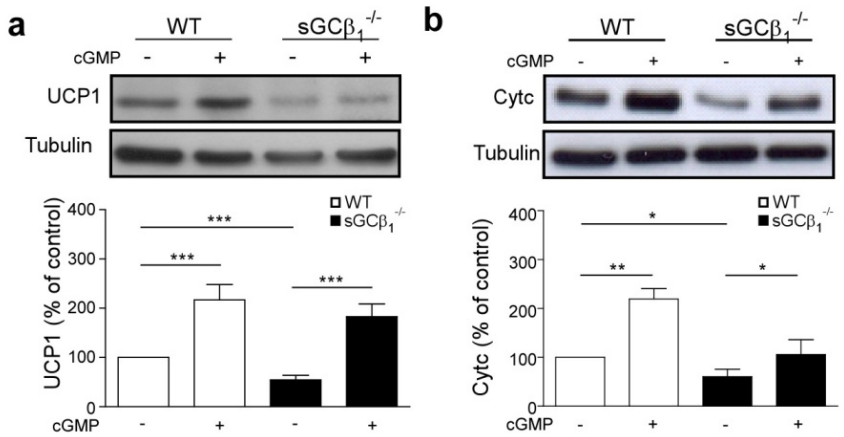

Figure 11: Loss of sGC influences thermogenic program.

Western blot analysis of brown WT and $sGC\beta_1^{-/-}$ adipocytes differentiated in absence or presence of 200 µM 8-pCPT cGMP. (a) Upper part representative Western blot of UCP1, lower part densitometric quantification normalized to Tubulin. (b) Upper part representative Western blot of Cytc lower part densitometric quantification normalized to Tubulin; n>4 independent cell cultures. All data are represented as mean ± SEM and statistical testing was performed using Student t-test *p<0.05; **p<0.01; ***p<0.005.

A similar expression pattern was detectable for Cytc. In comparison to untreated WT cells, the protein level was 219.5 ± 21.2 % increased after chronic cGMP treatment (Figure 11b). In contrast to untreated WT cells, the Cytc protein expression was significantly downregulated by 39.4 % in untreated sGCβ1$^{-/-}$ cells (Figure 11b). sGC$\beta_1^{-/-}$ cells treated with cGMP increased the expression of Cytc 1.7 fold compared to untreated sGC$\beta_1^{-/-}$ cells, which represents the basal expression level of Cytc in WT cells, thus cGMP treatment rescued protein levels of Cytc in sGC$\beta_1^{-/-}$ cells (Figure 11b).

3.3.2 sGC deletion impairs mitochondrial biogenesis and lipolysis

The finding that sGC$\beta_1^{-/-}$ cells and mice exhibited a diminished expression of UCP1, a protein located in the mitochondrial membrane, led to the analysis of mitochondrial biogenesis and BA function. Therefore, sGC$\beta_1^{-/-}$ and WT cells were differentiated in the presence or absence of cGMP and subsequently, expression of PGC-1α, a marker for mitochondrial biogenesis and the amount of mtDNA was determined.

The mRNA expression of PGC-1α was significantly increased in WT cells treated with cGMP (1.8 ± 0.4 fold) compared to untreated WT cells (Figure 12a). In contrast, untreated sGC$\beta_1^{-/-}$ cells expressed 65 % less PGC-1α in comparison to untreated WT cells (Figure 12a). sGC$\beta_1^{-/-}$ cells treated with cGMP showed similar PGC-1α expression as untreated WT cells (1.0 ± 0.4 fold). In comparison to untreated sGC$\beta_1^{-/-}$ cells, sGC$\beta_1^{-/-}$ cells treated with cGMP significantly increased (2.8 fold) the expression of PGC-1α (Figure 12a). Hence, cGMP rescued the reduction of PGC-1α levels in untreated sGC$\beta_1^{-/-}$ cells to the level detected in untreated WT cells (Figure 12a).

The mtDNA in sGC$\beta_1^{-/-}$ cells and WT was investigated in mature BAs. Therefore, genomic DNA was isolated and analyzed regarding the mitochondrial marker NADH dehydrogenase (Nd1), cytochrome b (Cytb) and cytochrome c oxidase subunit 1 (Co1). The expression of all three markers (Nd1, Cytb and Co1) was reduced by 47 %, 48 % and 28 %, respectively, compared to untreated WT cells (Figure 12b).

To investigate the functional activity of BAs, the glycerol release was measured in mature WT and sGC$\beta_1^{-/-}$ BAs. By adding the initiator of lipolysis, NE, lipolytic activity of BAs was investigated. This treatment reveals further stimulation of lipolysis as under basal conditions. The lipolytic activity was investigated in untreated (basal) and acute NE-stimulated mature BAs from sGC$\beta_1^{-/-}$ and WT cells. WT cells treated with NE acutely increased glycerol release 3.1 ± 0.4 fold compared to untreated WT cells (Figure 12c). In contrast to untreated WT cells, the lipolytic activity in untreated sGC$\beta_1^{-/-}$ cells was reduced by 46 %. Acute NE stimulation of sGC$\beta_1^{-/-}$ cells increased glycerol release 1.5 ± 0.3 fold compared to untreated WT cells (Figure 12c). sGC$\beta_1^{-/-}$ cells treated with NE significantly increased the lipolytic activity 2.9 fold compared to untreated sGC$\beta_1^{-/-}$ cells (Figure 12c). However, the glycerol release was still significantly lower in sGC$\beta_1^{-/-}$ cells treated with NE compared to WT cells treated with NE. These results show that sGCβ_1 is important for the mitochondrial biogenesis and lipolytic activity of BAs.

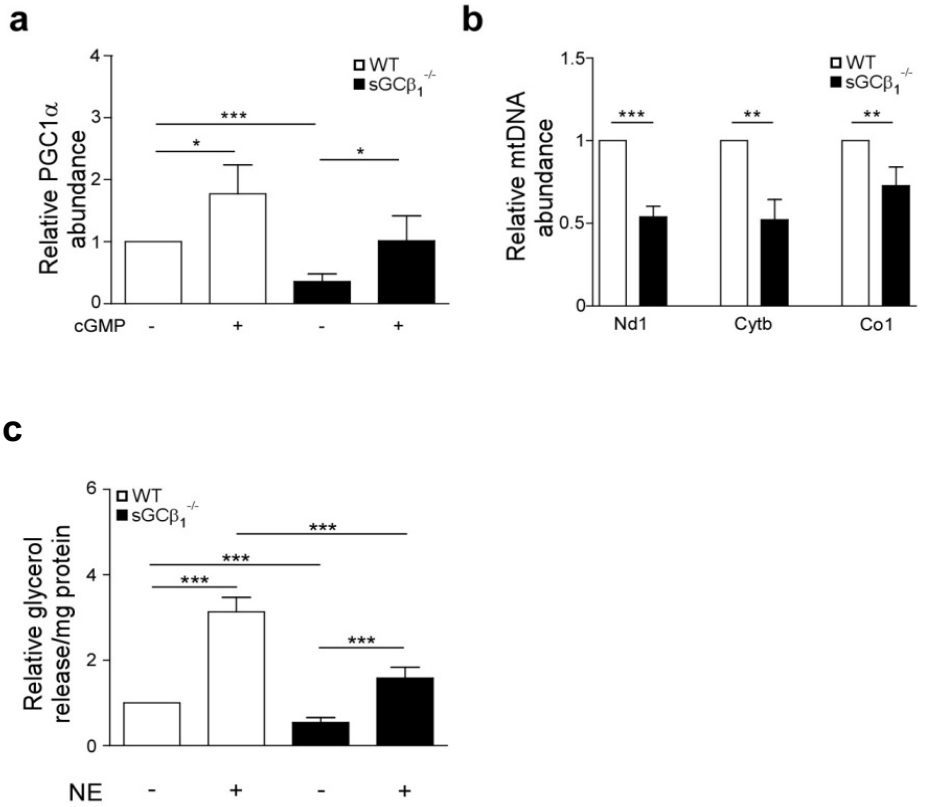

Figure 12: sGC deficiency leads to reduced mitochondrial biogenesis and BAs function.

(a) Gene expression levels of *PGC-1α* in brown WT and sGC$\beta_1^{-/-}$ adipocytes differentiated in absence or presence of 200 µM 8-pCPT-cGMP; n=7-8 independent cell cultures. (b) Abundance of mitochondrial DNA markers *NADH dehydrogenase* (*Nd1*); *cytochrome b* (*Cytb*) and c*ytochrome c oxidase subunit 1* (*Co1*) normalized to the chromosomal DNA encoded gene H19, n=3-5 independent cell cultures. (c) Lipolytic activity of WT and sGC$\beta_1^{-/-}$ adipocytes in the absence or presence of NE. All data are represented as mean ± SEM and statistical testing was performed using Student t-test *p<0.05; **p<0.01; ***p<0.005.

3.4 Pharmacological stimulation of sGC enhances BA function

3.4.1 Stimulation of sGC influences cGMP production and lipid accumulation

To address the question whether sGC might be a potential target to enhance BA differentiation, BAs were treated throughout differentiation with the sGC stimulator BAY 41-8543 in a concentration of 3 µM. As positive controls 200 µM cGMP and 50 µM DETA/NO as NO-Donor were used.

In a first approach cGMP concentration was measured in WT cells as described in 2.4.5. Untreated BAs released 3.2 ± 1.1 fmol cGMP/ µg protein (Figure 13a). After 15 min incubation with the NO-donor DETA/NO the cGMP level was significantly increased by 3.7 fold in comparison to untreated control cells (Figure 13a). Stimulation of sGC with BAY 41-8543 increased cGMP production 5.2 fold compared to untreated control cells (Figure 13a). A co-treatment of BAY 41-8543 and DETA/NO had a synergistic effect and led to a 14.4 fold increase of cGMP production in comparison to untreated control cells (Figure 13a).

In addition to its effect on cGMP production, the effect of BAY 41-8543 on lipid uptake was investigated. Therefore, lipid storage in BAs was visualized by Oil RedO (Figure 13b). Again, chronic cGMP treatment led to an enhanced lipid accumulation in BAs (Figure 13b). The NO-Donor DETA/NO increased the amount of lipid droplets compared to control cells (b). The pharmacological stimulation of sGC also led to an increased lipid accumulation when cells were chronically treated with BAY 41-8543 (Figure 13b).

In order to quantify the Oil RedO staining, TG assay was performed. In comparison to control cells, cGMP treated cells significantly incorporated 3.2 ± 0.9 fold more TG (Figure 13c). The TG content was 2.4 ± 0.8 fold increased in BAs treated with the NO-Donor DETA/NO compared to untreated control cells (Figure 13c). The highest increase in TG content was measured in BAs treated with BAY 41-8543 in comparison to control cells (Figure 13c). These results indicate that BAY 41-8543 increased cGMP concentration and led to a strong increase in TG content in BAs.

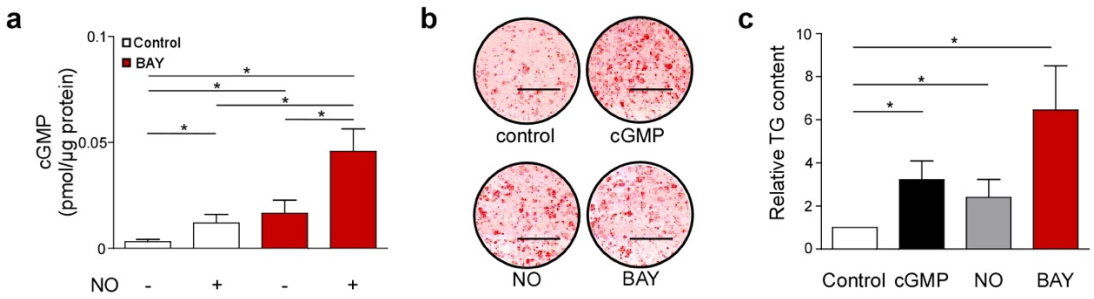

Figure 13: Stimulation of sGC influences cGMP production and lipid accumulation.
(a) Basal DETA/NO and BAY 41-8543 stimulated cGMP content of brown adipocytes n=5 independent cell cultures. (b) Representative Oil RedO staining of brown adipocytes differentiated in the presence of 200 µM 8-pCPT-cGMP, 50 µM DETA/NO and 3 µM BAY 41-8543. (c) Intracellular triglyceride content in brown adipocytes differentiated in the presence of 200 µM 8-pCPT-cGMP, 50 µM DETA/NO and 3 µM BAY 41-8543; n=5 independent cell cultures. All data are represented as mean ± SEM and statistical testing was performed using Student t-test *p<0.05.

3.4.2 sGC stimulator BAY 41-8543 enhances thermogenic and adipogenic program in BAs

Based on the finding that BAY 41-8543 enhanced cGMP level and TG content of BAs, the effect of BAY 41-8543 on the adipogenic and thermogenic programs in BAs was analyzed in more detail. For this reason, the cells were chronically incubated with BAY 41-8543 throughout differentiation. Again, PPARγ, aP2 as well as UCP1 and Cytc were used as markers for the adipogenic and thermogenic program, respectively.

In BAs treated with cGMP, PPARγ protein levels were increased to 185.0 ± 11.2 % in comparison to control cells (Figure 14a). The NO-Donor DETA/NO enhanced the expression to 141.8 ± 16.7 % compared to untreated control cells (Figure 14a). In comparison to untreated control cells, BAs treated with the sGC stimulator BAY 41-8543 significantly increased PPARγ expression by 75.5 ± 25.3 % (Figure 14a).

The other investigated adipogenic marker aP2 showed a similar expression pattern as PPARγ. Incubation with cGMP increased the protein level of aP2 to 342.5 ± 123.7 % compared to control cells (Figure 14b). The NO-Donor DETA/NO increased the protein level to 288.3 ± 78.9 % (Figure 14b). BAY 41-8543 had the strongest significant effect on the expression of aP2, the expression was increased to 425.0 ± 178.9 % compared to untreated control cells (Figure 14b). These results support the previous findings that stimulation of sGC is a strong enhancer of BA differentiation by increasing the adipogenic program.

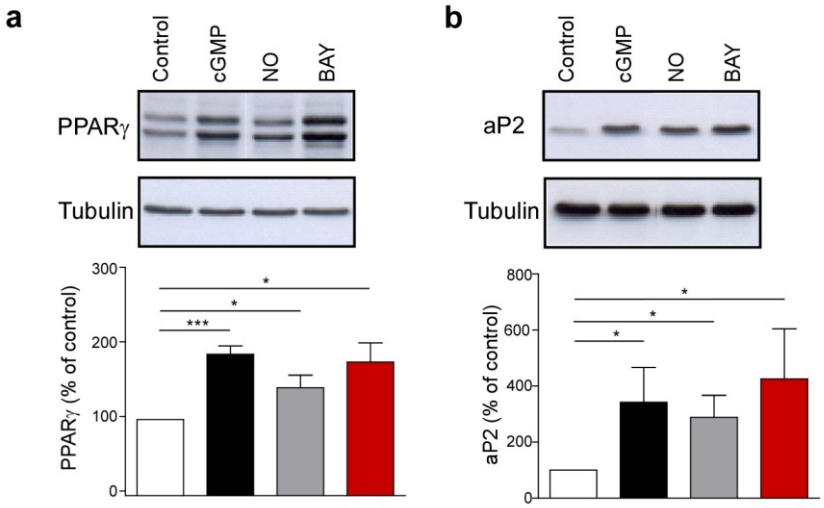

Figure 14: Chronic stimulation of sGC increases adipogenic program.

Western blot analysis of brown adipocytes differentiated in the presence of 200 µM 8-pCPT-cGMP, 50 µM DETA/NO and 3 µM BAY 41-8543. (a) Upper part representative Western blot of PPARγ, lower part densitometric quantification normalized to Tubulin. (b) Upper part representative Western blot of aP2, lower part densitometric quantification normalized to Tubulin; n>4 independent cell cultures. All data are represented as mean ± SEM and statistical testing was performed using Student t-test *p<0.05; ***p<0.005.

UCP1 protein levels revealed that the chronic treatment with cGMP led to a significant increase in UCP1 expression compared to control cells (Figure 15a). The NO-Donor increased the UCP1 protein level by 12.1 ± 34.9 % in comparison to control cells (Figure 15a). The strongest increase in UCP1 protein level, 225.1 ± 28.2 %, was measured when cells were chronically treated with BAY 41-8543 compared to untreated control cells (Figure 15a).

Chronic treatment with cGMP significantly increased the Cytc expression to 116 ± 24.6 % in comparison to control cells (Figure 15b). In comparison to control cells, DETA/NO enhanced the protein expression by 23.4 ± 26.5 % (Figure 15b). In line with the strongest increase in UCP1 expression, BAY 41-8543 treatment also led to the strongest increase in Cytc expression (134.0 ± 25.6 %) compared to control cells (Figure 15b). In summary, pharmacological stimulation of the sGC resulted in a significant increase in differentiation which was based on an upregulation of the adipogenic and thermogenic program.

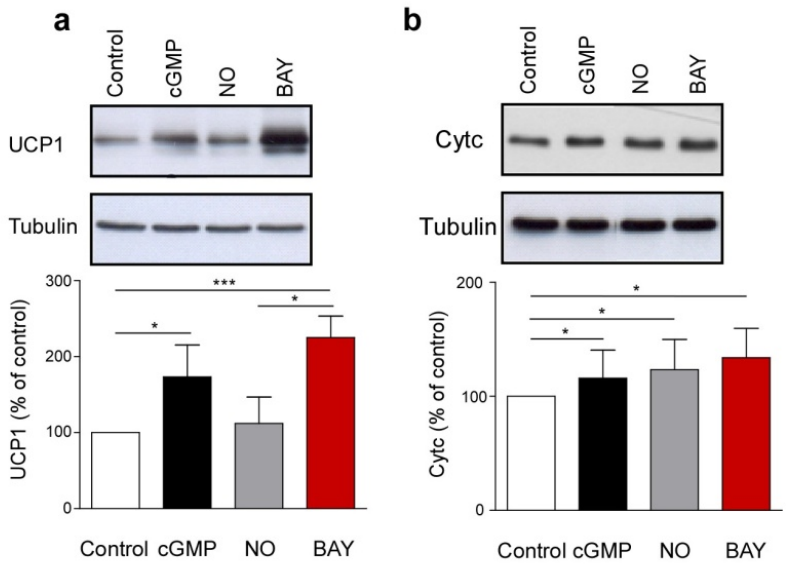

Figure 15: Chronic stimulation of sGC increases thermogenic program.

Western blot analysis of brown adipocytes differentiated in presence of 200 µM 8-pCPT-cGMP, 50 µM DETA/NO and 3 µM BAY 41-8543. (a) upper part representative Western blot of UCP1, lower part densitometric quantification normalized to Tubulin (b) upper part representative Western blot of Cytc, lower part densitometric quantification normalized to Tubulin; n>4 independent cell cultures. All data are represented as mean ± SEM and statistical testing was performed using Student t-test, *p<0.05; ***p<0.005.

For an enhanced BAT function, it is not only important that the adipogenic and thermogenic program are elevated, moreover, functionally active BAs are necessary. An indicator of BA activity is lipolytic activity. The basal lipolytic activity was measured in BAs treated with either cGMP, DETA/NO or BAY 41-8543 throughout differentiation.

Cells acutely treated with NE released 2.1 ± 0.6 fold more glycerol than unstimulated control cells (Figure 16). Chronic treatment with cGMP throughout differentiation increased basal lipolytic activity 1.9 ± 0.4 fold in comparison to untreated control cells (Figure 16). Chronic treatment with cGMP and a 2 h stimulation with NE increased the glycerol release 5.5 ± 1.5 fold compared to untreated control cells (Figure 16). The NO-Donor DETA/NO enhanced basal lipolytic activity 2.1 ± 0.34 fold compared to control cells (Figure 16). The treatment of BAs with DETA/NO and acute treatment with NE caused a significantly additional increase in glycerol release 5.8 ± 1.8 fold compared to untreated cells (Figure 16). The pharmacological stimulation of sGC with BAY 41-8543 increased basal lipolytic activity by 1.6 ± 0.2 fold in comparison to untreated control cells (Figure 16). An acute treatment with NE significantly enhanced the glycerol release in BAY 41-8543 treated BAs 3.9 ± 1.0 fold in comparison to untreated control cells (Figure 16). In summary, chronic treatment with BAY 41-8543 increases basal lipolytic activity, comparable to acute NE-treated cells. Moreover, not only the basal lipolytic activity is increased, additionally BAs chronically treated with BAY 41-8543 and acutely stimulated with NE exhibit enhanced lipolytic activity and this argues for an enhanced BA function.

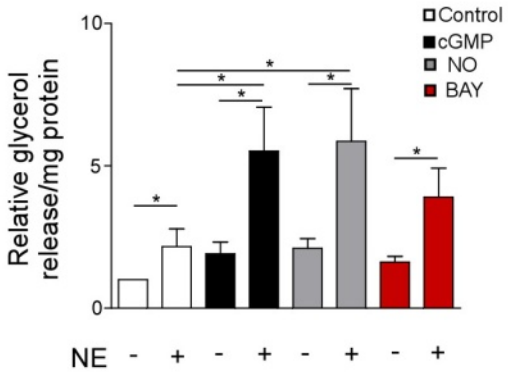

Figure 16: Pharmacological stimulation of sGC leads to an enhanced BAT function.
Measurement of glycerol release under basal and NE-stimulated conditions in brown adipocytes differentiated in presence of 200 µM 8-pCPT-cGMP, 50 µM DETA/NO and 3 µM BAY 41-8543, n>4 independent cell cultures. All data are represented as mean ± SEM and statistical testing was performed using Student t-test *p<0.05.

3.5 sGC stimulation protects against diet-induced obesity

3.5.1 Pharmacological stimulation of sGC protects against weight gain

After identifying promising results *in vitro*, the effect of sGC stimulation on whole body metabolism was analyzed in more detail *in vivo*. Therefore, WT mice were fed a control diet (CD), high fat diet (HFD) or high fat diet supplemented with the sGC stimulator BAY 41-8543 (HFD+BAY41) for 12 weeks and changes in body weight were recorded weekly (Figure 5).

During the recorded time, mice fed the HFD and HFD+BAY41 gained more weight compared to mice fed the CD and at the 12 weeks' time point, mice fed a HFD gained 42.8 % more weight than mice fed the CD (Figure 17a). Addition of BAY41 to the HFD significantly decreased body weight gain resulting in 14.6 % less body weight at the 12 weeks' time point in comparison to mice fed only a HFD (Figure 17a).

It is well known that body weight changes are accompanied with changes in body composition(Kushner et al., 1990). Therefore, body composition was analyzed using NMR. Mice fed a HFD for 12 weeks had 88.0 % more fat mass than mice receiving CD (Figure 17b). In contrast, HFD+BAY41 mice exhibited only 59.0 % more fat mass compared to mice on a CD (Figure 17b). The weight of the water content was not significantly changed between all three groups (Figure 17b). The lean mass of mice fed a CD or a HFD was not changed, whereas the lean mass of HFD+BAY41 mice increased by 7.0 % in comparison to mice on CD (Figure 17b). In summary, pharmacological stimulation of sGC in combination with the HFD reduced gain in fat mass compared to mice on a HFD.

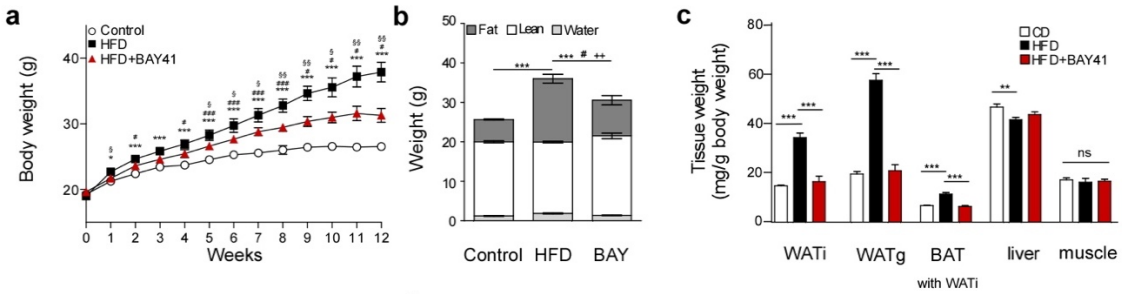

Figure 17: Pharmacological stimulation of sGC protects against weight gain.
(a;b) Effects of a control diet (CD), a high fat diet (HFD) with or without BAY 41-8543 (HFD+BAY41) on body weight (a) and body composition (b). (a) Significant *HFD versus CD; #BAY versus CD; §BAY versus HFD and for (b) *fat; ‘lean; + free water(c). Tissue weights of inguinal WAT (WATi) and gonadal WAT (WATg), interscapular brown adipose tissue with WAT (BAT), liver and muscle after treatment with or without BAY. All data are represented as mean ± SEM and statistical testing was performed for **a** two-way of variance (ANOVA) and **b** and **c** Student t-test was used, **p<0.01; ***p< 0.005.

The detected changes in body composition let to the hypothesis that also tissue weights were altered upon HFD. Therefore, after 12 weeks of feeding a CD, a HFD or a HFD+BAY41, the mice were sacrificed and the tissue weights were analyzed. The weight of WATi of mice fed the HFD was 124 % increased in comparison to mice fed the CD (Figure 17c). In contrast, HFD+BAY41 resulted only in an increase of 20 % in WATi weight compared to CD fed mice (Figure 17c). Mice that had been fed with a HFD+BAY41 exhibited a reduction in the weight of WATg by 55 % and BAT by 38.0 % when compared to mice fed only a HFD (Figure 17c).

The liver weight of mice on a HFD was 7.3 % lighter than the liver weight of mice on a CD for 12 weeks, whereas feeding the HFD+BAY41 did not result in significant changes (Figure 17c). The tissue weights of the muscle remained unaffected (Figure 17c). These results are contradictory to the obtained body composition as mice fed a HFD+ BAY41 had a higher lean mass. Nonetheless, these *in vivo* results reveal that mice treated with the sGC stimulator plus a HFD possess lighter adipose tissues than mice only fed a HFD.

3.5.2 Enhanced metabolic effects after sGC stimulation

Next, metabolic cages were used to record indirect calorimetry, which means VO_2 consumption over 24 h, energy intake and the locomotion activity over the night and day period. As before, mice were fed for 12 weeks with CD, HFD or HFD+ BAY41-8543 and the measurements were taken during the last week of the study in metabolic cages.

Indirect calorimetry showed no significant changes between CD and mice on HFD during the day period (0600-1800) (Figure 18a, b). Interestingly, HFD+BAY41 mice had a significant increase in O_2 consumption compared to mice fed a CD or HFD during the day cycles (Figure 18a, b). The indirect calorimetric measurement by oxygen consumption has one limitation as it does not consider the body weight, which was shown to be significantly altered after feeding the mice the HFD and HFD+BAY41 when compared to mice on CD (Figure 17a). Therefore, mean energy expenditure was correlated with body weight and indeed, this correlation confirmed that HFD+BAY41 mice had the highest O_2 consumption (Figure 18c).

Measurement of the energy intake showed that mice fed HFD consumed 32.7 % less energy than mice on the CD (Figure 18d). Interestingly, HFD+BAY41 mice ingested 25.0 % more energy than mice fed CD (Figure 18d). To rule out that the different diets and energy intake levels had an influence on the motility, the locomotion activity was analyzed. Surprisingly, there was no significant difference between all three groups (Figure 18e). These results demonstrate that mice fed a HFD+BAY41 have a higher energy expenditure, an increased food intake and a comparable locomotor activity compared to mice fed only a HFD, but unexpectedly their body weight remained significantly lower.

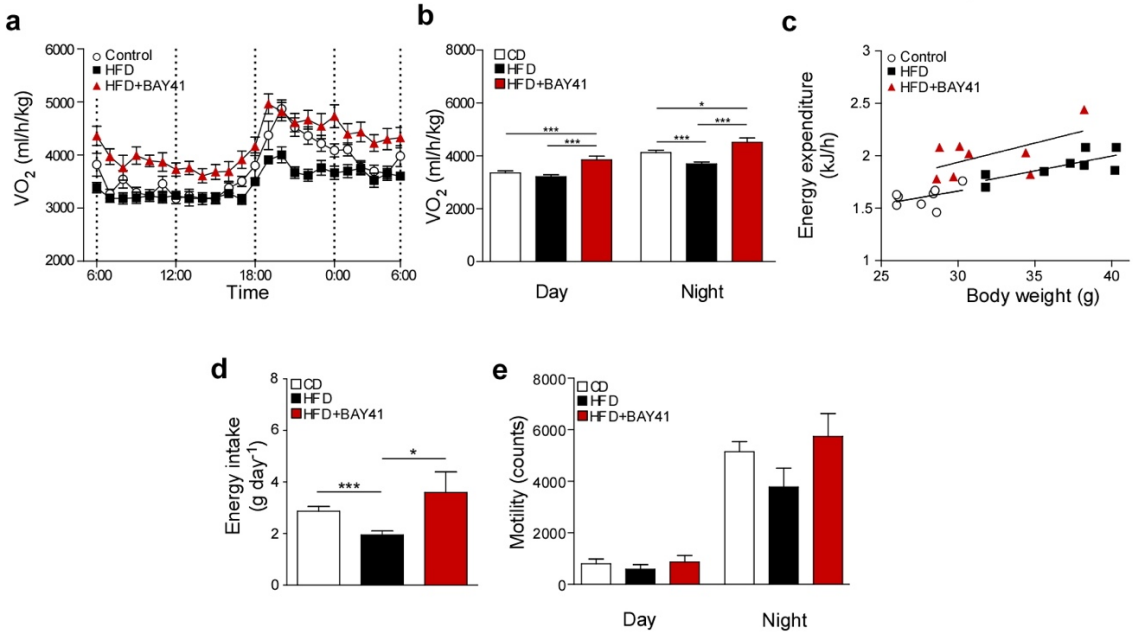

Figure 18: Metabolic measurements after 12 weeks feeding with CD, HFD and HFD+sGC stimulator.

(a;b) Oxygen consumption (VO_2) (a) and mean oxygen consumption during day and night (b) after feeding 12 weeks a control diet (CD), high fat diet (HFD) or high fat diet with sGC stimulator BAY 41-8543 (HFD+BAY41).(c) Mean energy expenditure in relation to the body weight. (d) Energy intake of mice within 24 h. (e) Motility during light and dark cycles within 24h of mice fed a CD, HFD or HFD+BAY 41-8543 All data are represented as mean ± SEM and statistical testing was performed using Student t-test, * $p< 0.05$; ***$p<0.005$.

3.5.3 sGC stimulator BAY 41-8543 enhances glucose clearance.

A long-term high fat diet could result in the development of diabetic phenotypes and therefore, a glucose tolerance test (GTT) was performed in the last week of the study. The mice were weighed and then their basal glucose level was measured. After intraperitoneal injection of a glucose solution, blood glucose level was measured every 30 min. The basal glucose level was significantly increased in mice fed a HFD or HFD+BAY41 compared to CD fed mice (Figure 19a). 30 min after the glucose injection there was no significant difference in glucose level of mice fed a HFD or a HFD+BAY41 (HFD:410.3 ± 19.8 mg/dl; HFD+BAY41:414.0 ± 14.5 mg/dl) (Figure 19a).

A significant change between mice fed a HFD or HFD+BAY41 could be observed after one hour post glucose injection, when mice treated with the sGC stimulator had cleared already 25.0 % more glucose than mice fed

HFD only (Figure 19a). Interestingly, two hours after glucose injection the difference in the glucose level between HFD+BAY41 mice and mice fed a CD was only 14 %, whereas the glucose level in mice fed the HFD was still significantly higher (Figure 19a).

Based on the finding that mice fed the sGC stimulator had a better glucose clearance, the insulin plasma levels of these mice were analyzed. The insulin plasma level of mice fed a HFD was increased by 729.2 % compared to mice on a CD (Figure 19b). Interestingly, HFD+BAY41 mice had a 50.0 % reduction in plasma insulin in comparison to mice fed only HFD (Figure 19b). These results demonstrate that mice treated with the pharmacological compound did not develop a diabetic phenotype.

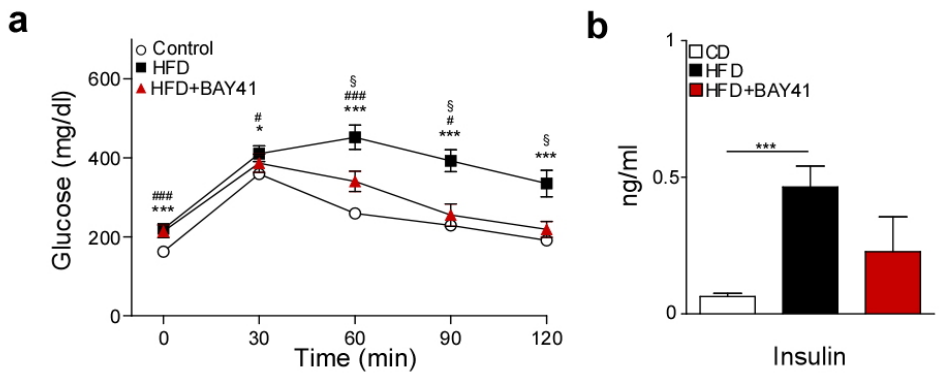

Figure 19: sGC stimulator BAY 41-8543 enhances glucose clearance after 12 weeks on a HFD.

(a) Glucose tolerance test after 12 weeks on a control diet (CD); a high fat diet (HFD) with or without BAY 41-8543 (HFD+BAY41); *HFD versus CD; # BAY versus CD, § BAY versus HFD. (b) Insulin plasma level at the end of the study. All data are represented as mean ± SEM and statistical testing was performed using Student t-test, *** p< 0.005.

3.6 Metabolic changes in brown adipose tissue after sGC stimulation

3.6.1 Acute NE stimulation increases BAT activity in mice treated with sGC stimulator

To investigate whether the BAT activity is increased in mice treated with HFD+BAY41, NE-induced thermogenesis was measured. Therefore, the resting metabolic rate (RMR) was analyzed and then NE (as mimic for cold stimulation) was subcutaneously injected. Afterwards, O_2 consumption was recorded for 2 h.

Interestingly, the basal O_2 consumption was significantly increased in HFD+BAY41 mice compared to mice fed a HFD (Figure 20a). After NE injection HFD+BAY41 mice consumed significantly more O_2 than mice only fed a CD or HFD (Figure 20a). Furthermore, after calculating the area under the curve (AUC) of the mean oxygen consumption after NE injection, HFD+BAY41 mice consumed significantly more O_2 than mice fed a CD or a HFD, whereas there were no significant changes between mice fed a CD or a HFD (Figure 20b). These results indicate that mice fed the sGC stimulator have an enhanced BAT activity and a higher O_2 consumption after acute NE stimulation.

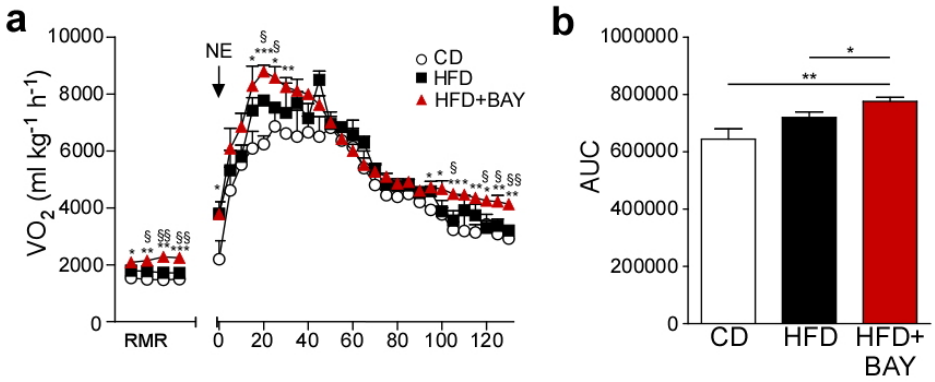

Figure 20: sGC stimulator BAY 41-8543 enhances BAT activity after acute cold stimulation.
(a) Norepinephrine (NE) induced thermogenesis in BAY41-8543 treated mice. Mice were fed a control diet (CD); a high fat diet (HFD) with or without BAY 41-8543 (HFD+BAY41) for 12 weeks. The resting metabolic rate (RMR) was analyzed at thermoneutrality (30°C). NE was used to induce maximal thermogenesis *BAY+HFD versus CD; # HFD versus CD, § BAY versus HFD. (b) Area under the curve (AUC) of mean oxygen consumption after NE injection; n=3 mice per group. All data are represented as mean ± SEM and statistical testing was performed using Student t-test, *p<0.05 ** p< 0.01.

3.6.2 Treatment with the sGC stimulator BAY 41-8543 increases lipid uptake in BAT

The sGC stimulator highly activates BAT after acute NE stimulation. To characterize BAT function in mice fed a CD, HFD or a HFD+BAY41 for 12 weeks in more detail, the following assays were performed: uptake of radioactive-labelled lipids, relative mRNA abundance of proteins involved in lipid uptake and thermogenic program as well as mitochondrial biogenesis. The lipid uptake assay revealed that mice fed a HFD contained 44.0 % less radioactive-labelled lipids than mice on a CD (a). On the contrary, HFD+BAY41 mice incorporated 50.0 % more radioactive-labelled lipids compared to mice on a HFD (Figure 21a).

Next, the expression levels of *CD36* and *LPL*, two proteins involved in lipid uptake, were analyzed. The expression of *CD36* in mice fed a HFD was 1.3 ± 0.4 fold, whereas *LPL* expression increased 3.5 ± 1.3 fold, both related to mice fed a CD (Figure 21b). HFD+BAY41 mice, however, had a more dramatic and thus significant increase in mRNA expression of both proteins, *CD36* increased 1.9 ± 0.5 fold and *LPL* 17.4 ± 6.3 fold, respectively, compared to mice fed a CD (Figure 21b).

The thermogenic marker *Ucp1* was 1.7 ± 0.6 fold and *Adrb3* was 3.5 ± 1.2 fold increased in mice fed a HFD compared to CD fed mice (b). *Ucp1* and *Adrb3* expression were increased 3.1 ± 0.7 fold and 4.8 ± 1.7 fold, respectively, in HFD+BAY41 mice compared to CD fed mice (Figure 21b).

The markers for mitochondrial biogenesis like *Pgc-1a* and *Nrf1* were increased 1.2 ± 0.4 fold and 1.6 ± 0.2 fold, respectively, in mice fed a HFD in comparison to mice fed a CD (Figure 21b). In HFD+BAY41 mice *Pgc-1a* and *Nrf1* expression were significantly increased by 1.9 ± 0.5 fold and 4.3 ± 0.9 fold, respectively, compared to CD fed mice (Figure 21b).

As all these marker proteins are differentially expressed in mice fed a HFD and treated with the sGC stimulator, also expression levels of proteins involved in glucose uptake were analyzed. Gene expression of *SLC2A1* was 4.41 ± 1.28 fold increased whereas *SLC2A4* was only 2.8 ± 1.2 fold increased in mice fed a HFD compared to mice on a CD (Figure 21c). In contrast, HFD+BAY41 mice expressed 11.9 ± 3.1 fold more *SLC2A1* and 4.1 ± 2.0 fold more *SLC2A4* than mice fed a CD (Figure 21c).

Taken together, these results show that the sGC stimulator enhanced the lipid uptake in BAT and increased the expression of functional markers for BAT activity.

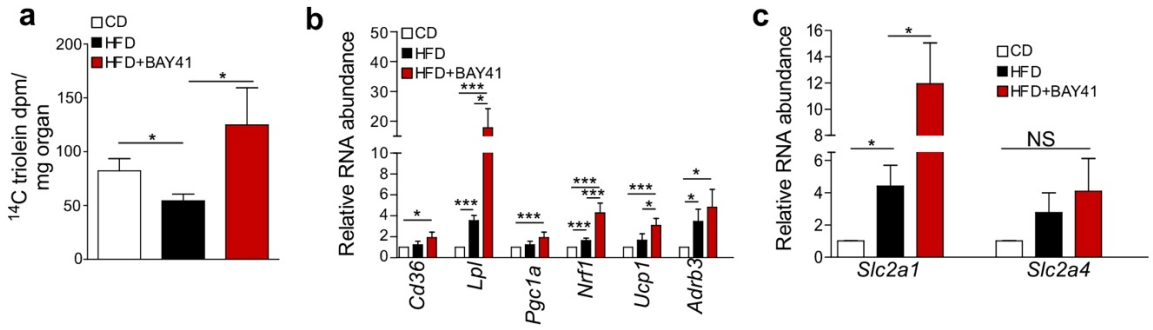

Figure 21: sGC stimulator BAY 41-8543 increases lipid uptake in BAT.
(a) Lipid uptake (^{14}C-Triolein) into BAT in mice fed for 12 weeks a control diet (CD), a high fat diet (HFD) with or without BAY 41-8543 (HFD+BAY41). (b) Expression level of marker for lipid uptake (*CD36* and *LPL)*, thermogenesis (*Ucp1* and *Adrb3*) and mitochondrial biogenesis (*Pgc-1α* and *Nrf1*). (c) Relative mRNA expression of glucose uptake markers (*SLC2A1* and *SLC2A4*). All data are represented as mean ± SEM and statistical testing was performed using Student t-test, *p<0.05, *** p< 0.005.

3.6.3 Mice treated with the sGC stimulator BAY 41-8543 exhibit improved BAT function

The previous results highlight that mice fed the sGC stimulator during HFD gained less weight and incorporated more lipids, the underlying mechanism for the improved BAT activity, however, remained unclear. Hence, histological sections of BAT of mice fed a CD, HFD or HFD with BAY 41-8543 for 12 weeks were analyzed and the expression levels of UCP1 as well as the mitochondrial content and *Vegf* mRNA expression were determined.

The histological section revealed an increased lipid content in mice fed a HFD for 12 weeks. In contrast, HFD+BAY41 mice stored less lipids in BAT (Figure 22a). The UCP1 expression showed no obvious difference between the three groups (Figure 22a). For quantification, the protein levels of UCP1 were analyzed. Mice fed a HFD did not exhibit a significant increase in expression compared to mice fed a CD (Figure 22b). Contrariwise, HFD+BAY41 mice expressed significantly, 78.0 ± 42.8 %, more UCP1 than mice fed a CD (Figure 22b).

Moreover, DNA marker for mitochondrial content were measured by qRT-PCR. The expression levels of *Cytb* and *Co1* in BAT were not significantly increased in mice fed a HFD, the expression of *Cytb* was 1.7 ± 0.6 fold and *Co1* was 1.2 ± 0.3 fold increased, respectively (Figure 22c and d). HFD+BAY41 mice, however, expressed 3.08 ± 0.83 fold more *Cytb* and 4.1 ± 1.5 fold more *Co1* compared to CD mice (Figure 22c and d).

To investigate whether the mtDNA content is also affected in WATi, which would be a hint for browning of WATi, *Cytb* and *Co1* content was measured in WATi. The expression level of *Cytb* and *Co1* in WATi were not significantly altered in mice fed a HFD, the expression of *Cytb* was 2.0 ± 1.5 fold and *Co1* was 1.7 ± 0.3 fold increased (Figure 22c and d). On the contrary, HFD+BAY41 mice exhibited an increased expression of *Cytb* (1.5 ± 0.8 fold) and *Co1* (1.5 ± 0.4 fold) compared to CD fed mice (Figure 22c and d).

The *Vegf* expression in mice fed a HFD was 1.3 ± 0.3 fold increased in comparison to CD mice (Figure 22e). Furthermore, in HFD+BAY41 mice the expression of *Vegf* was significantly (2.3 ± 0.1 fold) increased compared to mice fed a CD (Figure 22e). These results demonstrate that treatment with the sGC stimulator increased mitochondrial content in BAT and WATi as well as vascularization of BAT.

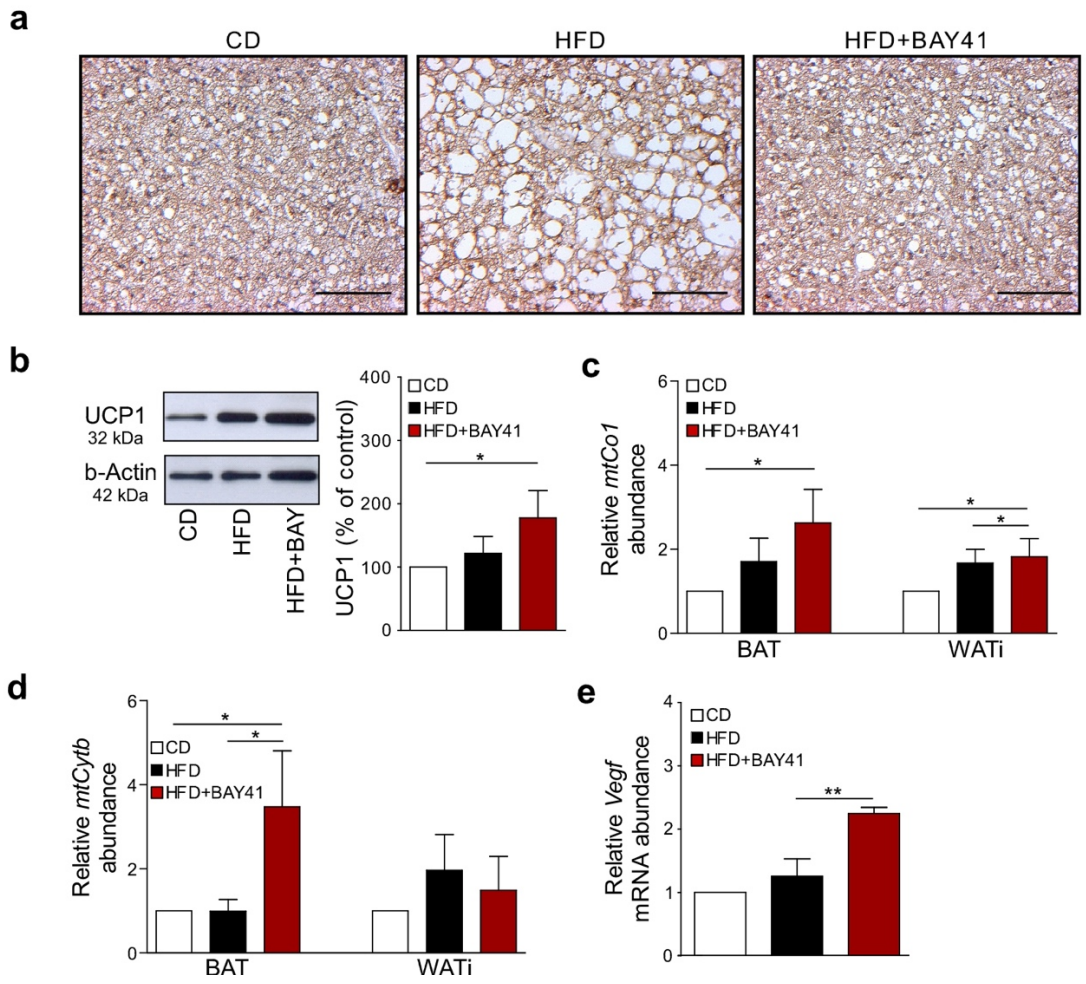

Figure 22: sGC stimulator BAY 41-8543 enhances BAT function.

Analysis of brown adipose tissue from mice fed a control diet (CD), a high fat diet (HFD) with or without BAY 41-8543 (HFD+BAY41) for 12 weeks. (a) Representative histology of BAT stained against UCP1 and hematoxylin, scale bar 100 µm (b) UCP1 protein expression in BAT, representative Western blot (left) and densitometric quantification normalized to β-Actin (right); n=8. (c and d) Mitochondrial DNA content in BAT and WATi. Abundance of mitochondrial DNA markers (c) *cytochrome c oxidase subunit 1* (*Co1*) and (b) *cytochrome b* (*Cytb*) and normalized to the chromosomal DNA encoded gene H19, n=5-7. (e) *Vegf* expression in BAT; n=8. All data are represented as mean ± SEM and statistical testing was performed using Student t-test, *p<0.05 ** p< 0.01.

3.7 Metabolic changes in white adipose tissue after sGC stimulation

3.7.1 Stimulation of sGC leads to an improved lipid uptake in WATi and reduces adipocytes diameter

It is common knowledge that redundant calories are stored in white adipose tissue, thus the existing hypothesis is that mice fed a HFD store more lipids in the adipose tissue (Hausman et al., 1997). To verify this in our settings, lipid uptake and TG content as well as adipocyte sizes were measured in mice fed a CD, HFD or HFD+BAY41 for 12 weeks.

The uptake of radioactive-labelled lipids in WATi of mice fed a HFD was 1.4 fold higher compared to mice fed a CD (Figure 23a). Interestingly, HFD+BAY41 mice incorporated 1.8 fold more radioactive-labelled lipids into WATi than mice fed a CD (Figure 23a).

The analyzed TG content demonstrated that mice on a HFD store 73.6 ± 46.7 % more lipids than mice fed a CD (Figure 23b). The TG content in WATi of HFD+BAY41 mice was not significantly increased in comparison to mice on a CD, leading only to an increase in TG content of 50.0 ± 32.5 % (Figure 23b). In summary, feeding mice a HFD supplemented with the sGC stimulator resulted in an enhanced lipid uptake in WATi but did not alter the lipid storage.

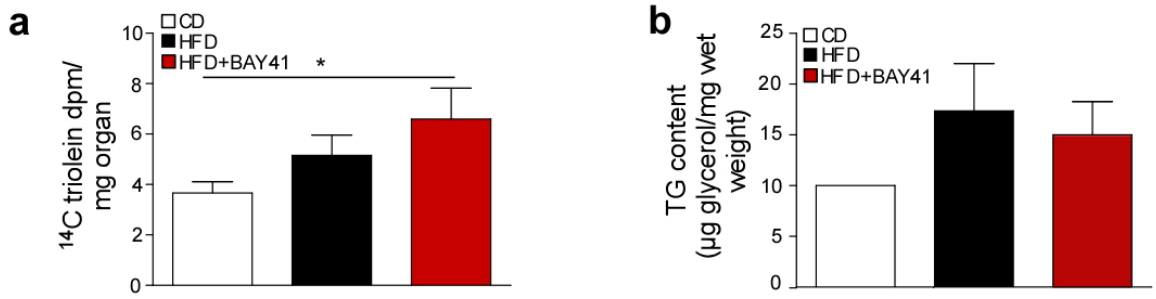

Figure 23: sGC stimulator BAY 41-8543 influences lipid uptake in WATi.
(a) Lipid uptake (^{14}C-Triolein) into WATi in mice fed 12 weeks a control diet (CD), a high fat diet (HFD) with or without BAY 41-8543 (HFD+BAY41). (b) TG content of WATi in mice on a diet for 12 weeks. All data are represented as mean ± SEM and statistical testing was performed using Student t-test, *p<0.05.

These results could support the hypothesis that in HFD fed mice redundant calories were stored in adipose tissue. The histological analyses of WATi of mice fed a HFD indeed revealed bigger lipid droplets than mice fed a CD. In contrast, WATi of HFD+BAY41 mice possessed lipid droplets that were greatly reduced in size when compared to mice fed a HFD (Figure 24a).

To quantify these results, the adipocytes diameter was measured in each group. Mice fed a HFD exhibited a significant, 1.7 fold bigger adipocytes diameter than mice fed a CD (Figure 24b). In contrast, the adipocytes diameter of HFD+BAY41 mice was not significantly altered compared to mice fed a CD (Figure 24b). These results demonstrate that the sGC stimulator protected mice against excess gain of adipose tissue mass.

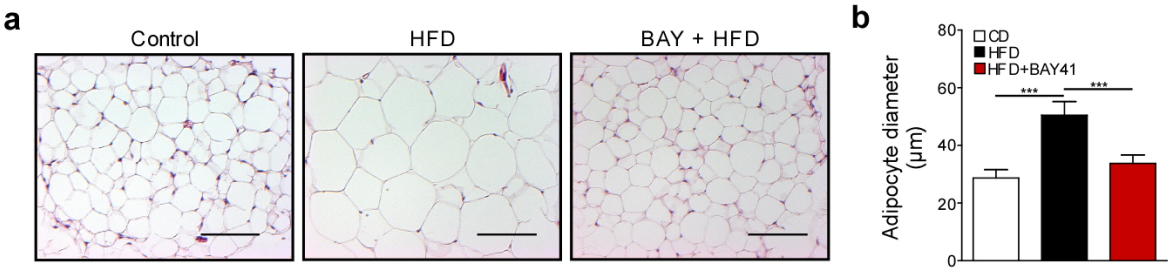

Figure 24: sGC stimulation leads to decreased adipocyte sizes.
(a) Representative images of WATi section stained with hematoxylin and eosin. (b) Adipocytes diameter of WATi adipocytes. All data are represented as mean ± SEM and statistical testing was performed using Student t-test, ***p<0.005.

3.7.2 Browning effect in WATi after sGC stimulation with BAY 41-8543

Earlier results from *in vitro* studies showed that the treatment with the sGC stimulator enhanced the function of the BAs. It has been shown by Mitschke et al. that activation of the cGMP/PKGI pathway also induces a browning effect in WAs (Mitschke et al., 2013). For this reason the ability of the sGC stimulator to induce browning was analyzed.

Therefore, WATi was stained against UCP1 and with haematoxylin to visualize the cell nucleus. Treatment with the HFD for 12 weeks reduced UCP1 expression in WATi compared to mice fed a CD (Figure 25). Surprisingly, HFD+BAY41 mice exhibited the highest UCP1 expression compared to CD and HFD fed mice. These results emphasize that the sGC stimulator induces browning in WATi.

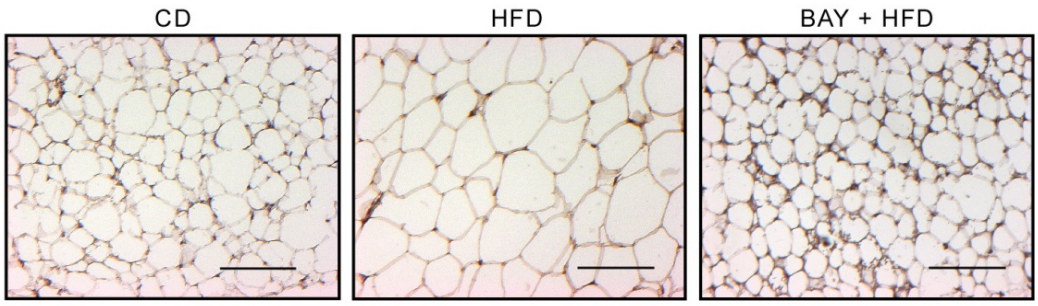

Figure 25: sGC stimulator enhances browning effect of WATi.
Analysis of browning capacity in WATi of mice fed 12 weeks a control diet (CD), a high fat diet (HFD) with or without BAY 41-8543 (HFD+BAY41). Representative images of WATi section stained with hematoxylin and UCP1, scale bar 100 µM.

3.8 sGC stimulation influences muscle metabolism

3.8.1 Increased lipid uptake into muscles after treatment with BAY 41-8543

Mice that had been fed for long term with HFD+sGC stimulator exhibit enhanced BAT activity, increased browning of WATi, and a minor weight gain compared to mice fed a HFD. Additionally, muscle weight was not altered by the three different diets. The NMR results, however, revealed an increased lean mass. Consequently, the effect of sGC stimulator on muscle metabolism was further analyzed. Therefore, the lipid uptake in soleus muscle of mice fed a CD, HFD or HFD+BAY41- was measured. Additionally, in these mice the TG content was determined and gene analysis in calf muscle was performed.

The ^{14}C-triolen uptake in muscle of mice fed a HFD was 2.6 fold increased in comparison to CD fed mice (Figure 26a). The highest amount of lipids was incorporated into the muscle of HFD+BAY41 mice leading to a 3.3 fold increase compared to CD fed mice (Figure 26a).

The question whether the increased lipid uptake in the muscle results in an enhanced lipid storage remains unsolved. Hence, the TG content of the calf muscle was measured. The TG content of muscle from mice fed a HFD was increased by 78.0 ± 48.7 % compared to mice that had received a CD (Figure 26b). In contrast, HFD+BAY41 led only to a 35.0 ± 35.8 % increase in TG content compared to mice fed a CD (Figure 26b). Even through the TG content results were overall not significant, they suggest that mice fed with a HFD supplemented with BAY 41-8543 incorporated an enhanced quantity of lipids but they did not store them within the muscle.

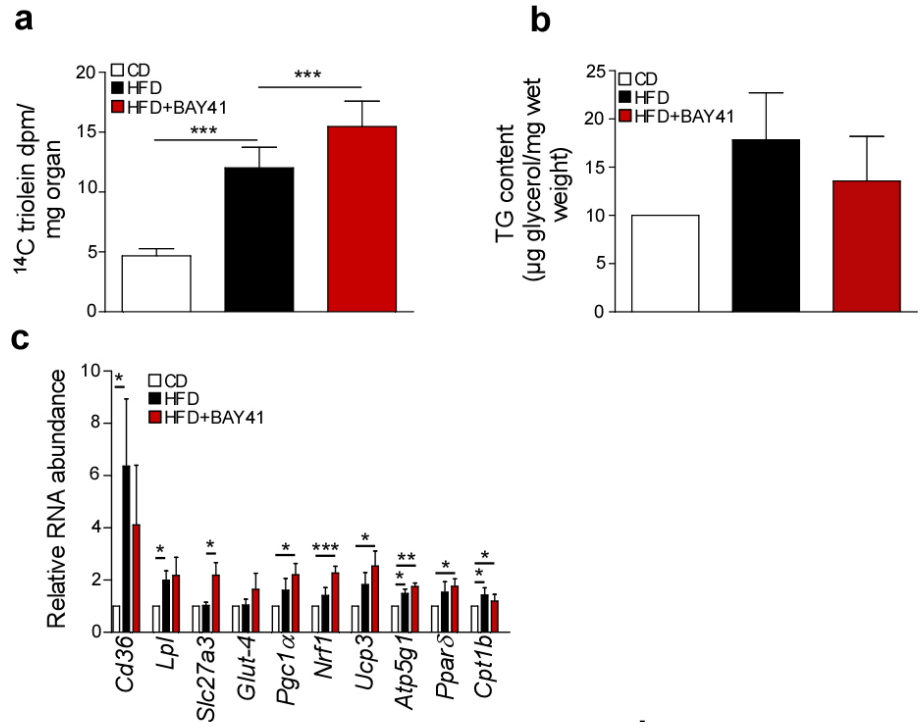

Figure 26: sGC stimulator enhances lipid uptake in muscle .

(a) Lipid uptake (^{14}C-Triolein) in muscle of mice fed a control diet (CD), a high fat diet (HFD) with or without BAY 41-8543 (HFD+BAY41) for 12 weeks; n= 6-8 per group. (b) TG content of muscle from mice fed a CD, HFD or BAY+HFD; n=8 per group. Gene expression marker of lipid uptake (Cd36, Lpl and SLC7A3), glucose uptake (Glut4), mitochondrial biogenesis (Pgc-1α and Nrf1), mitochondrial function (Ucp3 and Atp5g1) and fatty acid catabolism (Pparδ and Cpt1b), n=8 per group. All data are represented as mean ± SEM and statistical testing was performed using Student t-test, *p<0.05, **p<0.001, ***p<0.005.

Due to this finding, the question of how the lipids are further processed still remains. Therefore, the expression pattern of different marker proteins was analyzed to investigate whether the muscle metabolism was altered. As marker proteins involved in lipid uptake, the mRNA levels of *Cd36, Lpl* and *Slc27A3* were determined. Feeding a HFD over 12 weeks significantly increased the expression of *Cd36* (6.4 ± 2.6 fold) and *Lpl* (1.99 ± 0.35 fold) but did not alter the expression of *Scl27a3* (1.0 ± 0.1 fold) in comparison to CD fed mice (Figure 26c). Muscle of HFD+BAY41 mice showed an enhanced expression of all lipid uptake markers: *Cd36* increased 4.1 ± 2.3 fold, *Lpl* 2.2 ± 0.7 fold and *Scl27a3* 2.2 ± 0.5 fold in comparison to CD fed mice (Figure 26c). The expression of glucose uptake markers in the muscle was not significantly altered in HFD+BAY41 or HFD fed mice compared to CD fed mice (Figure 26c).

Marker for the mitochondrial biogenesis were not significantly increased in mice fed a HFD. The expression of *Pgc-1a* and *Nrf1* was 1.6 ± 0.4 fold and 1.0 ± 0.3 fold increased, respectively, compared to mice treated with CD (Figure 26c). In comparison to CD mice, the expression of *Pgc-1a* was 2.2 ± 0.4 fold and *Nrf1* 2.3 ± 0.3 fold increased in HFD+BAY41 fed mice, which represent significant changes in the expression levels. Analyzed expression markers for mitochondrial function are *Ucp3* and *Atp5g1*. In mice fed a HFD for 12 weeks, expression of *Ucp3* was not significantly increased, the levels of *Atp5g1*, however, were significantly increased (Figure 26c). Interestingly, expression of both marker was significantly enhanced in muscle of HFD+BAY41 mice compared to mice fed a CD (Figure 26c).

Expression levels of markers for the fatty acid catabolism, namely *Pparδ* and *Cpt1b*, were augmented in muscle of mice fed a HFD in comparison to mice fed a CD. *Pparδ* was 1.5 ± 0.5 fold and *Cpt1b* was 1.7 ± 0.3 fold increased (Figure 26c). A similar expression pattern was observed in the muscle of HFD+BAY41 mice. The expression levels of both markers were significantly increased (Figure 26c). These results highlight that stimulation with the sGC stimulator resulted not only in an increased lipid uptake in the muscle, it furthermore also augmented the expression of several marker proteins involved in lipid metabolism in the muscle.

3.8.2 Muscle fiber type switch in mice fed a HFD+BAY 41-8543

In addition to analyzing the muscle metabolism, changes in muscle fibre types were explored as the sGC stimulator may not only improve the muscle metabolism but could also induce a muscle fiber switch. For this purpose, the calf muscle was analyzed for expression of myosin heavy chains (*MHC*) which are an indicator for the function and endurance. The expression of the myosin heavy chain I (*MHCI*) was increased in HFD fed mice in comparison to mice fed a CD (3.2 ± 1.4 fold) (Figure 27a). Also, mice fed HFD+BAY41 expressed higher levels of MHCI (2.5 ± 0.9 fold) compared to mice fed a CD, however only the HFD+BAY41 fed mice exhibited a significant increase in *MHCI* expression (Figure 27a). The gene expression of *MHCIIa* and *MHCIIb* was not significantly increased in mice fed a HFD in comparison to mice receiving the CD (Figure 27a). In contrast, an increased expression of *MHCIIa* by 2.1 ± 0.5 fold and *MHCIIb* by 1.8 ± 0.2 fold was detected in HFD+BAY41 mice compared to CD (Figure 27a). The expression of *MHCIIx* was not affected neither by HFD nor by HFD+BAY41 (Figure 27a).

As a next step the genomic DNA from calf muscle was isolated and analyzed regarding the expression of the mitochondrial marker *NADH dehydrogenase* (*Nd1*); *cytochrome b* (*Cytb*) and *cytochrome c oxidase subunit 1* (*Co1*) to investigate if the mitochondrial biogenesis was also affected upon addition of the sGC stimulator. No significant changes, however, could be observed for any of the analyzed marker proteins, neither in mice fed a HFD nor in mice fed a HFD+BAY41 compared to CD fed mice (Figure 27b). Taken together, these results demonstrate that treatment with the sGC stimulator altered the composition of the muscle fiber type but it had no significant impact on mitochondrial DNA expression.

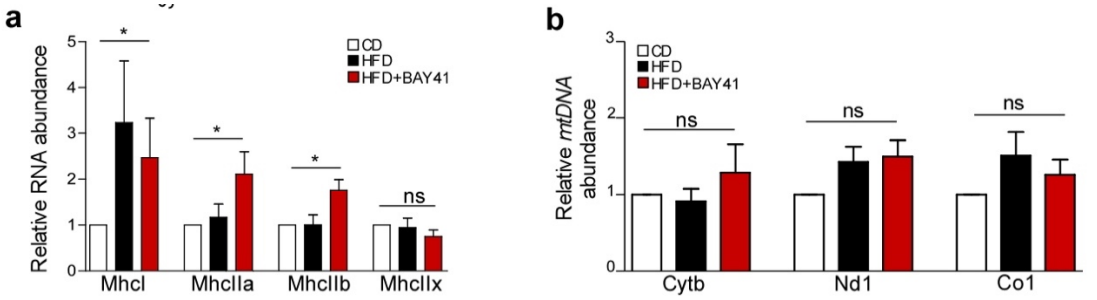

Figure 27: sGC stimulator leads to a muscle fiber type switch.

(a) Relative mRNA abundance of muscle fiber (myosin heavy chain I, IIa, IIb and IIx) of mice fed 12 weeks a control diet (CD), a high fat diet (HFD) with or without BAY 41-8543 (HFD+BAY41); n= 7-8 per group. (b) Abundance of mitochondrial DNA markers *NADH dehydrogenase* (*Nd1*); *cytochrome b* (*Cytb*) and c*ytochrome c oxidase subunit 1* (*Co1*) normalized to the chromosomal DNA encoded gene H19, n=8 per group. All data are represented as mean ± SEM and statistical testing was performed using Student t-test, *p<0.05.

3.9 BAY 41-8543 protects against liver steatosis

Treatment with BAY 41-8543 accounts for an enhanced muscle metabolism, reduced body weight and diminished adipocytes size. Nevertheless, it remains ambiguous where the excess amount of lipids is stored as it is not deposited in the adipose tissue. Another tissue prone to store excess lipids is the liver, a condition resulting in liver steatosis.

To investigate this, the lipid uptake in the liver and the TG content of the liver were measured. Measurements of lipid uptake in the liver revealed that mice on HFD incorporated significantly (1.7 fold) more lipids than mice fed a CD (Figure 28a). Interestingly, HFD+BAY41 mice incorporated even more lipids (2.2 fold) into the liver compared to mice on a CD (Figure 28a). These results could strengthen the hypothesis that treatment with the sGC stimulator triggers a severe fatty liver in mice. To rule out the subsequent development of a fatty liver, TG assay was performed. Mice fed with a HFD for 12 weeks stored 83.0 % more TG in the liver than mice fed a CD (Figure 28b). In contrast, HFD+BAY41 mice had only a minor increase of 3 % in the TG content compared to mice on a CD (Figure 28b).

The underlying mechanisms of exceeded lipid uptake in mice fed a HFD+BAY41, however, remained elusive. To gain more insights in liver function, expression of a marker for hepatic gluconeogenesis (Glucose6-Phosphatase=Gcp6), of the oxidative stress detoxifying gene (catalase=Cat) and energy dissipation gene (uncoupling protein 2=Ucp2)

in the liver was analyzed. The gene expression of the marker for hepatic *Gcp6* showed a 1.7 ± 0.5 fold increase in mice fed a HFD over 12 weeks (Figure 28c), whereas its expression level remained unaffected in mice fed a HFD+BAY41, both conditions compared to mice fed a CD (Figure 28c). The mRNA expression of *Cat* was 2.5 ± 0.1 fold enhanced in mice fed a HFD in comparison to CD fed mice (Figure 28c). Again, the expression of *Cat* was not significantly affected in HFD+BAY41 mice compared to mice fed a CD (Figure 28c). Finally, the expression of the energy dissipation marker *Ucp2* remained independent of the different diets. Taken together, the sGC stimulator represents a potent drug against the development of a liver steatosis in mice, which is a comorbidity of obesity.

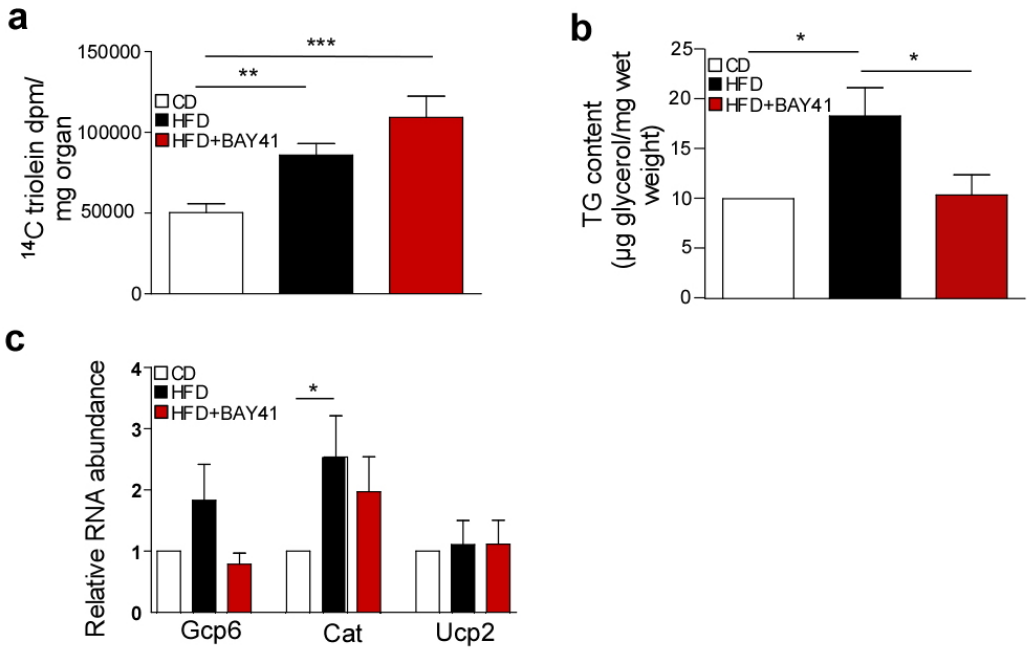

Figure 28: sGC stimulator enhances liver metabolism.

(a) Lipid uptake (^{14}C-Triolein) in liver of mice fed 12 weeks a control diet (CD), a high fat diet (HFD) with or without BAY 41-8543 (HFD+BAY41); n= 6-8 per group (Study performed by Prof. Heeren's lab.). (b) TG content of liver from mice fed a CD, HFD or BAY+HFD; n=8 per group. Gene expression marker of hepatic gluconeogenesis (Glucose6-Phosphatase=Gcp6), oxidative stress detoxifying genes (catalase=Cat) and energy dissipation (Ucp2) in liver, n=8 per group. All data are represented as mean ± SEM and statistical testing was performed using Student t-test, *p<0.05, **p<0.001, ***p<0.005.

3.10 Effects of sGC stimulator BAY 41-8543 on already established obesity

In addition to the prevention study described above, another and more clinical relevant approach was undertaken, in which the effect of the sGC stimulator in mice with already established obesity was investigated. Not only the effect of sGC stimulation and a HFD was analyzed, also the consequences after a diet change and additional treatment with the sGC stimulator were investigated. Therefore, body weight, glucose tolerance test, metabolic measurements and tissue weights as well as plasma level of leptin, adiponectin and insulin were analyzed.

3.10.1 sGC stimulator BAY 41-8543 influences body weight.

Mice were fed a HFD for 12 weeks and after this, the diet was changed for 6 additional weeks. One group was fed a HFD (HFD-HFD) and the second group was fed a HFD+BAY 41-8543 (HFD-BAY+HFD). The third group was switched to CD (HFD-CD) and the fourth group was fed a CD plus the sGC stimulator BAY 41-8543 (HFD-BAY+CD). The fifth group was fed a CD from the beginning (CD). Before changing the diet, all mice on a HFD weighed 39.9 ± 1.4 g, mice just receiving the CD weighed 27.7 ± 0.7 g (Figure 29a). At the end of the study HFD-HFD mice weighed 47.9 ± 1.2 g (Figure 29a). HFD-BAY+HFD mice weighed 13 % less than HFD-HFD mice (Figure 29a). Interestingly, a diet switch reduced the body weight in HFD-CD to 29.4 ± 0.7 g and HFD-BAY+CD mice exhibited a reduction in body weight by 8 % in comparison to HFD-CD fed mice at the end of the study (Figure 29b). In contrast, mice fed a CD from the beginning of the study weighed 29.1 ± 0.6 g after 18 weeks. These results demonstrate that BAY 41-8543 can boost the reduction of the body weight also in combination with a CD.

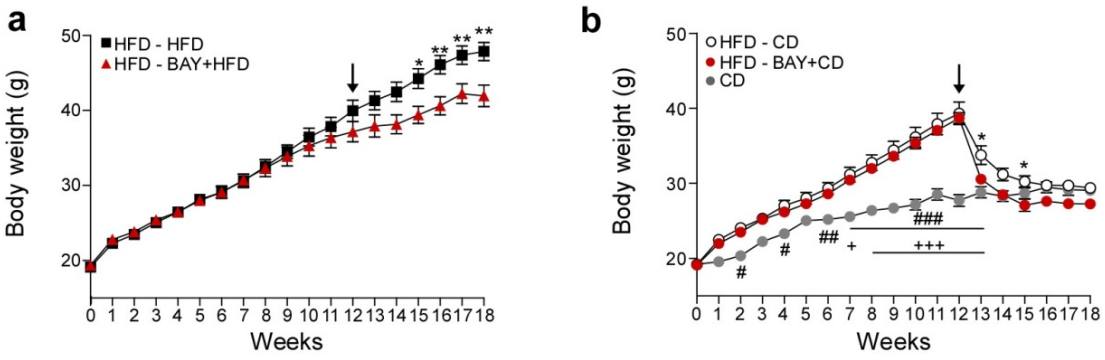

Figure 29: Effects of sGC stimulator BAY 41-8543 on already established obesity.
(a;b) Effects of weight gain after already established obesity. Therefore, mice were fed a HFD for 12 weeks and then diet was changed, to (a) HFD (HFD-HFD) or HFD plus BAY 41-8543 (HFD-BAY+HFD) for additional six weeks, (b) or CD (HFD-CD) and CD plus BAY 41-8543 (HFD-BAY+CD) also for the six additional weeks, n=8 mice per group, #CD versus HFD-CD, + CD versus HFD-CD+BAY, *HFD-CD versus HFD-CD+BAY. All data are represented as mean ± SEM and statistical testing was performed using two-way analysis of variance (ANOVA). $^{*,\#,+}$p<0.05, $^{**,\#\#,++}$p<0.01, $^{\#\#\#,+++}$p<0.005.

3.10.2 BAY 41-8543 increases energy expenditure and improves glucose clearance

At the end of the study O_2 consumption and glucose clearance were measured. HFD-BAY+HFD mice consumed significantly more O_2 during day and night compared to HFD-HFD mice (Figure 30a). Surprisingly, the diet change to CD plus BAY 41-8543 for additional six weeks (HFD-BAY+CD) did not significantly enhance the O_2 consumption compared to mice fed only a CD (Figure 30b).

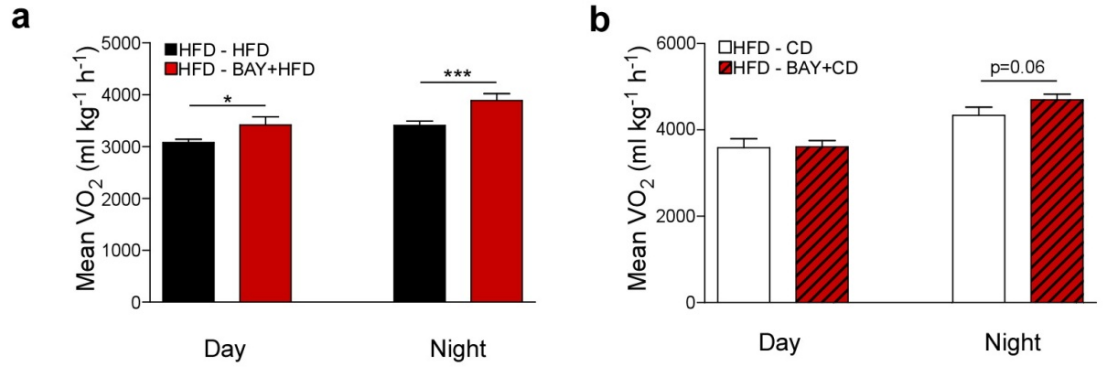

Figure 30: BAY 41-8543 increases energy expenditure after already established obesity.
(a;b) Mean energy expenditure (VO_2) during day and night cycle after established obesity. Therefore, mice were fed a HFD for 12 weeks and then diet was changed, to (a) HFD (HFD-HFD) or HFD plus BAY 41-8543 (HFD-BAY+HFD) for additional six weeks, (b) or CD (HFD-CD) and CD plus BAY 41-8543 (HFD-BAY+CD) also for six additional weeks, n=8 mice per group. All data are represented as mean ± SEM and statistical testing was performed using Student t-test, *p<0.05, ***p<0.005.

Furthermore, GTT was performed to validate if the sGC stimulator also improves the glucose clearance after already established obesity. The basal glucose level was not significantly different between HFD-HFD and HFD-BAY+HFD fed mice (Figure 31a). Two hours after glucose injection, HFD-BAY+HFD mice had a reduced glucose level by 26.9 % compared to HFD-HFD mice (Figure 31a).

The basal glucose level of HFD-CD or HFD-BAY+CD mice was not significantly different (Figure 31b). Two hours after glucose injection the glucose level of mice fed HFD-BAY+CD was reduced by 21 % compared to mice fed a CD (HFD-CD) (Figure 31b). These results reveal that the sGC stimulator improves glucose clearance after already established obesity and triggers a higher glucose clearance when mice were fed a HFD+BAY41.

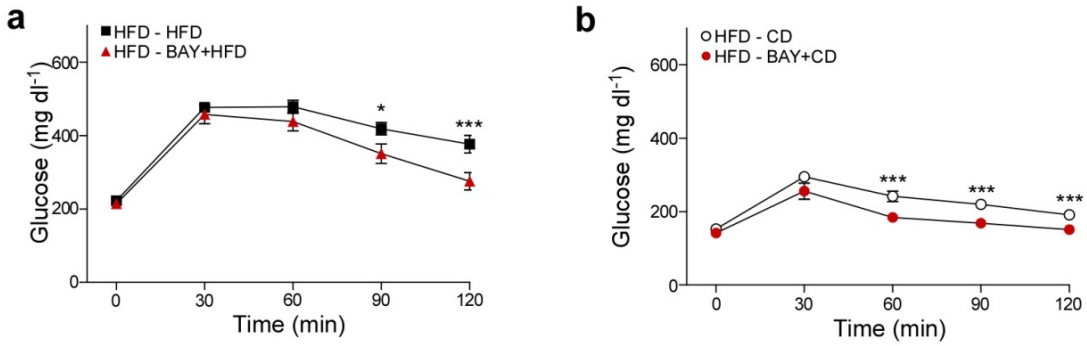

Figure 31: BAY 41-8543 improves glucose clearance after already established obesity.
(a;b) Glucose tolerance test after established obesity. Therefore, mice were fed a HFD for 12 weeks and then diet was changed, to (a) HFD (HFD-HFD) or HFD plus BAY 41-8543 (HFD-BAY+HFD) for additional six weeks, (b) or CD (HFD-CD) and CD plus BAY 41-8543 (HFD-BAY+CD) also for six additional weeks, n=8 mice per group. All data are represented as mean ± SEM and statistical testing was performed using Student t-test, $^{*}p<0.05$, ***p<0.005.

3.10.3 The sGC stimulator BAY 41-8543 decreases adipose tissue weight and plasma level of insulin, leptin and adiponectin

To unravel how the treatment of obese mice with the sGC stimulator improves their health in comparison to HFD fed mice, tissue weights were measured and the plasma level of insulin, leptin and adiponectin were analyzed. The WATi of HFD-BAY+HFD mice was 27 % reduced compared to HFD-HFD mice (Figure 32a) whereas WATi weight of HFD-BAY+CD mice was decreased by 24 % compared to HFD-CD mice (Figure 32a). The weight of WATg from HFD-BAY+HFD mice was 13 % reduced compared to HFD-HFD mice (Figure 32a). Surprisingly, HFD-BAY+CD mice possessed a decreased WATg weight by 39 % compared to HFD-CD mice (Figure 32a). The weight of BAT and muscle was not significantly altered in all four groups (Figure 32a).

The plasma level of insulin showed a significant (56.3 %) decrease after changing the diet from HFD to HFD+BAY 41-8543 (HFD-BAY+HFD) compared to mice on HFD-HFD (Figure 32b). Interestingly, diet change from HFD to CD (HFD-CD) decreased the insulin plasma level to the same extent as a change from HFD to BAY+HFD did (Figure 32b). Addition of BAY41 to CD did not further decrease insulin plasma level compared to HFD-CD mice (Figure 32b).

Leptin plasma levels were not significantly decreased in HFD-BAY+HFD mice compared to HFD-HFD mice (Figure 32b). Interestingly, HFD-BAY+CD mice possessed a significant decrease in leptin plasma level by 46.7 % compared to HFD-CD mice (Figure 32b). The levels of adiponectin were not significantly different between all four groups (Figure 32b). Together these results demonstrate that the sGC stimulator decreased the weight of WATi and WATg as well as the plasma levels of insulin and leptin after already established obesity.

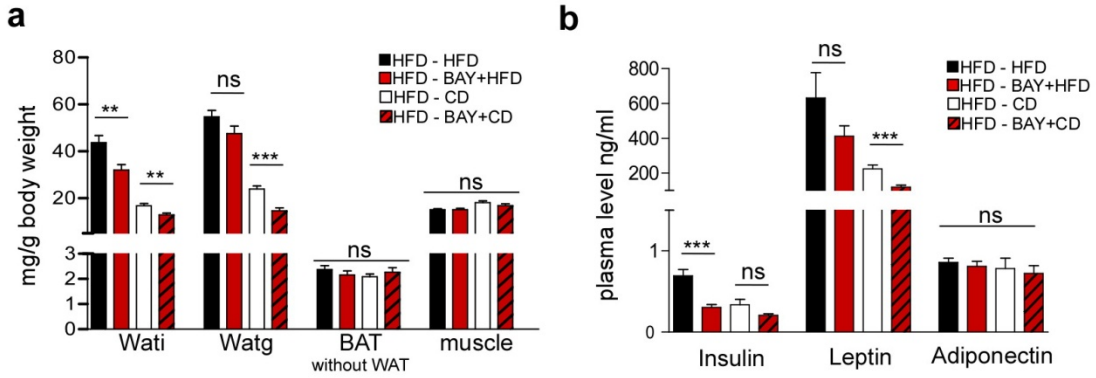

Figure 32: BAY 41-8543 decreases adipose tissue weight and improves insulin and leptin secretion after already established obesity.

(a;b) Tissue weights and plasma level after established obesity. Therefore, mice were fed a HFD for 12 weeks and then diet was changed, to HFD (HFD-HFD) or HFD plus BAY 41-8543 (HFD-BAY+HFD) for additional 6 weeks, or CD (HFD-CD) and CD plus BAY 41-8543 (HFD-BAY+CD) also for six additional weeks, n=8 mice per group. (a) Tissue weights after 18 weeks of treatment of WATi, WATg, BAT and muscle. (b) Plasma level of insulin, leptin and adiponectin after 18 weeks of treatment. All data are represented as mean ± SEM and statistical testing was performed using Student t-test, *p<0.05, ***p<0.005.

3.11 Effects of sGC stimulator BAY 41-8543 on mice fed a CD

3.11.1 sGC stimulator BAY 41-8543 does not influence body weight nor body composition

After identifying that the stimulation of sGC influenced the body weight in two different approaches, one question remained unsolved: What are the effects of sGC stimulator on weight gain in mice just fed CD for 12 weeks? Hence, their body weight was measured every week and additionally, in the last week, body composition was determined. The body weight was not significantly changed after treatment with BAY 41-8543 over the period of 12 weeks. At the end of the study the body weight was not significantly changed in both groups (Figure 33a). Body composition showed no significant alteration in fat, lean mass and water content (Figure 33b).

After sacrificing the mice, tissue weights were measured. The sGC stimulator did not affect the WATi weight compared to mice fed a CD only (Figure 33c). Interestingly, treatment with BAY 41-8543 significantly decreased the tissue weight of WATg by 20 % compared to mice fed the CD (Figure 33c). BAT weight and muscle weight was not affected by the stimulation of sGC (Figure 33c). Taken together, the sGC stimulator does not affect body weight nor body composition but reduces WATg weight.

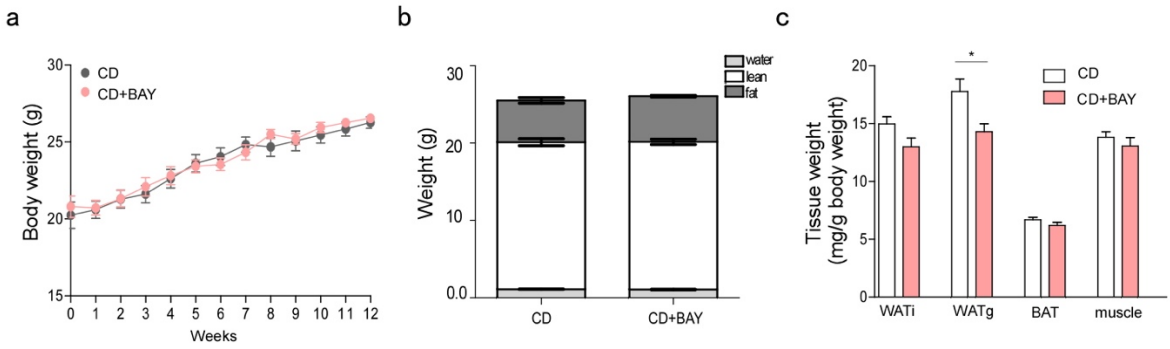

Figure 33: Effects of sGC stimulator BAY 41-8543 on body weight and composition in mice fed a CD.

(a;b) Effects of control diet (CD) with or without BAY 41-8543 (CD+BAY) on body weight (a) and body composition (b). (c) Tissue weights of inguinal WAT (WATi) and gonadal WAT (WATg), interscapular brown adipose tissue with WAT (BAT) and muscle after treatment with or without BAY 41-8543. All data are represented as mean ± SEM and statistical testing was performed using Student t-test, *$p<0.05$.

3.11.2 The sGC stimulator BAY 41-8543 improves glucose clearance, but does not affect NE-induced thermogenesis

Treatment of non-obese mice with the sGC stimulator did not show as strong effects as seen in obese mice or mice fed a HFD. The only effect discovered so far was a decreased WATg weight. Hence, GTT and NE-induced thermogenesis were analyzed in addition.

The treatment with the sGC stimulator enhanced the glucose clearance over time compared to mice on a CD. Interestingly, the basal glucose level was already 12 % reduced in mice fed the sGC stimulator compared to mice only fed a CD (Figure 34a). The AUC was significantly reduced upon treatment with the sGC stimulator compared to mice fed only a CD (Figure 34b).

To investigate BAT activity, NE-induced thermogenesis was measured. Remarkably, the RMR was significantly increased in mice fed a CD supplemented with the sGC stimulator compared to mice fed a CD (Figure 34c). After NE injection, mice fed a CD+BAY consumed more O_2 than mice only fed a CD (Figure 34c). The AUC revealed that mice fed a CD+BAY consumed 12 % more O_2 than mice fed only a CD (Figure 34d). Hence, these results strengthen that sGC stimulation not only acts on obese mice, it also improves glucose clearance and BAT activity in mice fed a CD.

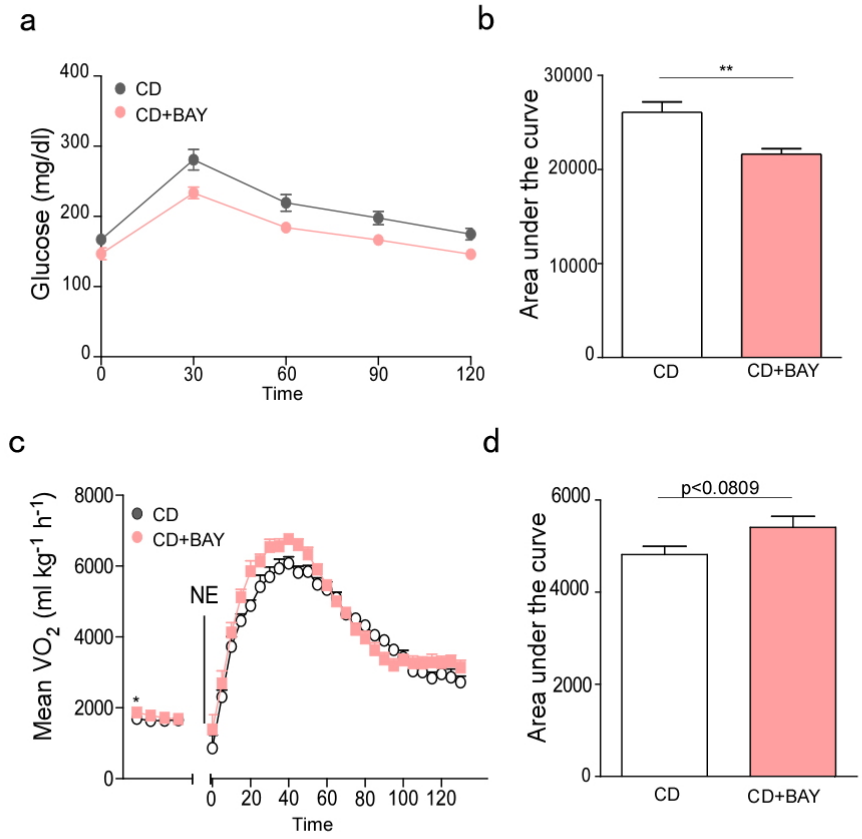

Figure 34: Enhanced glucose clearance after BAY 41-8543 treatment in CD mice.
(a;b) Effects of control diet (CD) with or without BAY 41-8543 on glucose clearance (a). (b) Calculation of the area under the curve (AUC). (c) Norepinephrine-induced (NE) thermogenesis in BAY 41-8543 treated mice. Mice were 12 weeks fed a control diet (CD) with or without BAY 41-8543 (CD+BAY). The resting metabolic rate was analyzed at thermoneutrality (30°C). NE (subcutaneous injection 1mg/kg body weight) was used to induce maximal thermogenesis (b) Area under the curve (AUC) of mean oxygen consumption after NE injection; n=7 mice per group. All data are represented as mean ± SEM and statistical testing was performed using Student t-test, ** p< 0.01.

4 Discussion

4.1 sGC is crucial for BA differentiation and thermogenesis

Genetic ablation of the β_1 subunit of sGC in mice leads to severe phenotypes like, dysmotility of the gastrointestinal tract, dysfunctional smooth muscle relaxation, high blood pressure and postnatal death (Friebe et al., 2007). The β_1 subunit of sGC contains a heme–binding domain, making it indispensable for proper functioning of sGC upon activation by NO and sGC stimulator (Hoffmann et al., 2009; Stasch et al., 2002b). Current understanding of the metabolic consequences resulting from sGC ablation is rudimentary. Therefore, this thesis aims to add important knowledge about the role of sGC in metabolism, especially in BAT and WATi, using *in vitro* and *in vivo* models.

The cGMP pathway is a crucial regulator of BAT thermogenesis (Haas et al., 2009; Pfeifer and Hoffmann, 2015). The second messenger cGMP is generated by two different enzymes, sGCs and pGCs (Friebe and Koesling, 2009b; Garbers et al., 2006). PKGI, the major downstream target of cGMP, is essential for differentiation of BAs *in vitro* and *in vivo*, as well as for browning of WATi (Haas et al., 2009; Mitschke et al., 2013). Mice lacking the β_1 subunit of sGC have a reduced BAT mass and exhibit a decreased UCP1 expression, resulting in diminished BAT-derived thermogenesis. To unravel the underlying molecular mechanisms, further analyses were performed using BAs *in vitro*. Basal cGMP concentration in mature BAs is reduced in sGC$\beta_1^{-/-}$ cells, compared to untreated WT cells. Stimulation with NO increases intracellular cGMP only in WT cells but not in sGC$\beta_1^{-/-}$ cells, indicating that sGCβ_1 is required for NO-dependent cGMP production in BAs.

Lipid uptake in adipocytes, their subsequent esterification and storage (as TGs within the lipid droplets) is important for expansion of adipose tissue and maintenance of metabolic homeostasis (Rutkowski et al., 2015). TG content of sGC$\beta_1^{-/-}$ BAs is significantly reduced in comparison to untreated WT BAs. Addition of 200 µM of a cGMP analog increases BAs differentiation, marked by enhanced UCP1, PGC1α and aP2 expression and an increased TG content (Haas et al., 2009).

Chronic cGMP treatment of sGC$\beta_1^{-/-}$ BAs throughout differentiation protocol restores lipid content in these cells, demonstrating that the signaling pathway downstream of cGMP remains intact in sGC$\beta_1^{-/-}$ BAs. Importantly, NO-dependent cGMP production is dependent on sGCβ_1.

The impact of sGC on the adipogenic program was investigated by analyzing expression levels of PPARγ and aP2. Deletion of sGCβ_1 leads to decreased expression of PPARγ and aP2 *in vitro*. Earlier studies have shown that PPARγ is a master regulator of adipogenesis, regulating the expression of genes such as aP2 and C/EBPα (Carmona et al., 2005; Nedergaard et al., 2005). It has been previously shown that also the loss of PKGI leads to reduced PPARγ and aP2 expression in BAs (Haas et al., 2009). The mitochondrial thermogenic program is a hallmark of BAs and is highly regulated by PGC-1α (Cannon and Nedergaard, 1996). Furthermore, PGC-1α is a major regulator of mitochondrial biogenesis and energy homeostasis (Fernandez-Marcos and Auwerx, 2011). sGC$\beta_1^{-/-}$ cells exhibit a decreased expression of UCP1 and PGC-1α. Moreover, similar observations are made upon genetic ablation of PKGI in BAs (Haas et al., 2009). In this study, mtDNA expression analysis revealed that sGC$\beta_1^{-/-}$ cells express less PGC-1α and mtDNA (*Nd1*, *Cytb*, *Co1*). These results are in line with the previously published data where PGC-1α activates nuclear and non-nuclear receptors, like mitochondrial transcription factor (mtTFA) and nuclear respiratory factors (NRF) 1 and 2, which are important for replication and transcription of mitochondrial DNA (Bogacka et al., 2005).

In comparison to WT cells, basal lipolytic activity is decreased in sGC$\beta_1^{-/-}$ cells. After stimulation with NE, an increased lipolytic activity is observed in sGC$\beta_1^{-/-}$ cells compared to untreated sGC$\beta_1^{-/-}$ cells. However, lipolysis in NE-stimulated sGC$\beta_1^{-/-}$ cells increases by a lesser extent than in NE-treated WT cells. These results indicate that the deletion of sGC decreases the NE-induced lipolytic activity. NE release (from sympathetic nerves in BAT) is dramatically increased upon cold exposure (Young et al., 1982). Intracellular levels of eNOS, NO and cGMP are modulated by NE.

This leads to upregulated eNOS expression, enhanced NO production, increased intracellular cGMP level and a corresponding upregulation of UCP1 expression (Giordano et al., 2002). Nevertheless, this is not working in $sGC\beta_1^{-/-}$ cells because NO cannot activate sGC in this cells. NE induces also PGC-1α expression, which binds to the UCP1 promotor and increases UCP1 expression (Lowell and Spiegelman, 2000). NE, by binding with β-ARs, elevates intracellular cAMP production, which results in activation of the PKA pathway. This leads to an increased lipolysis of FFA from TG. FFA are then oxidized by mitochondria to produce heat (Cannon and Nedergaard, 2004). $VASP^{-/-}$ BAs have an increased β-ARs expression, which leads to enhanced lipolytic activity (Jennissen et al., 2012). Moreover, $VASP^{-/-}$ cells show increased TG accumulation and adipogenic marker expression, thus highlighting the importance of VASP and cGMP signaling in BAs (Jennissen et al., 2012). Deletion of VASP in BAs leads to increased Rac-1 activity, which enhances sGC expression and consequently, leads to higher cGMP production (Jennissen et al., 2012). Diminished NE-induced lipolytic activity in $sGC\beta_1^{-/-}$ BAs suggests that the absence of sGC leads to decreased β-AR expression, which in turn reduces lipolytic activity in adipocytes.

To summarize, $sGC\beta_1$ is crucial for normal BAT differentiation. Deletion of $sGC\beta_1$ inhibits adipogenic (TG content and PPARγ and aP2 expression) and thermogenic programs (diminished mitochondrial biogenesis and lipolytic activity) *in vitro*.

4.2 Stimulation of sGC with BAY 41-5843 influences adipogenesis of brown adipocytes

As demonstrated, sGC is crucial for adipogenic differentiation and thermogenic function of BAs. Consequently, the effects of pharmacological stimulation of sGC with BAY 41-8543 was assessed in BAs. The sGC stimulator BAY 41-8543 is known to stimulate sGC in a NO- and heme dependent manner, thus resulting in enhanced cGMP production. To date, effects of the sGC stimulator have only been investigated in smooth muscle cells, colon and aorta (Adderley et al., 2012; Monica et al., 2012; Soares et al., 2013; Thorsen et al., 2010). Accordingly, there are no functional data available describing the effects of sGC stimulation with BAY 41-8543 in adipocytes.

Application of BAY 41-8543 throughout differentiation positively influences the adipogenic differentiation as well as thermogenic program (increased UCP1 expression). In agreement, Nisoli et al. have shown an enhanced PPARγ expression in BAs upon treatment with an NO-Donor (Nisoli et al., 1998). Furthermore, a treatment with DETA/NO or BAY 41-8543 also increases the expression of the thermogenic marker UCP1, which is responsible for thermogenesis. In line with previously published work *in vitro* results presented here demonstrate increased UCP1 expression upon activation of the cGMP/PKGI pathway (Haas et al., 2009). Thus, pharmacological stimulation of sGC results in opposite effects as shown in sGC$\beta_1^{-/-}$ cells.

BAs treated with BAY 41-8543 exhibit an elevated TG content and lipolytic activity. Additionally, it has been reported that higher fat content in BAs provides an increased pool of lipids for lipolysis. TGs are broken down into diacylglycerols, then into monoglyceride and finally into fatty acids and glycerol (Lafontan, 2008). Thus, BAs treated with BAY 41-8543 have an enhanced lipolytic activity, as the rate-limiting step in adipose tissue lipolysis is the hydrolysis of TG by lipases.

Taken together, stimulation of the sGC/cGMP/PKGI pathway promotes BAs differentiation *in vitro*.

4.3 The effect of pharmacological stimulation of sGC on metabolism

4.3.1 Stimulation of sGC increases BAT activity and browning of WAT *in vivo*

After showing that stimulation of sGC increases BAs differentiation *in vitro*, the effects of BAY 41-8543 on the whole body metabolisms was investigated. A 12-week treatment with the sGC stimulator increases UCP1 expression in BAT. Consequently, enhanced BAT activity and higher oxygen consumption after acute NE stimulation is observed in mice co-fed a HFD and sGC stimulator compared to CD fed mice. In accordance, Gnad et al. have demonstrated that an acute NE treatment significantly increases O_2 consumption in mice fed a HFD (Gnad et al., 2014). Importantly, the sGC stimulator increases energy expenditure (EE) and lipid uptake into BAT under basal conditions. It has been shown that more than 50 % of nutrients lipids can be metabolized by active BAT, which leads to increased EE (Bartelt et al., 2011; Gnad et al., 2014; Moro et al., 2007; Ouellet et al., 2012). Likewise, muscle, WAT and liver also incorporate and subsequently utilize more lipids after treatment with the sGC stimulator. Congruently, the expression of lipid processing genes, such as *Adbr3*, *Nrf1*, *Pgc-1*α, *Lpl* and *Cd36,* is increased in BAT from mice treated a HFD with the sGC stimulator in comparison to CD mice. *Nrf1* and *Pgc-1*α are important for the transcription of mitochondrial DNA (Bogacka et al., 2005; Fernandez-Marcos and Auwerx, 2011). In agreement with these studies, expression of mitochondrial markers, such as *Co1* and *Cytb* is significantly increased in BAT from mice treated a HFD with sGC stimulator compared to CD. These results indicate that sGC stimulator mediated upregulation of mitochondrial markers may lead to increased energy supply in BAT.

Whitening of BAT is characterized by diminished β-adrenergic signaling, accumulation of large lipid droplets, mitochondrial dysfunction as well as loss of VEGF expression (Shimizu et al., 2014). In BAT sections of mice only fed a HFD whitening of BAT and adipocyte hypertrophy could be illustrated. This is in line with Gao et al. that showed that whitening of BAT is associated with adipocyte hypertrophy, increased expression of inflammation markers, excessive fat accumulation and ectopic lipid deposition (Gao et al., 2015).

In comparison to mice fed a HFD, mice co-fed a HFD and the sGC stimulator exhibit a reduced whitening in BAT, resulting in smaller lipid droplets, enhanced mitochondrial biogenesis, increased VEGF expression and β3-AR expression.

In mice fed with the sGC stimulator, the browning capacity of WATi is enhanced. Whereas, the white adipocyte diameter is decreased. This study adds the sGC stimulator BAY 41-8543 to the list of compounds capable to increase browning capacity of WATi. Increased cGMP levels in BAs and WAs result in elevated UCP1 expression (Bordicchia et al., 2012; Haas et al., 2009; Nisoli et al., 2003). Likewise, inhibition of PDEs increases intracellular cGMP level in WAs, thus leading to browning in WATi (Mitschke et al., 2013; Moro et al., 2007). Browning of WAs is induced by stimulation of the cGMP cascade (Mitschke et al., 2013; Roberts et al., 2015). Furthermore, browning of WAs can be stimulated by several other agents like sympathomimetics, prostaglandins, PPARγ activators, FGF21, NP and irisin (Bordicchia et al., 2012; Bostrom et al., 2012; Fisher et al., 2012; Petrovic et al., 2010; Vegiopoulos et al., 2010).

Mice treated with the sGC stimulator and HFD for 12 weeks have smaller white adipocytes diameter compared to mice fed only a HFD. Furthermore, mtDNA content in WATi of sGC stimulator treated mice is significantly increased compared to CD fed mice. Intriguingly, plasma insulin levels are similar in mice treated with the sGC stimulator and to CD fed mice, but lower compared to mice fed a HFD. It has previously been described that young adipocytes are relatively small, insulin sensitive and are characterized by increased adiponectin expression. During aging, cells increase in size and lose function and adiponectin synthesis (Yu and Zhu, 2004). Reduced adipocyte size is also an indicator for healthy fat expansion (Sun et al., 2011). Furthermore, mitochondrial biogenesis during adipocytes differentiation is increased but the amount of mitochondria is reduced in obese *db/db* mice (Choo et al., 2006). Mitochondrial biogenesis is essential for adipocyte differentiation while a reduction in mitochondrial mass causes adipocyte hypertrophy (Wilson-Fritch et al., 2003; Yu and Zhu, 2004). These findings highlight that the sGC stimulator leads to decreased expansion of WAT, higher mtDNA content and to a higher insulin sensitivity.

Mice treated with the sGC stimulator have a better glucose clearance and reduced plasma insulin levels compared to HFD fed mice. The loss of PKGI leads to abrogation of cGMP pathway, increased insulin resistance, and subsequently to suppression of BAT function and differentiation (Haas et al., 2009). It is known that RhoA, a small GTPase involved in insulin secretion, is inhibited by PKGI (Haas et al., 2009). The exact involvement of the NO/cGMP signaling pathway on the regulation of insulin secretion, however, remains elusive and there is no distinct explanation, why sGC stimulation leads to reduced plasma insulin level in mice (Kaneko et al., 2003; Ropero et al., 2010).

Moreover, it is known that regulation of adiponectin secretion inversely correlates with BMI and body fat (Arita et al., 1999). Although fat mass is reduced in obese mice treated with BAY 41-8543, no significant changes in plasma adiponectin levels are observed. Different studies on adiponectin secretion have revealed an inhibition of hepatic glucose production, increased glucose uptake in muscle, enhanced oxidation of fatty acids in muscle and liver, accompanied by increased EE (Berg et al., 2001; Combs et al., 2001; Fruebis et al., 2001). Furthermore, overexpression of adiponectin seems to be protective against insulin resistance and has anti-inflammatory effects (Kern et al., 2003; Maeda et al., 2002).

The cGMP/PKGI pathway, as described earlier, is a crucial regulator of BAT thermogenesis and for WATi browning (Haas et al., 2009; Mitschke et al., 2013; Pfeifer and Hoffmann, 2015). The here presented *in vivo* study shows that stimulation of sGC with BAY 41-8543 enhanced differentiation of BAT (comparable to *in vitro* experiments on BAs). Additionally, this study reveals that pharmacological stimulation of the sGC protects against DIO. Reduced weight gain is accompanied by improved overall metabolic status, indicated by reduced insulin signaling, improved glucose tolerance and decreased adipocyte diameter in WATi.

4.3.2 Pharmacological stimulation of sGC decreases fatty liver and enhances muscle function

sGC is ubiquitously expressed, thus oral sGC stimulator administration affects not only adipose tissue or adipocytes, but also other cells and organs (Potter, 2011). Skeletal muscle and liver from mice treated with sGC stimulator seem to be protected against excess fat accumulation, even though the lipid uptake is increased in both tissues. Importantly, mice treated with the sGC stimulator are insulin sensitive. Insulin resistance is strongly associated with skeletal and hepatic lipid content (Lee et al., 2014a; Morino et al., 2012). It develops in skeletal muscle and liver in case of an imbalance between uptake and utilization of intracellular lipids, such as diacylglycerol (Lee et al., 2014a). This lipid accumulation is primarily achieved by caloric intake exceeding the capacity of myocytes and hepatocytes, leading to obesity or metabolic syndrome (Birkenfeld and Shulman, 2014; Samuel and Shulman, 2012). These cell types metabolize and export fatty acids while refining or uncoupling mitochondrial respiration and enhancing lipid oxidation, which leads to an improved insulin sensitivity (Birkenfeld et al., 2011; Kumashiro et al., 2013; Lee et al., 2010; Neuschafer-Rube et al., 2014; Perry et al., 2013; Thielecke et al., 2010).

Nutrient excess in cultured hepatocytes and hepatic tissues promotes inflammatory signaling and insulin resistance. The study of Tateya et al. shows that during HFD liver NO levels are reduced. This triggers hepatic inflammation and impairment of insulin signaling (Tateya et al., 2011). Chronic treatment with PDE inhibitor Sildenafil, which inhibits cGMP degradation by PDE5, is able to prevent the HFD-dependent hepatic inflammation and insulin resistance (Tateya et al., 2011). Another study reports that deletion of PKGI reduces liver inflammation, fasting hyperglycemia and insulin tolerance (Lutz et al., 2011). Mice lacking eNOS are more resistant to insulin (Duplain et al., 2001; Shankar et al., 2000). Additionally, An et al. have shown that cGMP has a direct impact on liver homeostasis in terms of inflammatory status and insulin signaling. They have demonstrated that cGMP infusion (intraportal) in fasted, glucose-infused dogs decreases the glucose uptake in the liver.

Moreover, they have observed a decrease of NO after food consumption in dogs and they speculated that low cGMP levels might facilitate hepatic glucose uptake (An et al., 2012; Bandsma et al., 2001). In all three studies performed within this thesis - mice treated with BAY41-8543 and a HFD, a CD or after established obesity - BAY 41-8543 always improves the glucose clearance from blood circulation. This argues that administration of the sGC stimulator protects against liver inflammation and insulin intolerance.

Genes involved in gluconeogenesis (Gcp6), oxidative stress detoxification (CAT) and energy dissipation (Ucp2) in the liver have also been analyzed in this thesis. An increase in CAT mRNA expression in mice fed a HFD or a HFD with sGC stimulator can be explained by the fact that peroxisomal β-oxidation of fatty acids generates H_20_2, that needs to be efficiently removed by catalase. A higher H_20_2 content has been linked to in increased expression of CAT (Carmiel-Haggai et al., 2005). Moreover, *Ucp2* mRNA expression in liver of mice treated with a HFD or HFD plus sGC stimulator is unchanged compared to CD fed mice. Ucp2 is expressed in liver mitochondria and suppresses H_20_2 production. Chavin et al. demonstrate that increased *Ucp2* expression in fatty liver of *ob/ob* mice (Chavin et al., 1999). Gcp6 is a key enzyme in hepatic glucose metabolism. Alteration in Gcp6 activity leads to an impairment of lipid metabolism, as observed in patients with glycogen storage disease and diabetic states (Bandsma et al., 2001). Acute inhibition of the Gcp6 system stimulates hepatic de novo lipogenesis in rats and decreases circulating levels of insulin, which is a stimulator of lipogenesis (Bandsma et al., 2001). In line with these results, mice treated with the sGC stimulator have decreased Gcp6 levels and reduced plasma insulin levels, in comparison to mice fed a HFD. Therefore, it can be speculated that BAY 41-8543 inhibits the Gcp6 system and hence prevents the development of a fatty liver in mice.

Studies on mice overexpressing PKGI and fed a HFD have revealed a higher EE, lower fat mass and higher expression of mitochondrial biogenesis marker in skeletal muscle compared to WT mice (Miyashita et al., 2009). Similar results are obtained in WT mice fed the sGC stimulator and a HFD. Mice treated with the sGC stimulator have a higher EE, lower fat mass as well as higher mitochondrial biogenesis in skeletal muscle.

Additionally, qRT-PCR results on muscle from mice treated with BAY 41-8543 reveal significantly increased expression of the mitochondrial marker UCP3 and PGC-1α. *In vitro* experiments have pointed out that the NP/cGMP pathway stimulates mitochondrial biogenesis (Mitsuishi et al., 2008). In human myocytes, the NP/cGMP signaling pathway activates UCP3 and ATP/ADP translocase 1, which increases basal proton leak and energy uncoupling (Larsen et al., 2011). Furthermore, studies of Deshmukh et al. have shown a direct effect of cGMP on glucose uptake into muscle. Activation of the cGMP signaling in *ex vivo* human muscle strip increases cGMP levels and insulin–independent glucose transport and glycogen synthesis (Deshmukh et al., 2010). Similarly, mice treated with the sGC stimulator have increased mRNA expression of marker involved in glucose and lipid uptake, as well as fatty acid metabolism.

Skeletal muscles of mammalians contain myofibers that differ in mitochondrial content and contraction as well as metabolic properties. The most informative methods to describe muscle fiber types are based on specific myosin profiles, especially the myosin heavy chain (MHC). The comparison between slow (type I, slow twitch, MHCI) muscles and fast (type II, fast twitch, MHCIIa, IIb, IIx) muscles reveal that slow muscles are high in capillary density and mitochondrial volume, contain greater proportions of aerobic enzymes and are generally fatigue resistant (Koerker et al., 1990). It is widely accepted that healthy skeletal muscle can easily switch between glucose and fat oxidation and use fat as a source for energy. Interestingly, slow muscles have a greater sensitivity to insulin when compared to fast muscle phenotypes. Recent studies reported that MHC expression can be influenced by physical activity (Klitgaard et al., 1990; Minetto et al., 2013; Mosole et al., 2014), aging (Klitgaard et al., 1990; Mosole et al., 2014; Short et al., 2005; Vandervoort, 2002), and diet or obesity (Kriketos et al., 1996; Krotkiewski and Bjorntorp, 1986; Lillioja et al., 1987; Matsakas and Patel, 2009; Tanner et al., 2002). In a HFD study, it has been shown that fibers expressing MHC type I in rodent and human muscles are reduced, suggesting a decrease in overall oxidative capacity, insulin sensitivity and glucose tolerance (Kriketos et al., 1996; Lillioja et al., 1987).

In the 12-week study performed in this thesis, HFD increases albeit not significantly- the expression of MHCI, but does not affect expression of marker proteins for the fast twitch muscles. Interestingly, treatment with the sGC stimulator and HFD significantly increases the expression of MHCI, MHCIIa and MHCIIb. These results suggest that stimulation of sGC affects the muscle fiber type towards slow muscle, which are more sensitive to insulin. Additionally, the glucose tolerance test also reveals a greater glucose clearance in mice treated with the sGC stimulator, which argues for a higher insulin sensitivity. Another study on mice fed a HFD has demonstrated that HFD changed the muscle transcriptome and that the level of slow working muscle is increased (MHCI). This effect was explained by an increased expression of PGC-1α as an important regulator for muscle fiber type determination (de Lange et al., 2006; de Wilde et al., 2008). As described before, mice co-fed a HFD and the sGC stimulator also express more *PGC-1α* in muscles. Of note, the muscle study has its own limitations. Entire calf muscles were analyzed for MHC expression. The muscle, however, also includes soleus that expresses classical marker of type I fibers, and gastrocnemius that expresses low levels of MHCI and higher levels of MHC type II (Lin et al., 2002). Therefore, it cannot be ruled out that during RNA isolation different rates of soleus or gastrocnemius muscle were used, that may result in misleading expression levels, leading to minor effects.

To sum up, mice treated with the sGC stimulator exhibit increased lipid uptake, but are characterized by a reduced lipid storage. Interestingly, the stimulation with the sGC stimulator leads to a muscle fiber type switch and an increased mitochondrial biogenesis in muscle.

4.3.3 sGC stimulation as a potential therapeutic approach against obesity

Since obesity has reached pandemic proportions, an urgent need for reliable therapies is necessary. Currently, only two anti-obesity drugs are available in Europe; Orlistat and Liraglutide. Orlistat is a lipase blocker that reduces hydrolysation and absorption of fat by inhibition of pancreatic lipases. (Hogan et al., 1987). It is associated with gastrointestinal side effects such as cramps, flatulence and fatty stools (Lucas and Kaplan-Machlis, 2001). Since 2015, the GLP-1 analog Liraglutide is available (Pi-Sunyer et al., 2015a; Pi-Sunyer et al., 2015b). This drug imitates glucagon-like 1 peptide (GLP-1), an incretin hormone released by cells located in the ileum and colon (Flock et al., 2007; Hadjiyanni and Drucker, 2007; Yamada et al., 2008). This drug is a promising candidate to fight obesity due to numerous physiological effects: it increases insulin secretion, decreases glucagon secretion, slows gastric emptying and decreases appetite (Turton et al., 1996). Nonetheless, because of the low body weight reduction and the intense side effects, both drugs have limitations as anti-obesity drugs. Therefore, new potential drug targets need to be identified.

One such candidate to act as potential target for a new anti-obesity drugs is BAT. It is described that 60-100 g of activated BAT could burn 3-4 kg of fat per year (Virtanen et al., 2009). Beiroa et al. have investigated the effects of GLP-1 agonist on BAT thermogenesis and browning (Beiroa et al., 2014). A direct injection of Liraglutide in mice stimulates BAT thermogenesis and adipocytes browning independent of nutrient intake. In a human study on obese type 2 diabetic patients, treatment with Liraglutide for one year led to an increased in EE (Beiroa et al., 2014). In another study, Liraglutide affected the proliferation and differentiation of human adipose stem cells from subcutaneous adipose tissue. Liraglutide significantly reduced glucose uptake as well as intracellular lipid accumulation (Beiroa et al., 2014). Both studies clearly show the promising effects of these drugs on EE and adipose tissue differentiation, but still these drug show low body weight reduction and the intense side effects in long-term studies (Pi-Sunyer et al., 2015a; Pi-Sunyer et al., 2015b).

The sGC/cGMP pathway could represent another important target for anti-obesity drugs. It is an important signaling cascade that can be regulated at several levels and thus, the involvement of sGC in metabolism was investigated in detail.

This cascade starts with the endogenous ligand of sGC, NO. Organic nitrates for example have been used for more than 100 years to treat angina pectoris. NO treatment leads to an increased differentiation of BAs (Nisoli et al., 1998). NO is volatile and acts in the vascular system. However, a BAT specific treatment with a NO-analog against obesity is not possible due to nitrate tolerance after a long–term treatment (Munzel et al., 2014).

Another, well studied, enhancers of cGMP production are NPs. NPs activate NPR-A and NPR-B and have been shown to counteract in DIO as well as increase the expression of thermogenic markers in inducible BAs. Furthermore, they are capable of increasing EE in mice with concomitant browning of WAT (Bordicchia et al., 2012; Miyashita et al., 2009). A new designer NP, CD-NP, also activated cGMP production and promoted adipogenesis, as well as increased thermogenic markers in BAs (Glode et al., 2017). Mice treated 10 days with CD-NP showed increased browning capacity, but in this study divergent effects were observed depending on the duration of treatment (Glode et al., 2017). Recently, it has been shown that decreased expression of the NPRs in adipose tissue is associated with obesity, glucose intolerance and insulin resistance in humans (Kovacova et al., 2016). BNP, as one candidate of NPs, has been used as a drug to treat acute decompensated heart failure. Use of BNP might not be suitable for all obese patients as its safety has been questioned (Sackner-Bernstein et al., 2005a; Sackner-Bernstein et al., 2005b). An effect of administered NPs on body weight in clinical trials has not been published so far. Currently, there are two ongoing studies investigating the effects of NPs on metabolism.

Targeting cGMP signaling can be achieved not only by enhancing cGMP production, but also through inhibiting endogenous cGMP breakdown. One such therapeutically relevant target is PDE5. Sildenafil, a clinically approved PDE5 inhibitor, has been shown to increase intracellular cGMP levels (Turko et al., 1999).

Members of PDE5 inhibitors have been used mainly for erectile dysfunction for several years (Gareri et al., 2014; Salvi et al., 2004). Short-term treatment with Sildenafil results in browning, while chronic treatment results in less weight gain in mice on a HFD (Ayala et al., 2007; Mitschke et al., 2013). Sildenafil has adverse effects like headache, flushing, indigestion, blurred vision and most notably, it interacts with agents that lower blood pressure such as nitrates, sGC stimulator or alpha blockers. Furthermore, an increased risk of melanoma has also been reported (Kloner, 2004; Kloner et al., 2004; Schwartz and Kloner, 2010).

Therefore, alternative strategies to increase cGMP signaling in adipocytes are necessary for develop a viable anti-obesity therapy without or with less side effects. To increase intracellular cGMP levels via the sGC pathway, a new drug class was used: sGC stimulator. These compounds stimulate sGC in a heme-dependent manner and show a strong synergism with NO (Stasch and Hobbs, 2009). Soluble GC stimulation can be achieved even when the endogenous NO/cGMP signaling is impaired, due to reduced bioavailability of NO. Treatment of obese patients with a sGC stimulator could synergistically work with NO and consequently boost lipolysis in subcutaneous adipose tissue and therby decrease weight gain. A study on obese patients showed that gene expression and protein levels of eNOS are increased, but HSL protein levels are decreased compared to lean patient (Elizalde et al., 2000). This suggests that increased NO production (by eNOS) and decreased HSL levels may impede lipolysis in subcutaneous adipose tissue during obesity and might help in weight reduction (Elizalde et al., 2000).

The compound used in this study is chemically related to Riociguat, which is used for pulmonary hypertension and shows a favorable safety profile (Frey et al., 2011; Ghofrani et al., 2013b). Side effects, such as hypotension, headache, diarrhea and dizziness have been reported in patients treated with 2.5 mg of Riociguat, thrice a day (Ghofrani et al., 2013b; Ghofrani et al., 2016). Since patients with obesity were excluded from these studies, the effects of Riociguat in obese human subjects cannot be estimated. Notably, all the patients in the Riociguat clinical trial had a normal body weight (Ghofrani et al., 2013a; Ghofrani et al., 2013b).

In addition, patients suffering from pulmonary hypertension rather tend to have a lower body weight because of their severe disease. A significant change in body weight was not observed in the clinical trials (Ghofrani et al., 2013a; Ghofrani et al., 2013b; Ghofrani et al., 2016; Ghofrani et al., 2013c; Ghofrani et al., 2015).

Nevertheless, the sGC stimulator is a promising candidate as anti-obesity drug as it increases BAs activity and induces browning in WATi after sGC stimulation in mice (Figure 35). Moreover, sGC stimulation counteracts DIO-induced pathologies even in already established murine obesity, by increasing energy expenditure. Stimulation of sGC also results in increased lipid uptake and utilization, mainly by BAT. Overall, sGC stimulation leads to reduced body weight and improved metabolic phenotype in mice with DIO. Additionally, comorbidities of overweight like fatty liver and insulin resistance are curtailed after sGC stimulation.

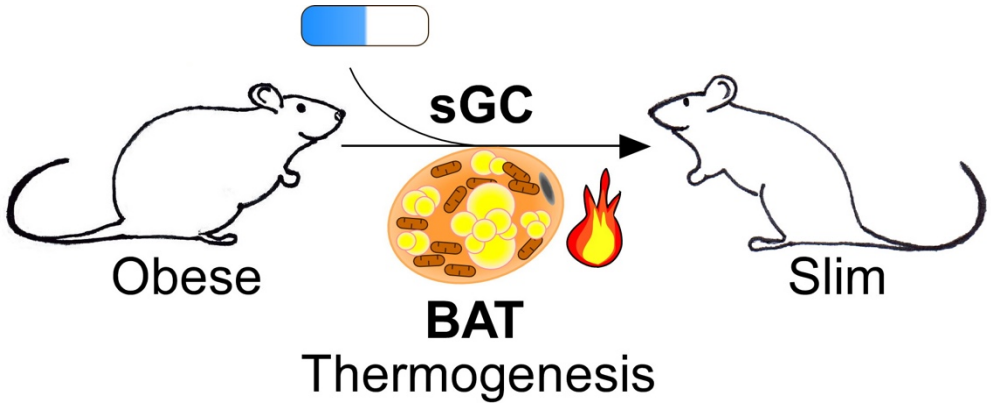

Figure 35: Pharmagological sGC stimulation counteracts against obesity.
Graphic overview about the effect of the pharmacological stimulation of sGC on mice fed a HFD.

In summation, sGC stimulation represents an innovative pharmacological principle, with sGC stimulators as potential candidates for developing viable anti-obesity therapies.

5 Summary

Obesity is a worldwide health problem characterized by a chronic positive energy balance. The excess energy is stored primarily as lipids (TGs) in white adipose tissue (WAT). In contrast, brown adipose tissue (BAT) utilizes energy to produce heat in response to cold exposure. BAT is a promising target for developing anti-obesity therapies. This thesis focusses on the role of soluble guanylate cyclase (sGC) in metabolism and identifies BAT-centered therapies.

Analysis of sGCβ_1 knockout mice revealed reduced BAT mass and less UCP1 expression in comparison to WT mice. Furthermore, differentiation and function of brown adipocytes was impaired in mice lacking the β_1 subunit of sGC. Congruently, chronic stimulation of sGC with 3 µM BAY 41-8543 during differentiation of brown adipocytes (BAs) resulted in improved adipogenic (PPARγ and aP2) and thermogenic marker (PGC-1α and UCP1) expression. Functionally, lipolysis, was also enhanced in BAs treated with BAY 41-8543.

Pharmacological stimulation of sGC during a high fat diet regime protects against weight gain. Stimulation of sGC increases function of BAs and energy consumption by UCP1 mediated thermogenesis. Importantly, BAY 41-8543 counteracts comorbidities of obesity, such as fatty liver and diabetes, even in already established obesity via increased energy expenditure. Notably, mice treated with the sGC stimulator exhibited reduced "whitening" of BAT and enhanced "browning" of WAT. In addition, sGC stimulation leads to increased expression of mitochondrial markers in muscle, which shows the overall effect of sGC stimulation. Stimulation of sGC results in increased lipid uptake and utilization by BAT, WATi, liver and muscle. Overall, sGC stimulation leads to reduced body weight gain, even in obese mice. Moreover, sGC stimulation improves metabolic phenotype in mice with diet-induced obesity (DIO), as well as on control diet (CD).

Therefore, sGC stimulators represent a novel pharmacological approach for the treatment of obesity and its comorbidities.

6 References

Adderley, S.P., Joshi, C.N., Martin, D.N., and Tulis, D.A. (2012). Phosphodiesterases Regulate BAY 41-2272-Induced VASP Phosphorylation in Vascular Smooth Muscle Cells. Front Pharmacol *3*, 10.

An, Z., Winnick, J.J., Moore, M.C., Farmer, B., Smith, M., Irimia, J.M., Roach, P.J., and Cherrington, A.D. (2012). A cyclic guanosine monophosphate-dependent pathway can regulate net hepatic glucose uptake in vivo. Diabetes *61*, 2433-2441. .

Arita, Y., Kihara, S., Ouchi, N., Takahashi, M., Maeda, K., Miyagawa, J., Hotta, K., Shimomura, I., Nakamura, T., Miyaoka, K.*, et al.* (1999). Paradoxical decrease of an adipose-specific protein, adiponectin, in obesity. Biochem Biophys Res Commun *257*, 79-83.

Asano, H., Kanamori, Y., Higurashi, S., Nara, T., Kato, K., Matsui, T., and Funaba, M. (2014). Induction of beige-like adipocytes in 3T3-L1 cells. J Vet Med Sci *76*, 57-64.

Ayala, J.E., Bracy, D.P., Julien, B.M., Rottman, J.N., Fueger, P.T., and Wasserman, D.H. (2007). Chronic treatment with sildenafil improves energy balance and insulin action in high fat-fed conscious mice. Diabetes *56*, 1025-1033.

Bandsma, R.H., Wiegman, C.H., Herling, A.W., Burger, H.J., ter Harmsel, A., Meijer, A.J., Romijn, J.A., Reijngoud, D.J., and Kuipers, F. (2001). Acute inhibition of glucose-6-phosphate translocator activity leads to increased de novo lipogenesis and development of hepatic steatosis without affecting VLDL production in rats. Diabetes *50*, 2591-2597.

Barnard, T. (1977). Brown adipose tissue as an effector of nonshivering thermogenesis. Experientia *33*, 1124-1126.

Bartelt, A., Bruns, O.T., Reimer, R., Hohenberg, H., Ittrich, H., Peldschus, K., Kaul, M.G., Tromsdorf, U.I., Weller, H., Waurisch, C.*, et al.* (2011). Brown adipose tissue activity controls triglyceride clearance. Nat Med *17*, 200-205.

Bartelt, A., and Heeren, J. (2014). Adipose tissue browning and metabolic health. Nat Rev Endocrinol *10*, 24-36.

Beiroa, D., Imbernon, M., Gallego, R., Senra, A., Herranz, D., Villarroya, F., Serrano, M., Ferno, J., Salvador, J., Escalada, J.*, et al.* (2014). GLP-1 agonism stimulates brown adipose tissue thermogenesis and browning through hypothalamic AMPK. Diabetes *63*, 3346-3358.

Bellingham, M., and Evans, T.J. (2007). The alpha2beta1 isoform of guanylyl cyclase mediates plasma membrane localized nitric oxide signalling. Cell Signal *19*, 2183-2193. Epub 2007 Jun 2129.

Berg, A.H., Combs, T.P., Du, X., Brownlee, M., and Scherer, P.E. (2001). The adipocyte-secreted protein Acrp30 enhances hepatic insulin action. Nat Med *7*, 947-953.

Biel, M., Zong, X., Ludwig, A., Sautter, A., and Hofmann, F. (1999). Structure and function of cyclic nucleotide-gated channels. Rev Physiol Biochem Pharmacol *135*, 151-171.

Birkenfeld, A.L., Lee, H.Y., Majumdar, S., Jurczak, M.J., Camporez, J.P., Jornayvaz, F.R., Frederick, D.W., Guigni, B., Kahn, M., Zhang, D.*, et al.* (2011). Influence of the hepatic eukaryotic initiation factor 2alpha (eIF2alpha) endoplasmic reticulum (ER) stress response pathway on insulin-mediated ER stress and hepatic and peripheral glucose metabolism. J Biol Chem *286*, 36163-36170.

Birkenfeld, A.L., and Shulman, G.I. (2014). Nonalcoholic fatty liver disease, hepatic insulin resistance, and type 2 diabetes. Hepatology *59*, 713-723.

Blondin, D.P., Labbe, S.M., Tingelstad, H.C., Noll, C., Kunach, M., Phoenix, S., Guerin, B., Turcotte, E.E., Carpentier, A.C., Richard, D.*, et al.* (2014). Increased brown adipose tissue oxidative capacity in cold-acclimated humans. J Clin Endocrinol Metab *99*, E438-446.

Bocciardi, R., Giorda, R., Buttgereit, J., Gimelli, S., Divizia, M.T., Beri, S., Garofalo, S., Tavella, S., Lerone, M., Zuffardi, O.*, et al.* (2007). Overexpression of the C-type natriuretic peptide (CNP) is associated with overgrowth and bone anomalies in an individual with balanced t(2;7) translocation. Hum Mutat *28*, 724-731.

Bogacka, I., Xie, H., Bray, G.A., and Smith, S.R. (2005). Pioglitazone induces mitochondrial biogenesis in human subcutaneous adipose tissue in vivo. Diabetes *54*, 1392-1399.

Bordicchia, M., Liu, D., Amri, E.Z., Ailhaud, G., Dessi-Fulgheri, P., Zhang, C., Takahashi, N., Sarzani, R., and Collins, S. (2012). Cardiac natriuretic peptides act via p38 MAPK to induce the brown fat thermogenic program in mouse and human adipocytes. J Clin Invest *122*, 1022-1036.

Bostrom, P., Wu, J., Jedrychowski, M.P., Korde, A., Ye, L., Lo, J.C., Rasbach, K.A., Bostrom, E.A., Choi, J.H., Long, J.Z.*, et al.* (2012). A PGC1-alpha-dependent myokine that drives brown-fat-like development of white fat and thermogenesis. Nature *481*, 463-468.

Boswell-Smith, V., Spina, D., and Page, C.P. (2006). Phosphodiesterase inhibitors. Br J Pharmacol *147 Suppl 1*, S252-257.

Bowman, A., Gillespie, J.S., and Soares-da-Silva, P. (1986). A comparison of the action of the endothelium-derived relaxant factor and the inhibitory factor from the bovine retractor penis on rabbit aortic smooth muscle. Br J Pharmacol *87*, 175-181.

Bradford, M.M. (1976). A rapid and sensitive method for the quantitation of microgram quantities of protein utilizing the principle of protein-dye binding. Anal Biochem *72*, 248-254.

Budworth, J., Meillerais, S., Charles, I., and Powell, K. (1999). Tissue distribution of the human soluble guanylate cyclases. Biochem Biophys Res Commun *263*, 696-701.

Cannon, B., and Nedergaard, J. (1996). Adrenergic regulation of brown adipocyte differentiation. Biochem Soc Trans *24*, 407-412.

Cannon, B., and Nedergaard, J. (2004). Brown adipose tissue: function and physiological significance. Physiol Rev *84*, 277-359.

Cao, W., Daniel, K.W., Robidoux, J., Puigserver, P., Medvedev, A.V., Bai, X., Floering, L.M., Spiegelman, B.M., and Collins, S. (2004). p38 mitogen-activated protein kinase is the central regulator of cyclic AMP-dependent transcription of the brown fat uncoupling protein 1 gene. Mol Cell Biol *24*, 3057-3067.

Carmiel-Haggai, M., Cederbaum, A.I., and Nieto, N. (2005). A high-fat diet leads to the progression of non-alcoholic fatty liver disease in obese rats. FASEB J *19*, 136-138.

Carmona, M.C., Hondares, E., Rodriguez de la Concepcion, M.L., Rodriguez-Sureda, V., Peinado-Onsurbe, J., Poli, V., Iglesias, R., Villarroya, F., and Giralt, M. (2005). Defective thermoregulation, impaired lipid metabolism, but preserved adrenergic induction of gene expression in brown fat of mice lacking C/EBPbeta. Biochem J *389*, 47-56.

Chang, F.J., Lemme, S., Sun, Q., Sunahara, R.K., and Beuve, A. (2005). Nitric oxide-dependent allosteric inhibitory role of a second nucleotide binding site in soluble guanylyl cyclase. J Biol Chem *280*, 11513-11519.

Chavin, K.D., Yang, S., Lin, H.Z., Chatham, J., Chacko, V.P., Hoek, J.B., Walajtys-Rode, E., Rashid, A., Chen, C.H., Huang, C.C.*, et al.* (1999). Obesity induces expression of uncoupling protein-2 in hepatocytes and promotes liver ATP depletion. J Biol Chem *274*, 5692-5700.

Choi, J.H., Banks, A.S., Estall, J.L., Kajimura, S., Bostrom, P., Laznik, D., Ruas, J.L., Chalmers, M.J., Kamenecka, T.M., Bluher, M.*, et al.* (2010). Anti-diabetic drugs inhibit obesity-linked phosphorylation of PPARgamma by Cdk5. Nature *466*, 451-456.

Choo, H.J., Kim, J.H., Kwon, O.B., Lee, C.S., Mun, J.Y., Han, S.S., Yoon, Y.S., Yoon, G., Choi, K.M., and Ko, Y.G. (2006). Mitochondria are impaired in the adipocytes of type 2 diabetic mice. Diabetologia *49*, 784-791.

Cinti, S. (2005). The adipose organ. Prostaglandins Leukot Essent Fatty Acids *73*, 9-15.

Combs, T.P., Berg, A.H., Obici, S., Scherer, P.E., and Rossetti, L. (2001). Endogenous glucose production is inhibited by the adipose-derived protein Acrp30. J Clin Invest *108*, 1875-1881.

Daff, S. (2010). NO synthase: structures and mechanisms. Nitric Oxide *23*, 1-11.

de Lange, P., Farina, P., Moreno, M., Ragni, M., Lombardi, A., Silvestri, E., Burrone, L., Lanni, A., and Goglia, F. (2006). Sequential changes in the signal transduction responses of skeletal muscle following food deprivation. FASEB J *20*, 2579-2581.

de Wilde, J., Mohren, R., van den Berg, S., Boekschoten, M., Dijk, K.W., de Groot, P., Muller, M., Mariman, E., and Smit, E. (2008). Short-term high fat-feeding results in morphological and metabolic adaptations in the skeletal muscle of C57BL/6J mice. Physiol Genomics *32*, 360-369.

Degerman, E., Belfrage, P., and Manganiello, V.C. (1997). Structure, localization, and regulation of cGMP-inhibited phosphodiesterase (PDE3). J Biol Chem *272*, 6823-6826.

Derbyshire, E.R., and Marletta, M.A. (2012). Structure and regulation of soluble guanylate cyclase. Annual Review of Biochemistry *81*, 533-559.

Deshmukh, A.S., Long, Y.C., de Castro Barbosa, T., Karlsson, H.K., Glund, S., Zavadoski, W.J., Gibbs, E.M., Koistinen, H.A., Wallberg-Henriksson, H., and Zierath, J.R. (2010). Nitric oxide increases cyclic GMP levels, AMP-activated protein kinase (AMPK)alpha1-specific activity and glucose transport in human skeletal muscle. Diabetologia *53*, 1142-1150.

Duplain, H., Burcelin, R., Sartori, C., Cook, S., Egli, M., Lepori, M., Vollenweider, P., Pedrazzini, T., Nicod, P., Thorens, B.*, et al.* (2001). Insulin resistance, hyperlipidemia, and hypertension in mice lacking endothelial nitric oxide synthase. Circulation *104*, 342-345.

Elizalde, M., Ryden, M., van Harmelen, V., Eneroth, P., Gyllenhammar, H., Holm, C., Ramel, S., Olund, A., Arner, P., and Andersson, K. (2000). Expression of nitric oxide synthases in subcutaneous adipose tissue of nonobese and obese humans. J Lipid Res *41*, 1244-1251.

Fernandez-Marcos, P.J., and Auwerx, J. (2011). Regulation of PGC-1alpha, a nodal regulator of mitochondrial biogenesis. Am J Clin Nutr *93*, 884S-890.

Fisher, F.M., Kleiner, S., Douris, N., Fox, E.C., Mepani, R.J., Verdeguer, F., Wu, J., Kharitonenkov, A., Flier, J.S., Maratos-Flier, E.*, et al.* (2012). FGF21 regulates PGC-1alpha and browning of white adipose tissues in adaptive thermogenesis. Genes Dev *26*, 271-281.

Flock, G., Baggio, L.L., Longuet, C., and Drucker, D.J. (2007). Incretin receptors for glucagon-like peptide 1 and glucose-dependent insulinotropic polypeptide are essential for the sustained metabolic actions of vildagliptin in mice. Diabetes *56*, 3006-3013.

Forstermann, U., and Sessa, W.C. (2012). Nitric oxide synthases: regulation and function. Eur Heart J *33*, 829-837.

Francis, S.H., Busch, J.L., and Corbin, J.D. (2010a). cGMP-dependent protein kinases and cGMP phosphodiesterases in nitric oxide and cGMP action. Pharmacol Rev *62*, 525-563.

Francis, S.H., Sekhar, K.R., Ke, H., and Corbin, J.D. (2010b). Inhibition of cyclic nucleotide phosphodiesterases by methylxanthines and related compounds. Handb Exp Pharmacol, 93-133.

Frayn, K.N., Arner, P., and Yki-Jarvinen, H. (2006). Fatty acid metabolism in adipose tissue, muscle and liver in health and disease. Essays Biochem *42*, 89-103.

Frey, R., Muck, W., Kirschbaum, N., Kratzschmar, J., Weimann, G., and Wensing, G. (2011). Riociguat (BAY 63-2521) and warfarin: a pharmacodynamic and pharmacokinetic interaction study. J Clin Pharmacol *51*, 1051-1060.

Friebe, A., and Koesling, D. (2009a). The function of NO-sensitive guanylyl cyclase: what we can learn from genetic mouse models. Nitric Oxide *21*, 149-156. doi: 110.1016/j.niox.2009.1007.1004. Epub 2009 Jul 1025.

Friebe, A., and Koesling, D. (2009b). The function of NO-sensitive guanylyl cyclase: what we can learn from genetic mouse models. Nitric Oxide *21*, 149-156.

Friebe, A., Mergia, E., Dangel, O., Lange, A., and Koesling, D. (2007). Fatal gastrointestinal obstruction and hypertension in mice lacking nitric oxide-sensitive guanylyl cyclase. Proceedings of the National Academy of Sciences of the United States of America *104*, 7699-7704.

Fruebis, J., Tsao, T.S., Javorschi, S., Ebbets-Reed, D., Erickson, M.R., Yen, F.T., Bihain, B.E., and Lodish, H.F. (2001). Proteolytic cleavage product of 30-kDa adipocyte complement-related protein increases fatty acid oxidation in muscle and causes weight loss in mice. Proc Natl Acad Sci U S A *98*, 2005-2010.

Galic, S., Oakhill, J.S., and Steinberg, G.R. (2010). Adipose tissue as an endocrine organ. Mol Cell Endocrinol *316*, 129-139.

Gao, M., Ma, Y., and Liu, D. (2015). High-fat diet-induced adiposity, adipose inflammation, hepatic steatosis and hyperinsulinemia in outbred CD-1 mice. PLoS One *10*, e0119784.

Garbers, D.L., Chrisman, T.D., Wiegn, P., Katafuchi, T., Albanesi, J.P., Bielinski, V., Barylko, B., Redfield, M.M., and Burnett, J.C., Jr. (2006). Membrane guanylyl cyclase receptors: an update. Trends Endocrinol Metab *17*, 251-258.

Gareri, P., Castagna, A., Francomano, D., Cerminara, G., and De Fazio, P. (2014). Erectile dysfunction in the elderly: an old widespread issue with novel treatment perspectives. Int J Endocrinol *2014*, 878670.

Ghofrani, H.A., D'Armini, A.M., Grimminger, F., Hoeper, M.M., Jansa, P., Kim, N.H., Mayer, E., Simonneau, G., Wilkins, M.R., Fritsch, A.*, et al.* (2013a). Riociguat for the treatment of chronic thromboembolic pulmonary hypertension. N Engl J Med *369*, 319-329.

Ghofrani, H.A., Galie, N., Grimminger, F., Grunig, E., Humbert, M., Jing, Z.C., Keogh, A.M., Langleben, D., Kilama, M.O., Fritsch, A.*, et al.* (2013b). Riociguat for the treatment of pulmonary arterial hypertension. N Engl J Med *369*, 330-340.

Ghofrani, H.A., Grimminger, F., Grunig, E., Huang, Y., Jansa, P., Jing, Z.C., Kilpatrick, D., Langleben, D., Rosenkranz, S., Menezes, F.*, et al.* (2016). Predictors of long-term outcomes in patients treated with riociguat for pulmonary arterial hypertension: data from the PATENT-2 open-label, randomised, long-term extension trial. Lancet Respir Med *4*, 361-371.

Ghofrani, H.A., Simonneau, G., and Rubin, L.J. (2013c). Riociguat for pulmonary hypertension. N Engl J Med *369*, 2268.

Ghofrani, H.A., Staehler, G., Grunig, E., Halank, M., Mitrovic, V., Unger, S., Mueck, W., Frey, R., Grimminger, F., Schermuly, R.T.*, et al.* (2015). Acute effects of riociguat in borderline or manifest pulmonary hypertension associated with chronic obstructive pulmonary disease. Pulm Circ *5*, 296-304.

Gillespie, J.S., Liu, X.R., and Martin, W. (1989). The effects of L-arginine and NG-monomethyl L-arginine on the response of the rat anococcygeus muscle to NANC nerve stimulation. Br J Pharmacol *98*, 1080-1082.

Giordano, A., Tonello, C., Bulbarelli, A., Cozzi, V., Cinti, S., Carruba, M.O., and Nisoli, E. (2002). Evidence for a functional nitric oxide synthase system in brown adipocyte nucleus. FEBS Lett *514*, 135-140.

Glode, A., Naumann, J., Gnad, T., Cannone, V., Kilic, A., Burnett, J.C., Jr., and Pfeifer, A. (2017). Divergent effects of a designer natriuretic peptide CD-NP in the regulation of adipose tissue and metabolism. Mol Metab *6*, 276-287.

Gnad, T., Scheibler, S., von Kugelgen, I., Scheele, C., Kilic, A., Glode, A., Hoffmann, L.S., Reverte-Salisa, L., Horn, P., Mutlu, S.*, et al.* (2014). Adenosine activates brown adipose tissue and recruits beige adipocytes via A2A receptors. Nature *516*, 395-399.

Gudi, T., Lohmann, S.M., and Pilz, R.B. (1997). Regulation of gene expression by cyclic GMP-dependent protein kinase requires nuclear translocation of the kinase: identification of a nuclear localization signal. Mol Cell Biol *17*, 5244-5254.

Haas, B., Mayer, P., Jennissen, K., Scholz, D., Berriel Diaz, M., Bloch, W., Herzig, S., Fassler, R., and Pfeifer, A. (2009). Protein kinase G controls brown fat cell differentiation and mitochondrial biogenesis. Sci Signal *2*, ra78.

Hadjiyanni, I., and Drucker, D.J. (2007). Glucagon-like peptide 1 and type 1 diabetes: NOD ready for prime time? Endocrinology *148*, 5133-5135.

Harms, M., and Seale, P. (2013). Brown and beige fat: development, function and therapeutic potential. Nat Med *19*, 1252-1263.

Hausman, D.B., Loh, M.Y., Flatt, W.P., and Martin, R.J. (1997). Adipose tissue expansion and the development of obesity: influence of dietary fat type. Asia Pac J Clin Nutr *6*, 49-55.

Hoffmann, L.S., Schmidt, P.M., Keim, Y., Schaefer, S., Schmidt, H.H., and Stasch, J.P. (2009). Distinct molecular requirements for activation or stabilization of soluble guanylyl cyclase upon haem oxidation-induced degradation. Br J Pharmacol *157*, 781-795.

Hofmann, F. (2005). The biology of cyclic GMP-dependent protein kinases. J Biol Chem *280*, 1-4.

Hofmann, F., Feil, R., Kleppisch, T., and Schlossmann, J. (2006). Function of cGMP-dependent protein kinases as revealed by gene deletion. Physiol Rev *86*, 1-23.

Hogan, S., Fleury, A., Hadvary, P., Lengsfeld, H., Meier, M.K., Triscari, J., and Sullivan, A.C. (1987). Studies on the antiobesity activity of tetrahydrolipstatin, a potent and selective inhibitor of pancreatic lipase. Int J Obes *11 Suppl 3*, 35-42.

Ignarro, L.J., Cirino, G., Casini, A., and Napoli, C. (1999). Nitric oxide as a signaling molecule in the vascular system: an overview. J Cardiovasc Pharmacol *34*, 879-886.

Jabs, A., Oelze, M., Mikhed, Y., Stamm, P., Kroller-Schon, S., Welschof, P., Jansen, T., Hausding, M., Kopp, M., Steven, S.*, et al.* (2015). Effect of soluble guanylyl cyclase activator and stimulator therapy on nitroglycerin-induced nitrate tolerance in rats. Vascul Pharmacol *71*, 181-191.

Jennissen, K., Siegel, F., Liebig-Gonglach, M., Hermann, M.R., Kipschull, S., van Dooren, S., Kunz, W.S., Fassler, R., and Pfeifer, A. (2012). A VASP-Rac-Soluble Guanylyl Cyclase Pathway Controls cGMP Production in Adipocytes. Sci Signal *5*, ra62.

Jespersen, N.Z., Larsen, T.J., Peijs, L., Daugaard, S., Homoe, P., Loft, A., de Jong, J., Mathur, N., Cannon, B., Nedergaard, J.*, et al.* (2013). A classical brown adipose tissue mRNA signature partly overlaps with brite in the supraclavicular region of adult humans. Cell Metab *17*, 798-805.

Kajimura, S., and Saito, M. (2013). A New Era in Brown Adipose Tissue Biology: Molecular Control of Brown Fat Development and Energy Homeostasis. Annu Rev Physiol *76*, 225-249.

Kaneko, Y., Ishikawa, T., Amano, S., and Nakayama, K. (2003). Dual effect of nitric oxide on cytosolic Ca2+ concentration and insulin secretion in rat pancreatic beta-cells. Am J Physiol Cell Physiol *284*, C1215-1222.

Kern, P.A., Di Gregorio, G.B., Lu, T., Rassouli, N., and Ranganathan, G. (2003). Adiponectin expression from human adipose tissue: relation to obesity, insulin resistance, and tumor necrosis factor-alpha expression. Diabetes *52*, 1779-1785.

Khaodhiar, L., McCowen, K.C., and Blackburn, G.L. (1999). Obesity and its comorbid conditions. Clin Cornerstone *2*, 17-31.

Kim, S.N., Jung, Y.S., Kwon, H.J., Seong, J.K., Granneman, J.G., and Lee, Y.H. (2016). Sex differences in sympathetic innervation and browning of white adipose tissue of mice. Biol Sex Differ *7*, 67.

Klish, W.J. (1995). Childhood obesity: pathophysiology and treatment. Acta Paediatr Jpn *37*, 1-6.

Klitgaard, H., Bergman, O., Betto, R., Salviati, G., Schiaffino, S., Clausen, T., and Saltin, B. (1990). Co-existence of myosin heavy chain I and IIa isoforms in human skeletal muscle fibres with endurance training. Pflugers Arch *416*, 470-472.

Kloner, R.A. (2004). Cardiovascular effects of the 3 phosphodiesterase-5 inhibitors approved for the treatment of erectile dysfunction. Circulation *110*, 3149-3155.

Kloner, R.A., Jackson, G., Emmick, J.T., Mitchell, M.I., Bedding, A., Warner, M.R., and Pereira, A. (2004). Interaction between the phosphodiesterase 5 inhibitor, tadalafil and 2 alpha-blockers, doxazosin and tamsulosin in healthy normotensive men. J Urol *172*, 1935-1940.

Koerker, D.J., Sweet, I.R., and Baskin, D.G. (1990). Insulin binding to individual rat skeletal muscles. Am J Physiol *259*, E517-523.

Kovacova, Z., Tharp, W.G., Liu, D., Wei, W., Xie, H., Collins, S., and Pratley, R.E. (2016). Adipose tissue natriuretic peptide receptor expression is related to insulin sensitivity in obesity and diabetes. Obesity (Silver Spring) *24*, 820-828.

Kozak, L.P., and Harper, M.E. (2000). Mitochondrial uncoupling proteins in energy expenditure. Annu Rev Nutr *20*, 339-363.

Kriketos, A.D., Pan, D.A., Lillioja, S., Cooney, G.J., Baur, L.A., Milner, M.R., Sutton, J.R., Jenkins, A.B., Bogardus, C., and Storlien, L.H. (1996). Interrelationships between muscle morphology, insulin action, and adiposity. Am J Physiol *270*, R1332-1339.

Krotkiewski, M., and Bjorntorp, P. (1986). Muscle tissue in obesity with different distribution of adipose tissue. Effects of physical training. Int J Obes *10*, 331-341.

Kuhn, M. (2003). Structure, regulation, and function of mammalian membrane guanylyl cyclase receptors, with a focus on guanylyl cyclase-A. Circ Res *93*, 700-709.

Kumashiro, N., Beddow, S.A., Vatner, D.F., Majumdar, S.K., Cantley, J.L., Guebre-Egziabher, F., Fat, I., Guigni, B., Jurczak, M.J., Birkenfeld, A.L.*, et al.* (2013). Targeting pyruvate carboxylase reduces gluconeogenesis and adiposity and improves insulin resistance. Diabetes *62*, 2183-2194.

Kushner, R.F., Kunigk, A., Alspaugh, M., Andronis, P.T., Leitch, C.A., and Schoeller, D.A. (1990). Validation of bioelectrical-impedance analysis as a measurement of change in body composition in obesity. Am J Clin Nutr *52*, 219-223.

Laemmli, U.K. (1970). Cleavage of structural proteins during the assembly of the head of bacteriophage T4. Nature *227*, 680-685.

Lafontan, M. (2008). Advances in adipose tissue metabolism. Int J Obes (Lond) *32 Suppl 7*, S39-51.

Larsen, F.J., Schiffer, T.A., Sahlin, K., Ekblom, B., Weitzberg, E., and Lundberg, J.O. (2011). Mitochondrial oxygen affinity predicts basal metabolic rate in humans. FASEB J *25*, 2843-2852.

Lee, H.Y., Choi, C.S., Birkenfeld, A.L., Alves, T.C., Jornayvaz, F.R., Jurczak, M.J., Zhang, D., Woo, D.K., Shadel, G.S., Ladiges, W.*, et al.* (2010). Targeted expression of catalase to mitochondria prevents age-associated reductions in mitochondrial function and insulin resistance. Cell Metab *12*, 668-674.

Lee, H.Y., Gattu, A.K., Camporez, J.P., Kanda, S., Guigni, B., Kahn, M., Zhang, D., Galbo, T., Birkenfeld, A.L., Jornayvaz, F.R.*, et al.* (2014a). Muscle-specific activation of Ca(2+)/calmodulin-dependent protein kinase IV increases whole-body insulin action in mice. Diabetologia *57*, 1232-1241.

Lee, P., Smith, S., Linderman, J., Courville, A.B., Brychta, R.J., Dieckmann, W., Werner, C.D., Chen, K.Y., and Celi, F.S. (2014b). Temperature-acclimated brown adipose tissue modulates insulin sensitivity in humans. Diabetes *63*, 3686-3698.

Levy, I., Horvath, A., Azevedo, M., de Alexandre, R.B., and Stratakis, C.A. (2011). Phosphodiesterase function and endocrine cells: links to human disease and roles in tumor development and treatment. Curr Opin Pharmacol *11*, 689-697.

Li, Z., Xi, X., Gu, M., Feil, R., Ye, R.D., Eigenthaler, M., Hofmann, F., and Du, X. (2003). A stimulatory role for cGMP-dependent protein kinase in platelet activation. Cell *112*, 77-86.

Lidell, M.E., Betz, M.J., Dahlqvist Leinhard, O., Heglind, M., Elander, L., Slawik, M., Mussack, T., Nilsson, D., Romu, T., Nuutila, P.*, et al.* (2013). Evidence for two types of brown adipose tissue in humans. Nat Med *19*, 631-634.

Lillioja, S., Young, A.A., Culter, C.L., Ivy, J.L., Abbott, W.G., Zawadzki, J.K., Yki-Jarvinen, H., Christin, L., Secomb, T.W., and Bogardus, C. (1987). Skeletal muscle capillary density and fiber type are possible determinants of in vivo insulin resistance in man. J Clin Invest *80*, 415-424.

Lin, J., Wu, H., Tarr, P.T., Zhang, C.Y., Wu, Z., Boss, O., Michael, L.F., Puigserver, P., Isotani, E., Olson, E.N.*, et al.* (2002). Transcriptional co-activator PGC-1 alpha drives the formation of slow-twitch muscle fibres. Nature *418*, 797-801.

Lobstein, T., Jackson-Leach, R., Moodie, M.L., Hall, K.D., Gortmaker, S.L., Swinburn, B.A., James, W.P., Wang, Y., and McPherson, K. (2015). Child and adolescent obesity: part of a bigger picture. Lancet *385*, 2510-2520.

Long, J.Z., Svensson, K.J., Tsai, L., Zeng, X., Roh, H.C., Kong, X., Rao, R.R., Lou, J., Lokurkar, I., Baur, W.*, et al.* (2014). A smooth muscle-like origin for beige adipocytes. Cell Metab *19*, 810-820.

Lowell, B.B., and Spiegelman, B.M. (2000). Towards a molecular understanding of adaptive thermogenesis. Nature *404*, 652-660.

Lucas, K.A., Pitari, G.M., Kazerounian, S., Ruiz-Stewart, I., Park, J., Schulz, S., Chepenik, K.P., and Waldman, S.A. (2000). Guanylyl cyclases and signaling by cyclic GMP. Pharmacol Rev *52*, 375-414.

Lucas, K.H., and Kaplan-Machlis, B. (2001). Orlistat--a novel weight loss therapy. Ann Pharmacother *35*, 314-328.

Lutz, S.Z., Hennige, A.M., Feil, S., Peter, A., Gerling, A., Machann, J., Krober, S.M., Rath, M., Schurmann, A., Weigert, C.*, et al.* (2011). Genetic ablation of cGMP-dependent protein kinase type I causes liver inflammation and fasting hyperglycemia. Diabetes *60*, 1566-1576.

Ma, X., Sayed, N., Baskaran, P., Beuve, A., and van den Akker, F. (2008). PAS-mediated dimerization of soluble guanylyl cyclase revealed by signal transduction histidine kinase domain crystal structure. J Biol Chem *283*, 1167-1178.

Maeda, N., Shimomura, I., Kishida, K., Nishizawa, H., Matsuda, M., Nagaretani, H., Furuyama, N., Kondo, H., Takahashi, M., Arita, Y.*, et al.* (2002). Diet-induced insulin resistance in mice lacking adiponectin/ACRP30. Nat Med *8*, 731-737.

Massberg, S., Sausbier, M., Klatt, P., Bauer, M., Pfeifer, A., Siess, W., Fassler, R., Ruth, P., Krombach, F., and Hofmann, F. (1999). Increased adhesion and aggregation of platelets lacking cyclic guanosine 3',5'-monophosphate kinase I. J Exp Med *189*, 1255-1264.

Matsakas, A., and Patel, K. (2009). Intracellular signalling pathways regulating the adaptation of skeletal muscle to exercise and nutritional changes. Histol Histopathol *24*, 209-222.

Matthias, A., Ohlson, K.B., Fredriksson, J.M., Jacobsson, A., Nedergaard, J., and Cannon, B. (2000). Thermogenic responses in brown fat cells are fully UCP1-dependent. UCP2 or UCP3 do not substitute for UCP1 in adrenergically or fatty scid-induced thermogenesis. J Biol Chem *275*, 25073-25081.

Mayer, B., and Hemmens, B. (1997). Biosynthesis and action of nitric oxide in mammalian cells. Trends Biochem Sci *22*, 477-481.

Minetto, M.A., Botter, A., Bottinelli, O., Miotti, D., Bottinelli, R., and D'Antona, G. (2013). Variability in muscle adaptation to electrical stimulation. Int J Sports Med *34*, 544-553.

Mitschke, M.M., Hoffmann, L.S., Gnad, T., Scholz, D., Kruithoff, K., Mayer, P., Haas, B., Sassmann, A., Pfeifer, A., and Kilic, A. (2013). Increased cGMP promotes healthy expansion and browning of white adipose tissue. FASEB J *27*, 1621-1630.

Mitsuishi, M., Miyashita, K., and Itoh, H. (2008). cGMP rescues mitochondrial dysfunction induced by glucose and insulin in myocytes. Biochem Biophys Res Commun *367*, 840-845.

Mittendorf, J., Weigand, S., Alonso-Alija, C., Bischoff, E., Feurer, A., Gerisch, M., Kern, A., Knorr, A., Lang, D., Muenter, K.*, et al.* (2009). Discovery of riociguat (BAY 63-2521): a potent, oral stimulator of soluble guanylate cyclase for the treatment of pulmonary hypertension. ChemMedChem *4*, 853-865.

Miyashita, K., Itoh, H., Tsujimoto, H., Tamura, N., Fukunaga, Y., Sone, M., Yamahara, K., Taura, D., Inuzuka, M., Sonoyama, T.*, et al.* (2009). Natriuretic Peptides/cGMP/cGMP-Dependent Protein Kinase Cascades Promote Muscle Mitochondrial Biogenesis and Prevent Obesity. Diabetes *58*, 2880-2892.

Monica, F.Z., Rojas-Moscoso, J., Porto, M., Schenka, A.A., Antunes, E., Cogo, J.C., and De Nucci, G. (2012). Immunohistochemical and functional characterization of nitric oxide signaling pathway in isolated aorta from Crotalus durissus terrificus. Comp Biochem Physiol C Toxicol Pharmacol *155*, 433-439.

Morino, K., Petersen, K.F., Sono, S., Choi, C.S., Samuel, V.T., Lin, A., Gallo, A., Zhao, H., Kashiwagi, A., Goldberg, I.J.*, et al.* (2012). Regulation of mitochondrial biogenesis by lipoprotein lipase in muscle of insulin-resistant offspring of parents with type 2 diabetes. Diabetes *61*, 877-887.

Moro, C., Klimcakova, E., Lafontan, M., Berlan, M., and Galitzky, J. (2007). Phosphodiesterase-5A and neutral endopeptidase activities in human adipocytes do not control atrial natriuretic peptide-mediated lipolysis. Br J Pharmacol *152*, 1102-1110.

Mosole, S., Carraro, U., Kern, H., Loefler, S., Fruhmann, H., Vogelauer, M., Burggraf, S., Mayr, W., Krenn, M., Paternostro-Sluga, T.*, et al.* (2014). Long-term high-level exercise promotes muscle reinnervation with age. J Neuropathol Exp Neurol *73*, 284-294.

Munzel, T., Sayegh, H., Freeman, B.A., Tarpey, M.M., and Harrison, D.G. (1995). Evidence for enhanced vascular superoxide anion production in nitrate tolerance. A novel mechanism underlying tolerance and cross-tolerance. J Clin Invest *95*, 187-194.

Munzel, T., Steven, S., and Daiber, A. (2014). Organic nitrates: update on mechanisms underlying vasodilation, tolerance and endothelial dysfunction. Vascul Pharmacol *63*, 105-113.

Murad, F. (2006). Shattuck Lecture. Nitric oxide and cyclic GMP in cell signaling and drug development. N Engl J Med *355*, 2003-2011.

Murrell, W. (1879). Nitro-glycerine as a remedy for angina pectoris. Lancet *1:80*.

Nakayama, K., Miyashita, H., Yanagisawa, Y., and Iwamoto, S. (2013). Seasonal effects of UCP1 gene polymorphism on visceral fat accumulation in Japanese adults. PLoS One *8*, e74720.

Nedergaard, J., Petrovic, N., Lindgren, E.M., Jacobsson, A., and Cannon, B. (2005). PPAR gamma in the control of brown adipocyte differentiation. Biochimica Et Biophysica Acta-Molecular Basis of Disease *1740*, 293-304.

Neuschafer-Rube, F., Lieske, S., Kuna, M., Henkel, J., Perry, R.J., Erion, D.M., Pesta, D., Willmes, D.M., Brachs, S., von Loeffelholz, C.*, et al.* (2014). The mammalian INDY homolog is induced by CREB in a rat model of type 2 diabetes. Diabetes *63*, 1048-1057.

Nisoli, E., Clementi, E., Paolucci, C., Cozzi, V., Tonello, C., Sciorati, C., Bracale, R., Valerio, A., Francolini, M., Moncada, S.*, et al.* (2003). Mitochondrial biogenesis in mammals: the role of endogenous nitric oxide. Science *299*, 896-899.

Nisoli, E., Clementi, E., Tonello, C., Sciorati, C., Briscini, L., and Carruba, M.O. (1998). Effects of nitric oxide on proliferation and differentiation of rat brown adipocytes in primary cultures. Br J Pharmacol *125*, 888-894.

Nossaman, B., Pankey, E., and Kadowitz, P. (2012). Stimulators and activators of soluble guanylate cyclase: review and potential therapeutic indications. Crit Care Res Pract *2012*, 290805.

Obata, H., Yanagawa, B., Tanaka, K., Ohnishi, S., Kataoka, M., Miyahara, Y., Ishibashi-Ueda, H., Kodama, M., Aizawa, Y., Kangawa, K.*, et al.* (2007). CNP infusion attenuates cardiac dysfunction and inflammation in myocarditis. Biochem Biophys Res Commun *356*, 60-66.

Okamatsu-Ogura, Y., Fukano, K., Tsubota, A., Uozumi, A., Terao, A., Kimura, K., and Saito, M. (2013). Thermogenic ability of uncoupling protein 1 in beige adipocytes in mice. PLoS One *8*, e84229.

Ouchi, N., Parker, J.L., Lugus, J.J., and Walsh, K. (2011). Adipokines in inflammation and metabolic disease. Nat Rev Immunol *11*, 85-97.

Ouellet, V., Labbe, S.M., Blondin, D.P., Phoenix, S., Guerin, B., Haman, F., Turcotte, E.E., Richard, D., and Carpentier, A.C. (2012). Brown adipose tissue oxidative metabolism contributes to energy expenditure during acute cold exposure in humans. J Clin Invest *122*, 545-552.

Perry, R.J., Kim, T., Zhang, X.M., Lee, H.Y., Pesta, D., Popov, V.B., Zhang, D., Rahimi, Y., Jurczak, M.J., Cline, G.W.*, et al.* (2013). Reversal of hypertriglyceridemia, fatty liver disease, and insulin resistance by a liver-targeted mitochondrial uncoupler. Cell Metab *18*, 740-748.

Petrovic, N., Walden, T.B., Shabalina, I.G., Timmons, J.A., Cannon, B., and Nedergaard, J. (2010). Chronic peroxisome proliferator-activated receptor gamma (PPARgamma) activation of epididymally derived white adipocyte

cultures reveals a population of thermogenically competent, UCP1-containing adipocytes molecularly distinct from classic brown adipocytes. J Biol Chem *285*, 7153-7164.

Pfeifer, A., Aszodi, A., Seidler, U., Ruth, P., Hofmann, F., and Fassler, R. (1996). Intestinal secretory defects and dwarfism in mice lacking cGMP-dependent protein kinase II. Science *274*, 2082-2086.

Pfeifer, A., and Hoffmann, L.S. (2015). Brown, beige, and white: the new color code of fat and its pharmacological implications. Annu Rev Pharmacol Toxicol *55*, 207-227.

Pfeifer, A., Kilic, A., and Hoffmann, L.S. (2013). Regulation of metabolism by cGMP. Pharmacol Ther *140*, 81-91.

Pfeifer, A., Klatt, P., Massberg, S., Ny, L., Sausbier, M., Hirneiss, C., Wang, G.X., Korth, M., Aszodi, A., Andersson, K.E.*, et al.* (1998). Defective smooth muscle regulation in cGMP kinase I-deficient mice. Embo J *17*, 3045-3051.

Pfeifer, A., Ruth, P., Dostmann, W., Sausbier, M., Klatt, P., and Hofmann, F. (1999). Structure and function of cGMP-dependent protein kinases. Rev Physiol Biochem Pharmacol *135*, 105-149.

Pi-Sunyer, X., Astrup, A., Fujioka, K., Greenway, F., Halpern, A., Krempf, M., Lau, D.C., le Roux, C.W., Violante Ortiz, R., Jensen, C.B.*, et al.* (2015a). A Randomized, Controlled Trial of 3.0 mg of Liraglutide in Weight Management. N Engl J Med *373*, 11-22.

Pi-Sunyer, X., Obesity, S., and Prediabetes, I. (2015b). Liraglutide in Weight Management. N Engl J Med *373*, 1781-1782.

Potter, L.R. (2011). Guanylyl cyclase structure, function and regulation. Cellular Signalling *23*, 1921-1926.

Potter, L.R., Abbey-Hosch, S., and Dickey, D.M. (2006). Natriuretic peptides, their receptors, and cyclic guanosine monophosphate-dependent signaling functions. Endocr Rev *27*, 47-72.

Roberts, L.D., Ashmore, T., Kotwica, A.O., Murfitt, S.A., Fernandez, B.O., Feelisch, M., Murray, A.J., and Griffin, J.L. (2015). Inorganic nitrate promotes the browning of white adipose tissue through the nitrate-nitrite-nitric oxide pathway. Diabetes *64*, 471-484. doi: 410.2337/db2314-0496. .

Robidoux, J., Kumar, N., Daniel, K.W., Moukdar, F., Cyr, M., Medvedev, A.V., and Collins, S. (2006). Maximal beta3-adrenergic regulation of lipolysis involves Src and epidermal growth factor receptor-dependent ERK1/2 activation. J Biol Chem *281*, 37794-37802.

Ropero, A.B., Soriano, S., Tuduri, E., Marroqui, L., Tellez, N., Gassner, B., Juan-Pico, P., Montanya, E., Quesada, I., Kuhn, M.*, et al.* (2010). The atrial natriuretic peptide and guanylyl cyclase-A system modulates pancreatic beta-cell function. Endocrinology *151*, 3665-3674.

Rosen, E.D., and Spiegelman, B.M. (2014). What we talk about when we talk about fat. Cell *156*, 20-44.

Rosen, E.D., Walkey, C.J., Puigserver, P., and Spiegelman, B.M. (2000). Transcriptional regulation of adipogenesis. Genes Dev *14*, 1293-1307.

Russwurm, M., Behrends, S., Harteneck, C., and Koesling, D. (1998). Functional properties of a naturally occurring isoform of soluble guanylyl cyclase. Biochem J *335*, 125-130.

Rutkowski, J.M., Stern, J.H., and Scherer, P.E. (2015). The cell biology of fat expansion. J Cell Biol *208*, 501-512.

Sackner-Bernstein, J.D., Kowalski, M., Fox, M., and Aaronson, K. (2005a). Short-term risk of death after treatment with nesiritide for decompensated heart failure: a pooled analysis of randomized controlled trials. Jama *293*, 1900-1905.

Sackner-Bernstein, J.D., Skopicki, H.A., and Aaronson, K.D. (2005b). Risk of worsening renal function with nesiritide in patients with acutely decompensated heart failure. Circulation *111*, 1487-1491. Epub 2005 Mar 1421.

Saito, M., Okamatsu-Ogura, Y., Matsushita, M., Watanabe, K., Yoneshiro, T., Nio-Kobayashi, J., Iwanaga, T., Miyagawa, M., Kameya, T., Nakada, K.*, et al.* (2009). High incidence of metabolically active brown adipose tissue in healthy adult humans: effects of cold exposure and adiposity. Diabetes *58*, 1526-1531.

Salvi, F., Sarzani, R., Giorgi, R., Donatelli, G., Pietrucci, F., Micheli, A., Baldoni, M., Minardi, D., Dessi-Fulgheri, P., Polito, M.*, et al.* (2004). Cardiovascular effects of sildenafil in hypertensive men with erectile dysfunction and different alleles of the type 5 cGMP-specific phosphodiesterase (PDE5). Int J Impot Res *16*, 412-417.

Samuel, V.T., and Shulman, G.I. (2012). Mechanisms for insulin resistance: common threads and missing links. Cell *148*, 852-871.

Sanchez-Gurmaches, J., Hsiao, W.Y., and Guertin, D.A. (2015). Highly selective in vivo labeling of subcutaneous white adipocyte precursors with Prx1-Cre. Stem Cell Reports *4*, 541-550.

Sanchez-Gurmaches, J., Hung, C.M., Sparks, C.A., Tang, Y., Li, H., and Guertin, D.A. (2012). PTEN loss in the Myf5 lineage redistributes body fat and reveals subsets of white adipocytes that arise from Myf5 precursors. Cell Metab *16*, 348-362.

Sandler, G., Ilahi, M.A., and Lawson, C.W. (1963). Glyceryl trinitrate in angina pectoris. Lancet *1*, 1130-1136.

Schermuly, R.T., Stasch, J.P., Pullamsetti, S.S., Middendorff, R., Muller, D., Schluter, K.D., Dingendorf, A., Hackemack, S., Kolosionek, E., Kaulen, C.*, et al.* (2008). Expression and function of soluble guanylate cyclase in pulmonary arterial hypertension. Eur Respir J *32*, 881-891.

Schmidt, P., Schramm, M., Schroder, H., and Stasch, J.P. (2003). Mechanisms of nitric oxide independent activation of soluble guanylyl cyclase. Eur J Pharmacol *468*, 167-174.

Schwartz, B.G., and Kloner, R.A. (2010). Drug interactions with phosphodiesterase-5 inhibitors used for the treatment of erectile dysfunction or pulmonary hypertension. Circulation *122*, 88-95.

Seale, P., Bjork, B., Yang, W., Kajimura, S., Chin, S., Kuang, S., Scime, A., Devarakonda, S., Conroe, H.M., Erdjument-Bromage, H.*, et al.* (2008). PRDM16 controls a brown fat/skeletal muscle switch. Nature *454*, 961-967.

Seale, P., Conroe, H.M., Estall, J., Kajimura, S., Frontini, A., Ishibashi, J., Cohen, P., Cinti, S., and Spiegelman, B.M. (2011). Prdm16 determines the thermogenic program of subcutaneous white adipose tissue in mice. J Clin Invest *121*, 96-105.

Sell, H., Berger, J.P., Samson, P., Castriota, G., Lalonde, J., Deshaies, Y., and Richard, D. (2004). Peroxisome proliferator-activated receptor gamma agonism increases the capacity for sympathetically mediated thermogenesis in lean and ob/ob mice. Endocrinology *145*, 3925-3934.

Shabalina, I.G., Petrovic, N., de Jong, J.M., Kalinovich, A.V., Cannon, B., and Nedergaard, J. (2013). UCP1 in brite/beige adipose tissue mitochondria is functionally thermogenic. Cell Rep *5*, 1196-1203.

Shankar, R.R., Wu, Y., Shen, H.Q., Zhu, J.S., and Baron, A.D. (2000). Mice with gene disruption of both endothelial and neuronal nitric oxide synthase exhibit insulin resistance. Diabetes *49*, 684-687.

Shao, D., and Lazar, M.A. (1997). Peroxisome proliferator activated receptor gamma, CCAAT/enhancer-binding protein alpha, and cell cycle status regulate the commitment to adipocyte differentiation. J Biol Chem *272*, 21473-21478.

Shih, M.F., and Taberner, P.V. (1995). Selective activation of brown adipocyte hormone-sensitive lipase and cAMP production in the mouse by beta 3-adrenoceptor agonists. Biochem Pharmacol *50*, 601-608.

Shimizu, I., Aprahamian, T., Kikuchi, R., Shimizu, A., Papanicolaou, K.N., MacLauchlan, S., Maruyama, S., and Walsh, K. (2014). Vascular rarefaction mediates whitening of brown fat in obesity. J Clin Invest *124*, 2099-2112.

Short, K.R., Bigelow, M.L., Kahl, J., Singh, R., Coenen-Schimke, J., Raghavakaimal, S., and Nair, K.S. (2005). Decline in skeletal muscle mitochondrial function with aging in humans. Proc Natl Acad Sci U S A *102*, 5618-5623.

Soares, M.O., Dumville, J.C., Ashby, R.L., Iglesias, C.P., Bojke, L., Adderley, U., McGinnis, E., Stubbs, N., Torgerson, D.J., Claxton, K.*, et al.* (2013). Methods to assess cost-effectiveness and value of further research when data are sparse: negative-pressure wound therapy for severe pressure ulcers. Med Decis Making *33*, 415-436.

Stasch, A., Ferbinteanu, M., Prust, J., Zheng, W., Cimpoesu, F., Roesky, H.W., Magull, J., Schmidt, H.G., and Noltemeyer, M. (2002a). Syntheses, structures, and surface aromaticity of the new carbaalane [(AlH)(6)(AlNMe(3))(2)(CCH(2)R)(6)] (R = Ph, CH(2)SiMe(3)) and a stepwise functionalization of the inner and outer sphere of the cluster. J Am Chem Soc *124*, 5441-5448.

Stasch, J.P., Alonso-Alija, C., Apeler, H., Dembowsky, K., Feurer, A., Minuth, T., Perzborn, E., Schramm, M., and Straub, A. (2002b). Pharmacological actions of a novel NO-independent guanylyl cyclase stimulator, BAY 41-8543: in vitro studies. Br J Pharmacol *135*, 333-343.

Stasch, J.P., and Hobbs, A.J. (2009). NO-independent, haem-dependent soluble guanylate cyclase stimulators. Handb Exp Pharmacol, 277-308.

Stuehr, D.J., Cho, H.J., Kwon, N.S., Weise, M.F., and Nathan, C.F. (1991). Purification and characterization of the cytokine-induced macrophage nitric oxide synthase: an FAD- and FMN-containing flavoprotein. Proc Natl Acad Sci U S A *88*, 7773-7777.

Sun, K., Kusminski, C.M., and Scherer, P.E. (2011). Adipose tissue remodeling and obesity. J Clin Invest *121*, 2094-2101.

Tanner, C.J., Barakat, H.A., Dohm, G.L., Pories, W.J., MacDonald, K.G., Cunningham, P.R., Swanson, M.S., and Houmard, J.A. (2002). Muscle fiber type is associated with obesity and weight loss. Am J Physiol Endocrinol Metab *282*, E1191-1196.

Tateya, S., Rizzo, N.O., Handa, P., Cheng, A.M., Morgan-Stevenson, V., Daum, G., Clowes, A.W., Morton, G.J., Schwartz, M.W., and Kim, F. (2011). Endothelial NO/cGMP/VASP signaling attenuates Kupffer cell activation and hepatic insulin resistance induced by high-fat feeding. Diabetes *60*, 2792-2801.

Tesmer, J.J., and Sprang, S.R. (1998). The structure, catalytic mechanism and regulation of adenylyl cyclase. Curr Opin Struct Biol *8*, 713-719.

Thielecke, F., Rahn, G., Bohnke, J., Adams, F., Birkenfeld, A.L., Jordan, J., and Boschmann, M. (2010). Epigallocatechin-3-gallate and postprandial fat oxidation in overweight/obese male volunteers: a pilot study. Eur J Clin Nutr *64*, 704-713.

Thonberg, H., Fredriksson, J.M., Nedergaard, J., and Cannon, B. (2002). A novel pathway for adrenergic stimulation of cAMP-response-element-binding protein (CREB) phosphorylation: mediation via alpha1-adrenoceptors and protein kinase C activation. Biochem J *364*, 73-79.

Thorsen, L.B., Eskildsen-Helmond, Y., Zibrandtsen, H., Stasch, J.P., Simonsen, U., and Laursen, B.E. (2010). BAY 41-2272 inhibits the development of chronic hypoxic pulmonary hypertension in rats. Eur J Pharmacol *647*, 147-154.

Towbin, H., Staehelin, T., and Gordon, J. (1979). Electrophoretic transfer of proteins from polyacrylamide gels to nitrocellulose sheets: procedure and some applications. Proc Natl Acad Sci U S A *76*, 4350-4354.

Trayhurn, P., and Beattie, J.H. (2001). Physiological role of adipose tissue: white adipose tissue as an endocrine and secretory organ. Proc Nutr Soc *60*, 329-339.

Tseng, Y.H., Kokkotou, E., Schulz, T.J., Huang, T.L., Winnay, J.N., Taniguchi, C.M., Tran, T.T., Suzuki, R., Espinoza, D.O., Yamamoto, Y.*, et al.* (2008). New role of bone morphogenetic protein 7 in brown adipogenesis and energy expenditure. Nature *454*, 1000-1004.

Turko, I.V., Ballard, S.A., Francis, S.H., and Corbin, J.D. (1999). Inhibition of cyclic GMP-binding cyclic GMP-specific phosphodiesterase (Type 5) by sildenafil and related compounds. Mol Pharmacol *56*, 124-130.

Turton, M.D., O'Shea, D., Gunn, I., Beak, S.A., Edwards, C.M., Meeran, K., Choi, S.J., Taylor, G.M., Heath, M.M., Lambert, P.D.*, et al.* (1996). A role for glucagon-like peptide-1 in the central regulation of feeding. Nature *379*, 69-72.

Unger, R.H., and Scherer, P.E. (2010). Gluttony, sloth and the metabolic syndrome: a roadmap to lipotoxicity. Trends Endocrinol Metab *21*, 345-352.

Vaandrager, A.B., Ehlert, E.M., Jarchau, T., Lohmann, S.M., and de Jonge, H.R. (1996). N-terminal myristoylation is required for membrane localization of cGMP-dependent protein kinase type II. J Biol Chem *271*, 7025-7029.

van Marken Lichtenbelt, W.D., and Schrauwen, P. (2011). Implications of nonshivering thermogenesis for energy balance regulation in humans. Am J Physiol Regul Integr Comp Physiol *301*, R285-296.

van Marken Lichtenbelt, W.D., Vanhommerig, J.W., Smulders, N.M., Drossaerts, J.M., Kemerink, G.J., Bouvy, N.D., Schrauwen, P., and Teule, G.J. (2009). Cold-activated brown adipose tissue in healthy men. N Engl J Med *360*, 1500-1508.

Vandervoort, A.A. (2002). Aging of the human neuromuscular system. Muscle Nerve *25*, 17-25.

Vegiopoulos, A., Muller-Decker, K., Strzoda, D., Schmitt, I., Chichelnitskiy, E., Ostertag, A., Berriel Diaz, M., Rozman, J., Hrabe de Angelis, M., Nusing, R.M.*, et al.* (2010). Cyclooxygenase-2 controls energy homeostasis in mice by de novo recruitment of brown adipocytes. Science *328*, 1158-1161.

Vijgen, G.H., Bouvy, N.D., Teule, G.J., Brans, B., Hoeks, J., Schrauwen, P., and van Marken Lichtenbelt, W.D. (2012). Increase in brown adipose tissue activity after weight loss in morbidly obese subjects. J Clin Endocrinol Metab *97*, E1229-1233.

Vijgen, G.H., Bouvy, N.D., Teule, G.J., Brans, B., Schrauwen, P., and van Marken Lichtenbelt, W.D. (2011). Brown adipose tissue in morbidly obese subjects. PLoS One *6*, e17247.

Virtanen, K.A., Lidell, M.E., Orava, J., Heglind, M., Westergren, R., Niemi, T., Taittonen, M., Laine, J., Savisto, N.J., Enerback, S.*, et al.* (2009). Functional brown adipose tissue in healthy adults. N Engl J Med *360*, 1518-1525.

Weissman, B.A., Jones, C.L., Liu, Q., and Gross, S.S. (2002). Activation and inactivation of neuronal nitric oxide synthase: characterization of Ca(2+)-dependent [125I]Calmodulin binding. Eur J Pharmacol *435*, 9-18.

WHO (2016). Obesity and Overweight (World Health Organization).

Wilson-Fritch, L., Burkart, A., Bell, G., Mendelson, K., Leszyk, J., Nicoloro, S., Czech, M., and Corvera, S. (2003). Mitochondrial biogenesis and remodeling during adipogenesis and in response to the insulin sensitizer rosiglitazone. Mol Cell Biol *23*, 1085-1094.

Wu, J., Bostrom, P., Sparks, L.M., Ye, L., Choi, J.H., Giang, A.H., Khandekar, M., Virtanen, K.A., Nuutila, P., Schaart, G.*, et al.* (2012). Beige adipocytes are a distinct type of thermogenic fat cell in mouse and human. Cell *150*, 366-376.

Yamada, C., Yamada, Y., Tsukiyama, K., Yamada, K., Udagawa, N., Takahashi, N., Tanaka, K., Drucker, D.J., Seino, Y., and Inagaki, N. (2008). The murine glucagon-like peptide-1 receptor is essential for control of bone resorption. Endocrinology *149*, 574-579.

Yamada, S., Deguchi, T., Nezasa, S., Tamaki, M., Ehara, H., Okano, M., and Kawada, Y. (1992). [Study on chemosensitivity test of urogenital tumors by ATP assay]. Nihon Hinyokika Gakkai Zasshi *83*, 2022-2028.

Yoneshiro, T., Aita, S., Matsushita, M., Okamatsu-Ogura, Y., Kameya, T., Kawai, Y., Miyagawa, M., Tsujisaki, M., and Saito, M. (2011). Age-related decrease in cold-activated brown adipose tissue and accumulation of body fat in healthy humans. Obesity (Silver Spring) *19*, 1755-1760.

Yoneshiro, T., Ogawa, T., Okamoto, N., Matsushita, M., Aita, S., Kameya, T., Kawai, Y., Iwanaga, T., and Saito, M. (2013). Impact of UCP1 and beta3AR gene polymorphisms on age-related changes in brown adipose tissue and adiposity in humans. Int J Obes (Lond) *37*, 993-998.

Young, J.B., Saville, E., Rothwell, N.J., Stock, M.J., and Landsberg, L. (1982). Effect of diet and cold exposure on norepinephrine turnover in brown adipose tissue of the rat. J Clin Invest *69*, 1061-1071.

Yu, Y.H., and Zhu, H. (2004). Chronological changes in metabolism and functions of cultured adipocytes: a hypothesis for cell aging in mature adipocytes. Am J Physiol Endocrinol Metab *286*, E402-410.